LOW FREQUENCY, MILLIMETER WAVELENGTH, INTERDIGITAL DIELECTROMETRY OF INSULATING MEDIA IN A TRANSFORMER ENVIRONMENT

by

PATRICK LI

S.B., Massachusetts Institute of Technology
(1985)

Submitted to the Department of
Electrical Engineering and Computer Science
in Partial Fulfillment of the Requirements
for the Degree of

MASTER OF SCIENCE
at the
MASSACHUSETTS INSTITUTE OF TECHNOLOGY 1987

Signature of Author_____
Department of Electrical Engineering and Computer Science
May 1987

Certified by_____
Thesis Supervisor

Accepted by_____
Chairman, Departmental Committee on Graduate Students

LOW FREQUENCY, MILLIMETER WAVELENGTH, INTERDIGITAL DIELECTROMETRY OF INSULATING MEDIA IN A TRANSFORMER ENVIRONMENT

by

PATRICK LI

Submitted to the Department of Electrical Engineering and Computer Science on May 19, 1987 in partial fulfillment of the requirement for the Degree of Master of Science

Abstract

A commercially available low frequency, millimeter wavelength, "microdielectric" sensor is adapted to measure the complex permittivity of insulating media in transformers. The following materials are studied: transformer oil, oil impregnated paper insulation, treated and untreated chromatographic grade silica gell, and cabosil particles. The goal is to be able to correlate changes in the dielectric properties of these insulating materials with changes in the condition of the transformer.

Sensor performance is extended from 1 Hz - 10 kHz to 0.005 Hz - 10 kHz. Studies were made of the sensor's performance, and a model developed to allow for accurate prediction of the sensor's behavior. Optimization of the sensor's measurement sensitivity is discussed.

The effects of moisture absorption by the materials from which the sensor is constructed are shown to obscure the desired response. A 5μm thick layer of Parylene C is found to be an effective barrier to moisture in transformer oil.

The ability to measure the complex permittivity of transformer oil using a parylene coated sensor is demonstrated. Changes in the complex permittivity of the oil are found upon oxidation. The effects of temperature are shown to have an Arhenius dependence.

Measurements are made of paper insulation showing the dependence of its conductivity on moisture. Ohmic conductivities are estimated for the paper in an initial analysis. Dispersion is then identified and frequency dependent complex permittivities are estimated for the paper. A power law dependence is hypothesized.

The possibility of measuring particlulate contamination in oil is explored. It is found that under very special conditions, the thickness of a sedimenting layer can be estimated. However, in a transformer, these conditions don't exist, and it becomes basically impossible to measure the level of contamination.

The use of chromatography particles packed on a parylene coated macro sensor is also explored to determine if the adsorption of degradation products from the oil affect the dielectric properties of the particle/oil mixture. A dispersive complex permittivity is estimated for the response of one such system.

Thesis Supervisor: James R. Melcher, Professor of Electrical Engineering

ACKNOWLEDGEMENTS

I would like to thank Professor Melcher for the quality of my overall research experience. He provided the guidance and support that was essential to the success of my research. More importantly, he helped me become more aware of the responsibilities that I, as an engineer, have for the work that I do and choices that I make.

I would also like to express my gratitude to Mark Zaretsky. He was always there to answer my silly questions and discuss my ideas. He helped shape much of my research and provided valuable insights into all sorts of problems that I encountered. Much of this thesis would not have been possible without the discussions that we shared.

Lastly, I would like to thank the consortium of electric utilities that made this research project possible. They helped me appreciate the engineering realities that are faced in industry.

Contents

List of Figures

List of Tables

Chapter 1

Introduction

Interest in monitoring large power transformers for diagnostic purposes has grown as power capacity has steadily increased and as performance levels have been pushed closer to operating limits. These newer and less conservative transformers, however, exact very high costs in both safety and dollars when they catastrophically fail. Sensors capable of measuring properties of the transformer, on-line, would increase the effectiveness of preventive maintenance programs. The goal of this thesis is to develop a planar, millimeter wavelength, interdigital electrode sensor to measure the complex dielectric properties of insulating media in a transfromer. The initial strategy will be to prototype a sensor capable of looking at changes in the bulk permittivity and conductivity (the complex dielectric constant) of the transformer oil as it is degraded in various controlled fashions. Then, various insulating media, such as paper insulation used in transformers, and diatomaceous/fuller's earth used for filtering and cleaning transformer oil, will be applied to the sensor and their complex dielectric properties monitored as degradation products are absorbed/adsorbed from transformer oil that has been degraded in a controlled fashion. Chapter 1 begins with a review of the methods currently used to monitor large power transformers. Then, section 1.2 presents the dielectric properties of transformer oil and reviews the current techniques and procedures used for acceptance testing and monitoring of transformer oil in light of its complex dielectric constant. Section 1.3 is an introduction to dielectrometry. The difference in the capabilities of two different wavelength versions of the sensor are explored and the general model for the interdigitated electrode structure described.

Chapter 2 describes the development of hardware for a prototype sensor and tests the validity of the model against actual data. Chapter 3 identifies potential contaminants in the oil that can poison the sensor and demonstrates a method for protecting against such contaminants. Chapter 4 outlines the method for estimating bulk parameters, and the dielectric properties of different transformer oils are estimated from gain and phase frequency responses. Chapter 5 explores the feasibility of measuring the dielectric properties of oil impregnated paper insulation and looks at the effects of moisture on the conductivity of paper. Chapter 6 looks at the possibility of detecting particles in the transformer oil using dielectrometry. Chapter 7 explores the possibility of dielectrically detecting the adsorption of degradation

products from the transformer oil using different types of particles.

1.1 Transformer Monitoring

When they fail, large power transformers (>1MVA) often do so catastrophically. Consequently, there is great interest in detecting the onset of such failures as early as possible. Various properties of the transformer have been studied and threshold levels determined for malfunctioning units. The fundamental properties of the transformer used in these diagnostics fall into three basic categories: mechanical (vibrations, heat transfer, corrosion); chemical (gas formation in the oil, oxidation, insulation deterioration, sludge formation); and electrical (dielectric properties of oil, electrical discharge activity, arcing, breakdown strength). The focus here will be upon the properties of the transformer oil and what they indicate about the condition of the transformer.

Transformer oil serves two basic functions: it is a good electrical insulator and a good conductor of heat. There are a variety of insulating fluids with these properties, but the napthenic type of petroleum crude has been found to be the most effective and is used in most large power transformers. The availability, however, of this type of crude is becoming limited and alternatives are being sought. An excellent review of the standard physical, chemical, and electrical properties of various brands of transformer oil is presented by Rouse [1]. Further information on other types of insulating fluids and their properties is presented by Wilson [2].

Current methods used for monitoring transformer oil are embodied by the ASTM standards. These are tests that have been established through experience for both quality control and diagnostic purposes. The oil's physical, chemical, and electrical properties of interest include the following: dielectric breakdown strength, power factor, dielectric loss, moisture content, dissolved gas content, acidity, interfacial tension, copper and iron content, and sludge and particulate counts. The first three tests have not been well correlated with specific degradation processes. However, changes in the other properties over time are indicative of specific problems. For example, the acidity and sludge content of the oil are good indicators that oxidation is occurring. The purpose here is not to give a detailed analysis of each of these tests. They are mentioned and referenced to provide background in the area of transformer monitoring [3].

Of all the methods available for monitoring transformer oil, dissolved gas analysis is perhaps the most important. Gas chromatography has been used extensively throughout the power industry to monitor the gas content of transformer oil. The absolute and relative quantities of combustible gases in oil are a good indicator of arcing and partial discharge activity as well as other types of faults. There is a fairly large data base of documented transformer failures that support the various diagnoses, based upon gas content, now routinely used in industry [4]. The ability to monitor combustible gas content in transformer oil is consequently of great importance in detecting malfunctioning transformers.

Liquid chromatographic analysis, on the other hand, is a technique that has only

recently been applied to transformer monitoring. Duval and Lamarre of the Hydro-Quebec Research Institute published some papers on the results of such analysis in the late 1970s [5] [6]. They used gel permeation and liquid/solid (adsorption) chromatography to analyze the oil. Even the most modern analytical techniques, however, are unable to separate the thousands of individual components contained in insulating oil. Instead, Duval and Lamarre separated the components by size (gel permeation chromatography) and aromaticity (adsorption chromatography). They used an RI (differential refractometer) detector and a UV detector to evaluate the eluted substances. They then compared the chromatograms of clean oil to that of oil degraded by gas-phase corona, sparking, strong arcing, and oxidation.

Significant differences were found in the chromatograms characterizing the clean and the degraded oil. Thus, monitoring degradation products other than combustible gases clearly has potential for becoming an important method of monitoring transformer oil. The only major drawback is that the complexity of transformer oil makes identification of individual components extremely difficult. Hence, identifying components to monitor and correlating them with specific types of failures becomes a monumental task. In addition, standardizing the tests, which is necessary for establishing a working data base, also becomes a more formidable obstacle.

It is clear that monitoring specific non-gaseous degradation products of transformer oil is most likely impractical. There are simply too many chemical components in transformer oil for even state of the art liquid chromatography to separate and identify. Another more tractable strategy is to look at the effects of known or suspected degradation processes which occur in transformers and to correlate them with changes in various properties of the transformer oil. This is the approach taken by Duval and Lamarre in their chromatographic analysis of the oil and is, in fact, the strategy used in developing most of the ASTM tests. The identification of specific combustible gases is the only exception.

Current techniques for monitoring transformer oil require, in almost all cases, that a sample be taken and the analysis done in a laboratory. Due to the high cost of such procedures, sampling is typically performed on an annual or semi-annual basis. If a problem is detected during one of these tests, more testing is performed on a much shorter time scale to try and conclusively determine if a problem really exists. However, there are clearly major drawbacks to such a scheme. In terms of trying to detect an impending failure, the testing is only effective if the time scale of the transformer's deterioration is on the order of the sampling time. Thus, it is possible for a transformer to pass a normally scheduled battery of tests and then fail catastrophically a short time later. There is at least one documented case where the time scale of failure was on the order of minutes [7]. Hence, there is clearly a need for on-line monitoring of transformers.

Efforts for development of on-line detectors have been concentrated in the area of gas detection. This is because of the wide variety of problems that can be detected in this manner, and the large data base that is available from experience with past transformer failures. However, there is a vast potential for a greater understanding of failure modes if other degradation products were detectable. One method for sensing such degradation products would be to look at their effects on the dielectric

properties of the oil, the paper insulation, or any other materials exposed to the oil. There are currently no such devices available for on-line monitoring of the dielectric properties of such materials in a transformer environment.

1.2 Dielectric Properties of Transformer Oil

Analysis of the dielectric properties of transformer oil has received considerable attention. However, research in this area has not reached a stage where many of the physical and chemical processes in the oil that affect its dielectric properties can be explained. Consequently, the complex dielectric constant is not a characteristic of the oil that utilities consistently look at when monitoring or even accepting transformer oil. Thus, there is not a lot of data from the field to help direct research efforts. In addition, many dielectric measurements of the oil are strongly dependent on the technique used in taking the measurement so that interpretation of available data can become difficult. To help ease this problem, a set of standards was developed by The American Society for Testing and Materials (ASTM) for many of the characteristics of petroleum based insulating oils. There are three tests for the dielectric properties of the transformer oil: dielectric breakdown voltage, power factor, and resistivity. The following three paragraphs describes briefly the test and its significance as stated by the ASTM.

The dielectric breakdown test (ASTM Method D877 D1816 D3300) is a measure of a liquids ability to withstand electrical stress. Low breakdown values would indicate the presence of contaminating agents such as water, dirt, or conducting particles in the liquid. The configuration of the test cell and summary of test conditions is presented in detail in the ASTM methods. This particular test will not be explored further as it is not a measurement that the microdielectric sensor is capable of making.

The power factor test (ASTM test D924) measures the ratio of the power dissipated in the oil to the product of the effective voltage and current at the terminals of the test cell when tested with a sinusoidal field under prescribed conditions. This is numerically equivalent to the sine of the loss angle. Thus, it is a measure of the dielectric losses in the oil which may be an indication of the level of soluble contaminants. The measurement is typically made at 60 Hz in a three terminal or guarded electrode test cell using a bridge circuit. Further details can be found in the test specifications [8].

Measurement of the resistivity (ASTM test D1169) of the transformer oil is performed at d-c potentials. The oil sample is tested in a three terminal, or guarded electrode test cell. An electric stress of 200 to 1200 V/mm is applied. The current flowing between the high voltage and guarded measuring electrode is measured at the end of one minute of electrification. The resistivity of a liquid is a measure of its electrical insulating properties. High resistivity indicates low content of free ions and conductive contaminants in the oil [8]. Unfortunately, the measured resistivity is not going to be determined by just the properties of the oil. The measurement will also be a function of the geometry of the cell and the strength and frequency of the applied field [9]. For example, electrode polarization in a d-c measurement can affect the field stressing the bulk of the oil.

The majority of dielectric studies of transformer oil are done using these standardized tests. This provides some common basis for comparing data from different studies. Before proceeding further with a review of the relevant literature, some

background theory on dielectric loss is presented. This will facilitate discussions in later sections concerning the literature.

1.2.1 Dielectric Loss Mechanisms

Dielectric losses in insulating fluids such as transformer oil are generally attributed to three mechanisms: ionic conduction, dipole orientation, and space charge polarization. Oils having aromatic, naphthenic, and paraffinic constituents exhibit all three losses. Silicone liquids and aromatic-free oils, on the other hand, generally do not exhibit dipole losses [10]. Ionic conduction and dipole orientation losses are processes that occur in the bulk of the insulating fluid whereas space charge polarization is strictly an interfacial phenomena occuring at the electrode-fluid boundary. Each of these loss mechanisms has distinctive characteristics which will be explored in this section.

Polarization effects at an electrode in an insulating dielectric fluid are, in general, not well understood. Quantitatively, there is an apparent increase in the permittivity at low frequencies. This affect is attributed to the formation of a high impedance layer due to blocking of ionic current at the electrode interface. At low frequencies, there is sufficient time for such blocking layers to form resulting in an increase in the measured capacitance. Consequently, such changes are not due to true increases in the permittivity of the bulk fluid [11] [12]. This is an effect to be aware of when actual measurements are made.

Ionic Conduction Losses

Ionic conduction losses occur when the electric field varies slowly enough so that ions have time to reverse direction and move from one half cycle to the next. The unipolar ionic conduction current in a fluid with ion concentration N, average mobility b, and average charge q is given by

$$\vec{J} = NqbE \tag{1.1}$$

where the conductivity is $\sigma = Nqb$. The conduction process is ohmic if it is comprised of both positive and negative ions which sum to zero net charge in the material. Using the constitutive relation for the current density, the permittivity and conductivity can be expressed as a single complex quantity:

$$\epsilon^* = \epsilon - \frac{j\sigma}{\omega} \tag{1.2}$$

where the permittivity ϵ may be dispersive. The real part is, by convention, the permittivity ϵ' and the imaginary part, the dielectric loss factor ϵ''. Thus, ionic conduction losses are characterized by an inverse angular frequency dependence by the dielectric loss factor. Another quantity of interest is the dielectric loss tangent $tan\delta = \epsilon''/\epsilon'$. It is the ratio of the energy dissipated per cycle to the energy stored per cycle. The ASTM power factor test is simply another manifestation of this same quantity ($sin\delta$).

Dipole Orientation Losses

At high enough frequencies, where the electric field is varying so quickly that the orientation of the dipoles lags the electric field and thermal energy is dissipated through viscous rotation, dispersions are encountered in both the permittivity ϵ' and the loss factor ϵ''. This phenomena is most simply modeled by the single relaxation time Debye model,

$$\epsilon' = \epsilon'_\infty + \frac{\epsilon'_0 - \epsilon'_\infty}{1 + (\omega\tau)^2} \tag{1.3}$$

and

$$\epsilon'' = \frac{(\epsilon'_0 - \epsilon'_\infty)\omega\tau}{1 + (\omega\tau)^2} \tag{1.4}$$

where ϵ'_0 is the permittivity at zero frequency and ϵ'_∞ is the permittivity at "infinite" frequency. The relaxation time, τ, for the dipole is given by

$$\tau = \frac{4\pi\eta r_D^3}{kT} \tag{1.5}$$

where η is the viscosity, r_D is the radius of the dipoles, k Boltzman's constant, and T the absolute temperature [13] [14]. The loss tangent is defined as before and is given by

$$tan\delta = \frac{(\epsilon'_0 - \epsilon'_\infty)\omega\tau}{\epsilon'_0 + \epsilon'_\infty(\omega\tau)^2} \tag{1.6}$$

which peaks at

$$\omega_0 = \frac{1}{\tau}\sqrt{\frac{\epsilon'_0}{\epsilon'_\infty}} \tag{1.7}$$

If the dipole radius is on the order of a few angstroms, then the relaxation time in room temperature for transformer oil, which has a viscosity of roughly .02 kg/ms, is approximately 10^{-9} seconds. Since the static and high frequency permittivity are of the same magnitude for transformer oil, the frequency for maximum dipolar loss is calculated to be of the order 10^7 Hz. Dipole losses are characterized by the dispersion seen in both the permittivity and the loss factor, and a maximum loss which occurs at a frequency determined by the dipolar relaxation time.

Microdielectric measurements (maximum frequency of 10 kHz) of transformer oil should experience only ionic conduction losses if no space charge polarization is observed. Dipole relaxation won't have an affect at such low frequencies. Thus, the permittivity should be frequency independent and the dielectric loss factor should scale inversely with the angular frequency ω. Actual experimental measurments will be shown later to confirm this theory.

1.2.2 Effects of Degradation on the Dielectric Properties of Transformer Oil

The majority of literature reporting on the effects of degradation processes on the dielectric properties of transformer oil concentrate on aging due to oxidation. This is a fairly slow process so that some sort of accelerated aging process is required when performing laboratory analyses. There are two ASTM tests designed to evaluate the oxidation resistance of the oil through accelerated aging. The tests and apparatus are described in ASTM tests D-2112 and D-2440. Basically, the oil is heated at high temperatures while exposed to oxygen and perhaps a catalyst such as copper. Typically, measurements of the loss tangent and conductivity are made after a certain aging period. Both ionic conduction and dipole losses have been examined in these tests. Attempts have been made to correlate oxidation with acidity, peroxide levels, dissolved copper content, and aromaticity. Some of these results are presented and the remainder are referenced.

Oxidation is believed to be one of the primary causes of oil degradation [1] [15]. It occurs where constituents in the oil react with free oxygen. The presence of catalysts such as copper can increase the rate of reaction and can itself contribute to losses when it becomes dissolved in the oil. The steps in the chemical process have been explored by various researchers [1] [13]. What has been found is that the by products of this reaction affect the loss mechanisms in the oil.

Hakim [13] performed accelerated oxidation experiments, on transformer oil, similar to the ASTM tests. The type of oil (aromatic, naphthenic, paraffinic) was not specified, but it was known that no oxidation inhibitors were present. The oil was heated for 68 hours at $115°C$ while exposed to air. This process was repeated up to three times with low frequency (1-10 kHz) and d.c. measurements of the resistivity made at the end of each run using a standard cell and bridge network at $50°C$. The applied field was 500 V/cm, well below the 200 kV/cm reported necessary for charge injection effects to occur [16]. Thus, the measured conductivity values should reflect ionic conduction losses. The d.c. conductivity measurements ranged from 5×10^{-13} mhos/m for new oil to 6.7×10^{-12} mhos/m after the third oxidation run. The a.c. conductivity measurements were found to be frequency independent in the ranges of interest and the values were similar to, but consistantly a little higher than, the d.c. values. It is suggested that the main product of oxidation may be the formation of acids and that therefore the primary conducting species in the oil are hydrogen ions. This would also be true for unoxidized oil because they both exhibit the same activation energies [13]. At least one other researcher has mentioned hydrogen ions as a possible conduction mechanism in oil [18].

Lamarre, Crine, and Duval [17] performed similar oxidation experiments but with the presence of copper to catalyze the reaction and oxidation inhibitors to retard the process. Correlations were made between the level of oxidation and the acidity, copper content, and peroxide levels in the oil. Each contaminant contributes to the conductivity of the oil. Overall, the conductivity of the oil was found to change two orders of magnitude from 2×10^{-13} mhos/m to 2×10^{-11} mhos/m from when it was new to after final oxidation. Measurements were made at room

temperature. Many other researchers have seen similar effects on low frequency and d.c. conductivity and associated loss tangents when oxidizing oil [15] [19] [20].

Oxidation products have also been found to have an effect upon dipolar losses. Upon oxidation of the oil, it has been shown that at any one temperature, the height of the loss peak as well as the distribution of relaxation time increases. The decrease in the maximum of the dielectric loss together with the absence of any change in the viscosity as a function of oxidation suggests, in light of eq. 1.5, that there is an increase in the radius of the dipole. From the data, the radius of the dipoles was estimated to have increased by a factor of 1.5. It is suggested that a upon oxidation, there develops a hydrogen bonding between the dipoles and its surrounding medium. Such hydrogen bonding would result from the many products of oxidation, particularly acids, and would increase the effective radius of the dipole [13].

Temperature was also shown to have a large effect upon the conductivity of the oil. The conductivity was found to have an Arrhenius type temperature dependency,

$$\sigma = \sigma_0 e^{-E_\sigma/RT} \tag{1.8}$$

where σ_0 is a constant and E_σ is the activation energy for electric conduction in the fluid. A typical value for transformer oil would be $E_\sigma = 15$ kcal/mole. The carrier mobility was found to have a similar temperature dependence with activation energy E_μ. The activation energy for electric conduction should be the sum of the activation energies for the mobilities of each species of ion, provided the ionic dissociation energy doesn't have an affect on the electric conduction process. These activation energies can provide insight on the conduction process. It was hypothesized from comparing these energies that the conduction process is due to the ionic nature of the impurities in the oil [21]. Besides providing information on the nature of the conduction process, the temperature dependence is important when comparing conductivity and loss measurements. For comparisons of different conductivity measurements taken at different temperatures to be meaningful, they must be normalized to some common temperature using the Arrhenius relation.

It has been argued that on-line monitoring of oxidation products isn't necessary because it is such a slow process under normal operating conditions. Unfortunately, not much else seems to be known about the effects of other forms of oil degradation upon the dielectric properties of the oil. Thus, the availability of on-line dielectric measurements of the transformer oil may not have immediate benefits. Perhaps changes in the dielectric properties of the oil can be correlated to other, faster, degradation mechanisms as experience with these measurements increases. In any case, the availability of such measurements will allow further exploration of the usefulness of dielectric measurements for transformer monitoring.

1.3 Microdielectrometry

1.3.1 Introduction

Microdielectrometry, as developed by Senturia et. al. [22], is a new technique for measuring complex dielectric dispersions using a planar interdigitated electrode structure. The device operates by driving one set of electrodes with a sinusoidal (2 volt pp) signal ranging in frequency from 0.005 Hz to 10 kHz and "listening" on the other set. The receiving electrode is connected to the gate of a high impedance charge flow transistor so that it is essentially allowed to "float" at some potential which is self consistent with Maxwell's equations and the complex dielectric properties of the adjacent media. The potential of the floating gate is a high impedance measurement made by using a feedback circuit utilizing an FET which is matched to a charge flow transistor (CFT). The information that is extracted from the sensor is a complex gain: $V_F e^{j\phi}/V_D$ expressed in decibels and degrees of relative phase difference from the driven gate.

Microdielectrometry has many advantages over conventional methods for taking dielectric measurements. Due to the planar geometry of the electrode structure, non-invasive measurements are made possible by simply placing the sensor against the media for which measurements are desired. This is not possible with conventional methods where the material must be sandwiched between two electrodes. Similarly, to make measurements of a liquid using conventional techniques, a sample must be taken and placed in a test cell. Microdielectrometry, on the other hand, requires simply placing the sensor in the fluid of interest. Also, many of the problems associated with test cell measurements such as the formation of blocking layers are not a problem when using microdielectrometry. Such layers, because of the high impedance measurement technique used, are easily recognized and accounted for using a continuum model. Finally, the low frequency (0.005Hz) measurements possible with microdielectrometry allows for identification of dielectric dispersions.

Thus, to monitor the oil on-line in a transformer, sensors can simply be mounted in strategic locations in the transformer or oil circulation loop and measurements made as often as desired. Also, because of the low frequencies possible with the microdielectrometer (.005 Hz), very low conductivities of about 1×10^{-13} mhos/m can be measured. The high frequency limit of 10 kHz allows conductivities up to about 1×10^{-7} mhos/m to be measured. The range of conductivities that are measureable with the microdielectrometer make it well suited for looking at transformer oil, which is a highly insulating fluid with a conductivity of typically 8×10^{-13} mhos/m when new.

1.3.2 Macro sensor vs. Micro sensor

In this section, the relevant attributes of two different versions of the dielectric sensor are described and the suitability of the sensors to the goals outlined earlier are explored.

There are currently two versions of the interdigitated electrode sensor which

are fundamentally characterized by the different spatial periodicity, or wavelength, of their electrode structures. They will be subsequently referred to as the macro sensor, which has a spatial wavelength of 1 mm; and the micro sensor, which has a spatial wavelength of 50μm. The sensors operate quasistatically if the wavelength of the applied signal is much greater than the spatial wavelengths of the sensors. This allows both sensors, theoretically, to operate in a quasistatic mode well into the gigahertz range (the maximum frequency of 10 kHz specified for the instrument is purely a limitation of the hardware). The quasistatic electric field generated by the sensor must, by Maxwell's laws, decay exponentially into the medium. The spatial wavelength determines the rate of this decay, and consequently, some characteristic depth where the electric field generated by the sensor has decayed essentially to zero. Beyond this point, the material no longer has any effect upon the response of the device. This maximum sensing range has been found, from modeling, to be approximately $\lambda/3$, which gives the micro sensor a range of 17μm and the macro sensor a range of 330μm.

The greater range of the macro sensor is necessary if coatings of paper insulation and diatomaceous earth are to be measured. This is simply because the paper insulation is 80 microns thick and the particles of diatomaceous earth are tens of microns in diameter. The micro sensor's shorter range would not allow it to "see" the bulk of the paper nor allow treatment of the oil particle mixture as a uniform medium. In addition, the shorter wavelength of the micro sensor makes it more sensitive to surface phenomena, such as space charge polarization, which could potentially interfere with bulk measurements of the oil at lower frequencies [25]. Thus, it is clear that the larger wavelength of the macro sensor makes it better suited for the desired configuration of measurements.

The micro sensor, because of the microfabrication techniques used to construct it, does have advantages over the macro sensor. These advantages relate to the electronics of the sensor as well as geometrical parameters which affect its sensitivity. These issues can be better understood once the model for the interdigitated electrode structure has been described.

1.3.3 Model Background

The macro electrode structures to be modeled are shown in Figures 1.1 and 1.2. Both of these sensor's, however, will be modeled initially in exactly the same manner. Differences in performance between the two macro sensors will be explored in a subsequent chapter. The micro sensor electrode structure, which basically has the same structure as that of the macro sensor illustrated in Figure 1.2, is also described using this model, but with input parameters reflecting differences in physical dimensions.

The basic structure of all these microdielectric sensors consist of an oxide layer sandwiched between the interdigitated electrode structure and a ground plane. Thus, there is coupling between the electrodes through the oxide layer and the media above the sensor plane, as well as coupling through the oxide layer between the electrodes and the ground plane. Development of a model for the interdig-

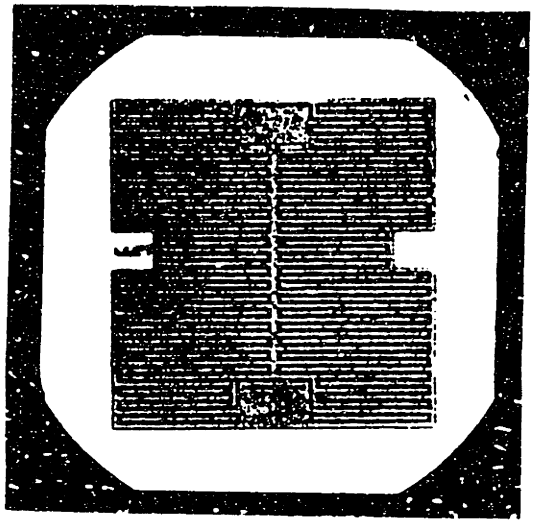

Figure 1.1: Macro Sensor Electrode Configuration 1: "Spine Structure" Sensor

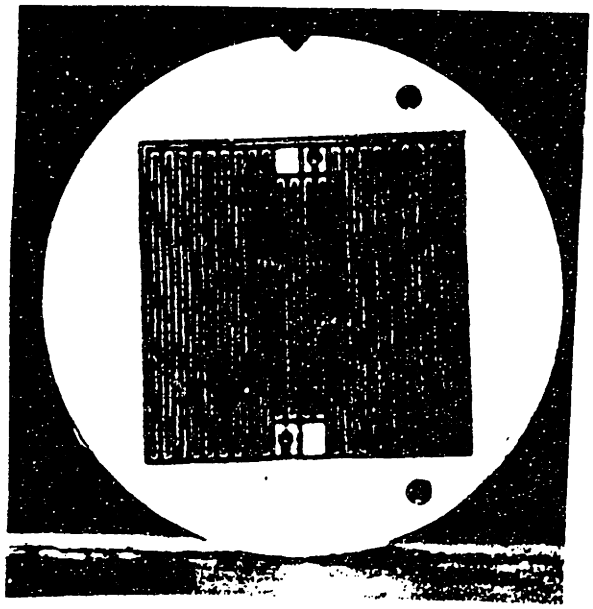

Figure 1.2: Macro Sensor Electrode Configuration 2: "Comb Structure" Sensor

itated electrode structure of the sensor was first done by Huan Lee at MIT. He used a finite difference simulation to solve Poisson's equation for lossy dielectrics in the sinusoidal steady state [23]. This solution, however, assumes that the sensor is responding to an infinite media with uniform bulk properties. Consequently, parameter estimation done with this model results in a best fit of the data to an infinite uniform media. This clearly sets limitations on the phenomena that can be addressed by this model.

Another strategy, first used by Lama Mouayad (MIT) and later refined by Mark Zaretsky (MIT) [25], was to use a continuum approach. It is a spectral analysis where all field quantities are expressed as fourier sums. The approximations made in developing this model were that the conduction process be linear in the electric field and the end effects and height of the electrodes be unimportant. Ignoring the end effects is a reasonable approximation if the area for which the electrodes are parallel is large compared to the number of ends. Ignoring the electrode height is also reasonable if it is much less than the spacing between electrodes. The validity of assuming a conduction process that is linear in the electric field will be demonstrated for transformer oil measurements within the frequency limitations of the instrument.

A graphical outline of the model is shown in Figure 1.3 There are two sets of inputs to the model. The first is a description of the electrode array structure which includes its spatial wavelength, the interelectrode spacing, the thickness of the oxide layer, and the permittivity of the oxide layer (see Figure 1.4). The second set of parameters describe the media above the electrode plane. This information is represented by a complex surface capacitance which describes the response of a linear media to one fourier component of the applied potential. Calculation of the surface capacitance is centered around the assumption that the properties of the media be uniform in the direction tangential to the electrode plane. Together, these two sets of parameters describe a completely specified problem.

The next step in developing the model was to solve the "mixed boundary value problem" for the potential along the electrode plane. The potential is constrained along the driven and floating electrodes and Gauss' law and conservation of charge govern the potential and electric field in the interelectrode region. To solve this problem, the interelectrode region is discretized by introducing a grid of unknown voltages at k collocation points. The potential is specified to vary linearly between these grid points. It is then expressed as a fourier sum in terms of the constrained values along the electrodes and the k unknown voltages in the interelectrode region. Integration of the conservation of charge boundary condition along surface segments bracketing the collocation points generates k equations in the k unknown potentials. Solving this system of equations then gives the values of the collocation voltages.

Electrical terminal variables are finally obtained by integrating current density over the surfaces of the electrodes. A pi network (see Figure 1.3) is used to represent the field solutions. Given the symmetry of the electrode structure, Y_{11} must equal Y_{22}. All of the admittances of the electrode can now be found by finding i_D and i_F with the floating electrode grounded. Once these admittances have been found, the floating gate can be allowed to float and the response determined for an arbitrary load. The complex gain is, as mentioned before, the ratio of the floating to driven

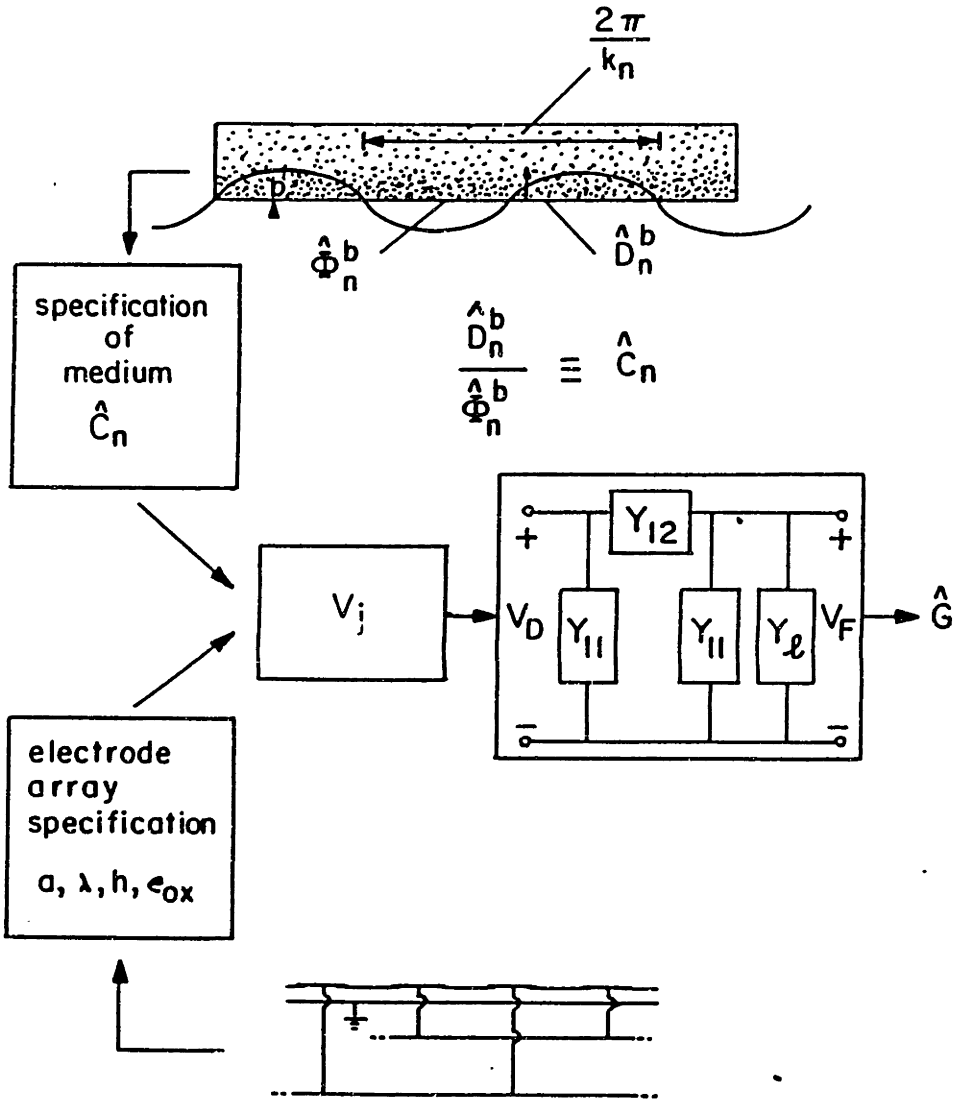

Figure 1.3: Block Diagram of Model (reprinted from [25])

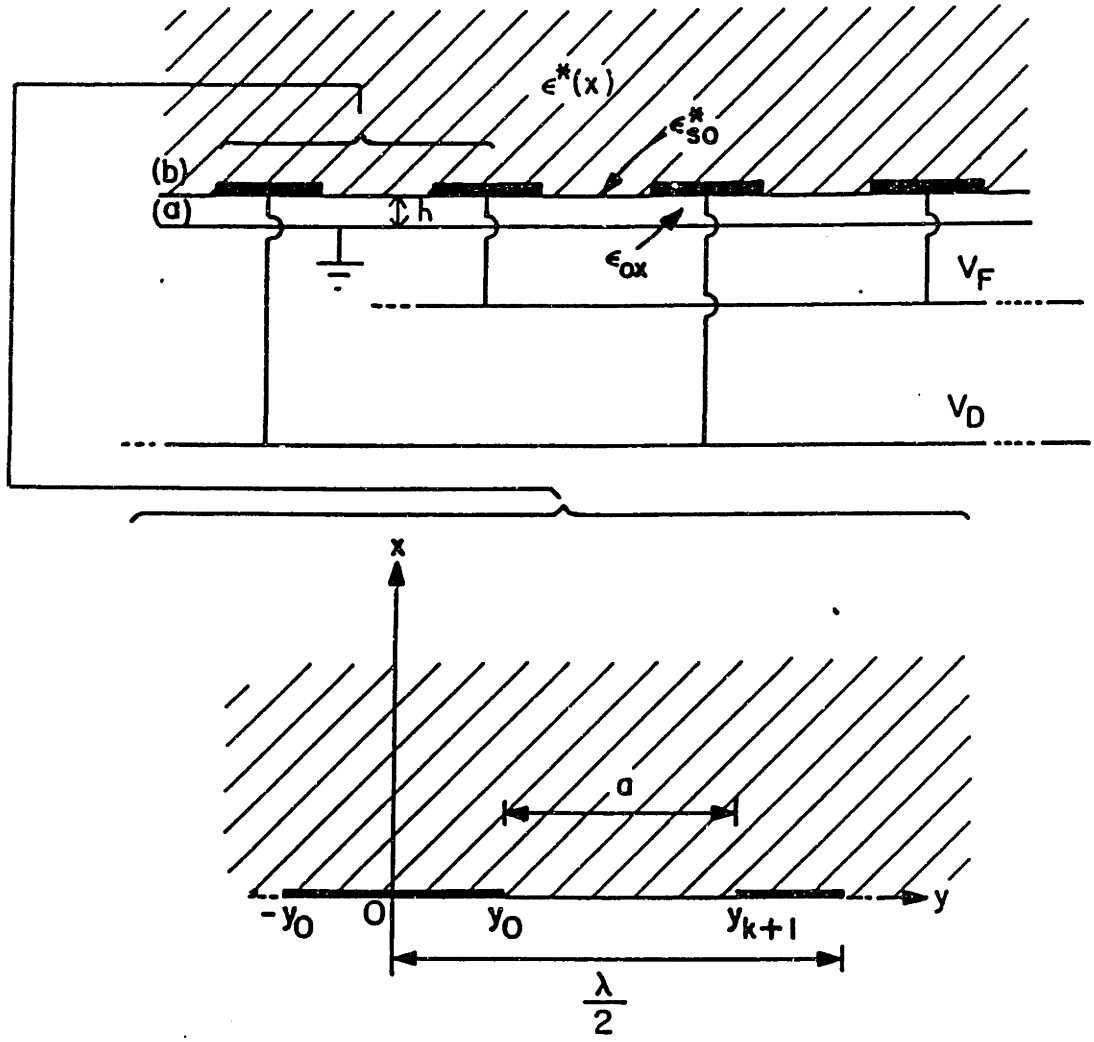

Figure 1.4: Parameters of Sensor Layout (reprinted from [25])

gate voltage (magnitude and phase) and is given by

$$\hat{G} = \frac{\hat{V}_F}{\hat{V}_D} = \frac{Y_{12}}{Y_{11} + Y_{12} + Y_l} \tag{1.9}$$

where Y_l is contributed by the CFT and associated connections in the interface hardware. Plots of the data are expressed in 20 log $\hat{G}$ vs. log frequency for the gain, and in degrees vs. log frequency for the phase.

1.3.4 Interpretation of Gain and Phase Response

From looking at the gain and phase outputs of the model, it is possible to immediately identify features of the response which indicate the properties of the media being modeled. For example, Figure 1.5 is the predicted response of the macro sensor to a uniform bulk medium of oil with a permittivity of $2.2\epsilon_0$ and a conductivity of 1×10^{-9} mhos/m. The gain at high frequency remains level with no relative phase difference. This indicates that the coupling between the electrodes is purely capacitive in this frequency regime. Thus, the "high frequency" response is only a function of the permittivity of the medium: the higher the permittivity, the higher the gain at these frequencies. As the frequency decreases, relaxation effects begin to dominate which is characterized by the excursion in the phase and the $-20dB$ per decade slope of the gain curve as it heads towards $0dB$. When the gain has reached unity and the phase has gone back to zero, it is an indication that the floating gate potential follows the driven gate potential exactly. Essentially, this means that the electrodes have been shorted by the medium. If the conductivity being modeled is outside the limits of the macro sensor, then the gain will either be 0 dB from .005 Hz to 10 kHz with no phase, indicating a short; or the gain will remain constant at some relative gain also with no phase, indicating that no conduction processes are detectable. These curve shapes are very important because the response of all uniform bulk media will have these characteristics. In addition, because of the assumption in the model that conduction processes be linear in the electric field, it is evident that their is a direct correlation between the frequency and the conductivity σ (see Equation 1.2). The consequences of this characteristic behavior is that the gain and phase curves have universal shapes which shift in frequency with the conductivity of the medium. For example, given a bulk frequency response to a material with some permittivity and conductivity, the response to a material with the same permittivity, and a conductivity an order of magnitude greater, would be the same curve but shifted to the right in frequency by a factor of ten. Thus, when interpreting data for a supposed bulk response, it is important to first establish that the predicted curve shapes of the model match the data. Once this is done, it becomes a matter of estimating the permittivity by matching the high frequency gain and determining the conductivity by matching the phase response. The interpretation of frequency responses to heterogeneous media can be approached using this same strategy because of the "universal" shapes that are predicted by the model.

Another characteristic gain and phase response is generated when the medium being modeled incorporates a surface conductivity along the electrode plane with

Fig: B1

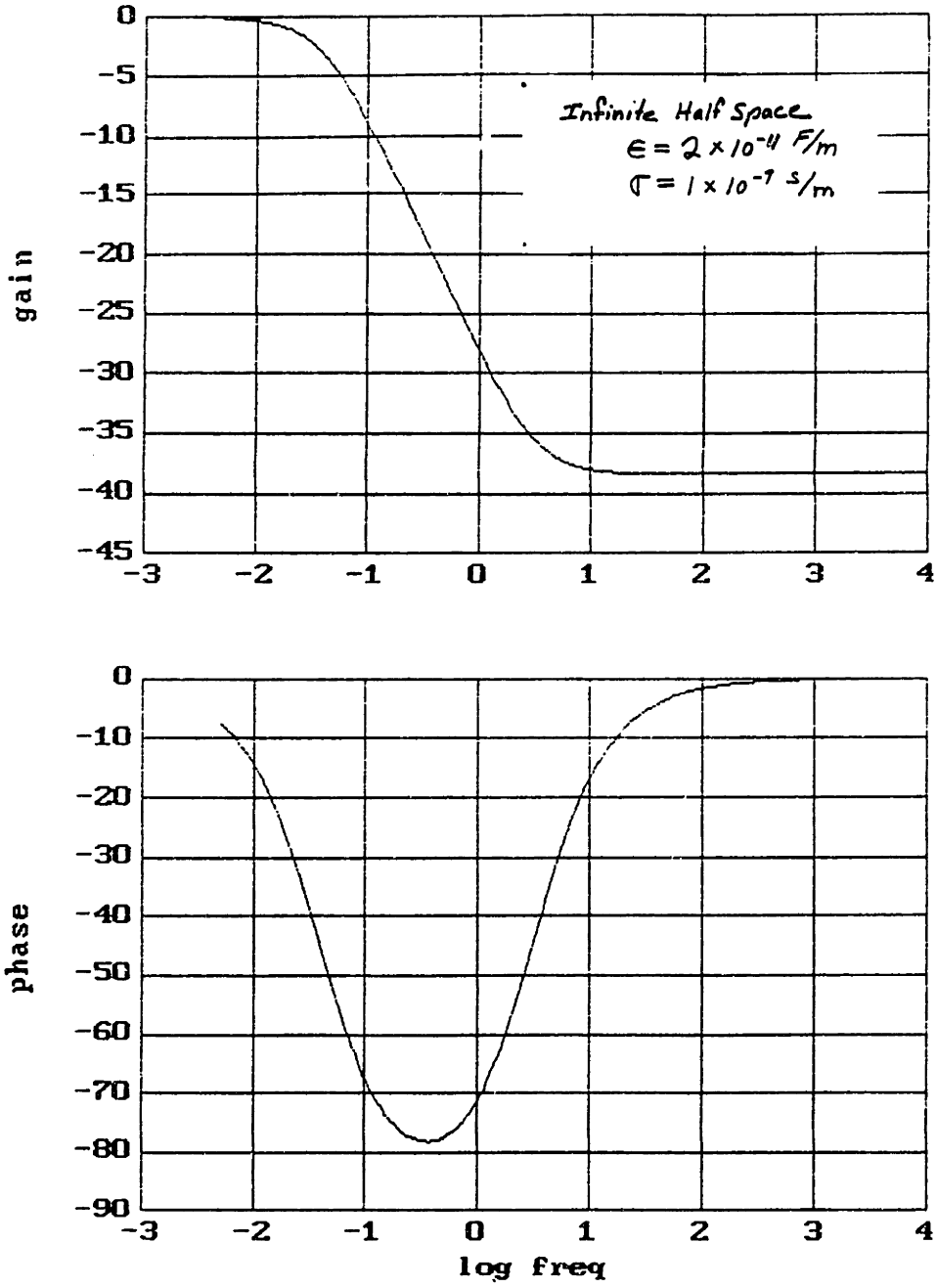

Figure 1.5: Predicted Bulk Response of Macro Sensor

an insulating infinite half space beyond. The frequency response of the macro and micro sensors to this surface conductivity are quite different and thus both will be shown. An explanation for the differences between the two will be presented in the next chapter. The surface response of the micro sensor (Figure 1.6) is characterized by an asymmetric phase curve and the steeper than $-20db$ per decade slope in the gain as it rises towards unity. The resonse of the macro sensor to a surface conductivity is illustrated in Figure 1.7. It's response is much closer to that of a medium with uniform bulk poperties. The only difference occurs in the slight tailing of the high frequency gain and the slightly different transition of the phase curve at high frequencies. The similarity between the "surface" and "bulk" responses makes it difficult to distinguish between the two. Again, both sets of curve shapes are universal and simply scale linearly in frequency with the surface conductivity. If the bulk medium is also conducting, whichever relaxation process has the shorter time constant will be the one that dominates. If the time constants are of the same magnitude, then a mixture of the curve shapes results.

Finally, there are the responses that are obtained when multiple layers are modeled. Figure 1.8 is the model output for a 50 μm layer with permittivity $3\epsilon_0$ and conductivity 1×10^{-12} and an infinite half space (i.e. any layer greater than 300 μm) with the permittivity of oil, $2.2\epsilon_0$, and conductivity 1×10^{-10}. The constant value of the gain at high frequency corresponds to the total capacitance due to the two layers. As the infinite half space becomes conducting at lower frequencies, the gain rises to a value corresponding to the capacitance of the lower layer capped by a perfect conductor. Each of the excursions in the phase curves correspond to the relaxation of charge in each of the layers. If the layer adjoining the electrodes was significantly more conducting than the infinite half space, the response of the dielectrometer would never reflect the relaxation of charge in the infinite half space. This is because once the closest layer becomes conducting, the sensor is essentially shorted, and layers further out no longer have any affect on its response.

With each layer added, an additional time constant reflecting the relaxation of charge in that layer is also added. Consequently, with enough layers given the right permittivities and conductivites, many different gain phase curves can be generated by the model. This is demonstrated in Figure 1.9 which represents an $40\mu m$ layer with a continuous conductivity profile which changes exponentially within the layer. The infinite half space beyond is insulating. The continuous conductivity profile gives essentially an "infinite" number of time constants which tends to smear out the gain and phase curves (see the appendix for details of modeling conductivity profiles). The gain transition is slower than that for the bulk and the phase curve is broader and asymmetric.

The attributes of the frequency response of the gain and phase can indicate a lot about the medium being measured without resorting to fitting exact parameters to a model. The lossless high frequency gain will always reflect the total capacitance of the medium being measured, and the number of phase excursions is an indication of the number of different conduction processes observed over the frequency range of the microdielectrometer. Also, the shapes of the gain and phase responses can point to a medium that is dispersive. A medium is suspected of being dispersive when

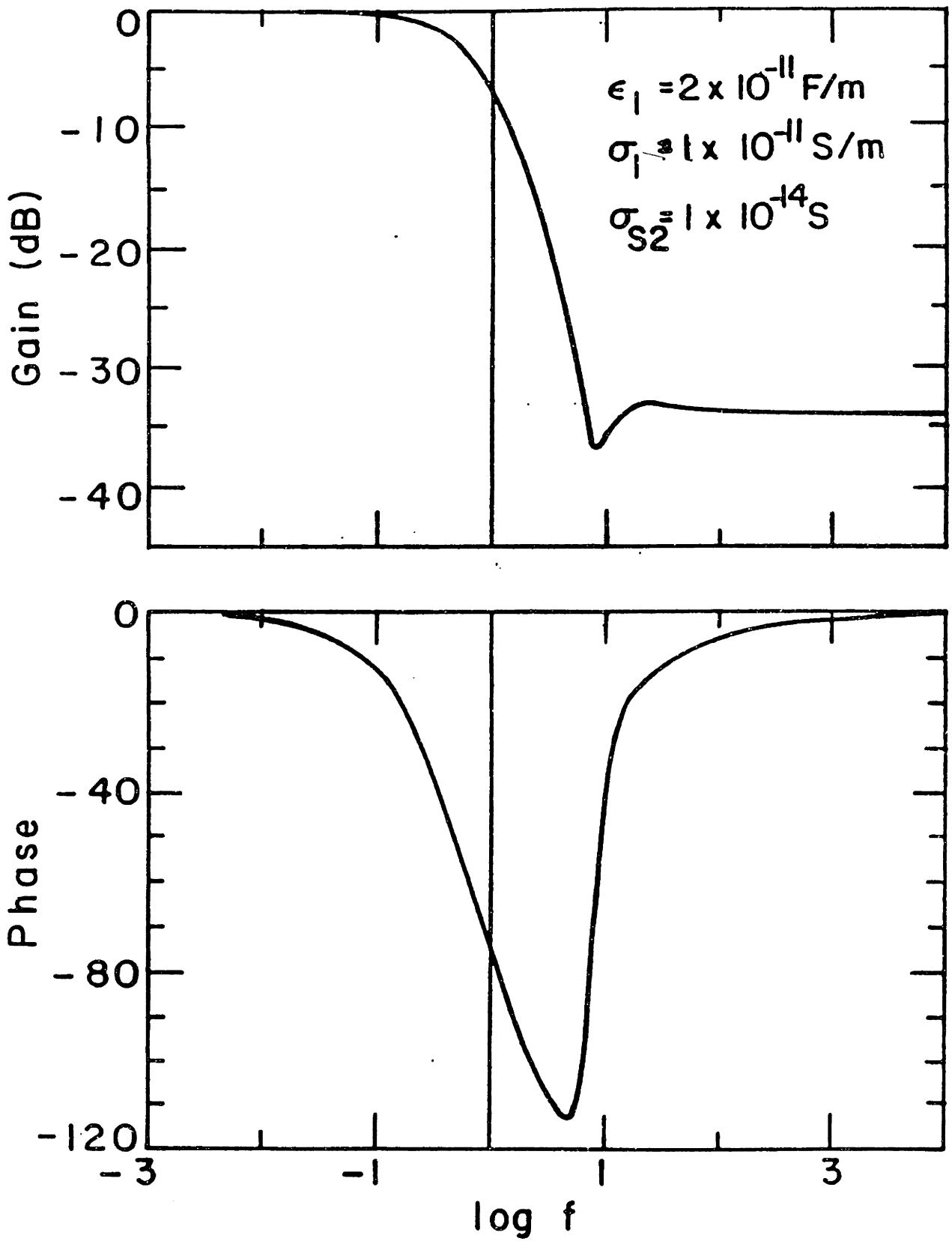

Figure 1.6: Predicted Response to Surface Conductivity: Micro Sensor (reprinted from [25])

Fig:surf

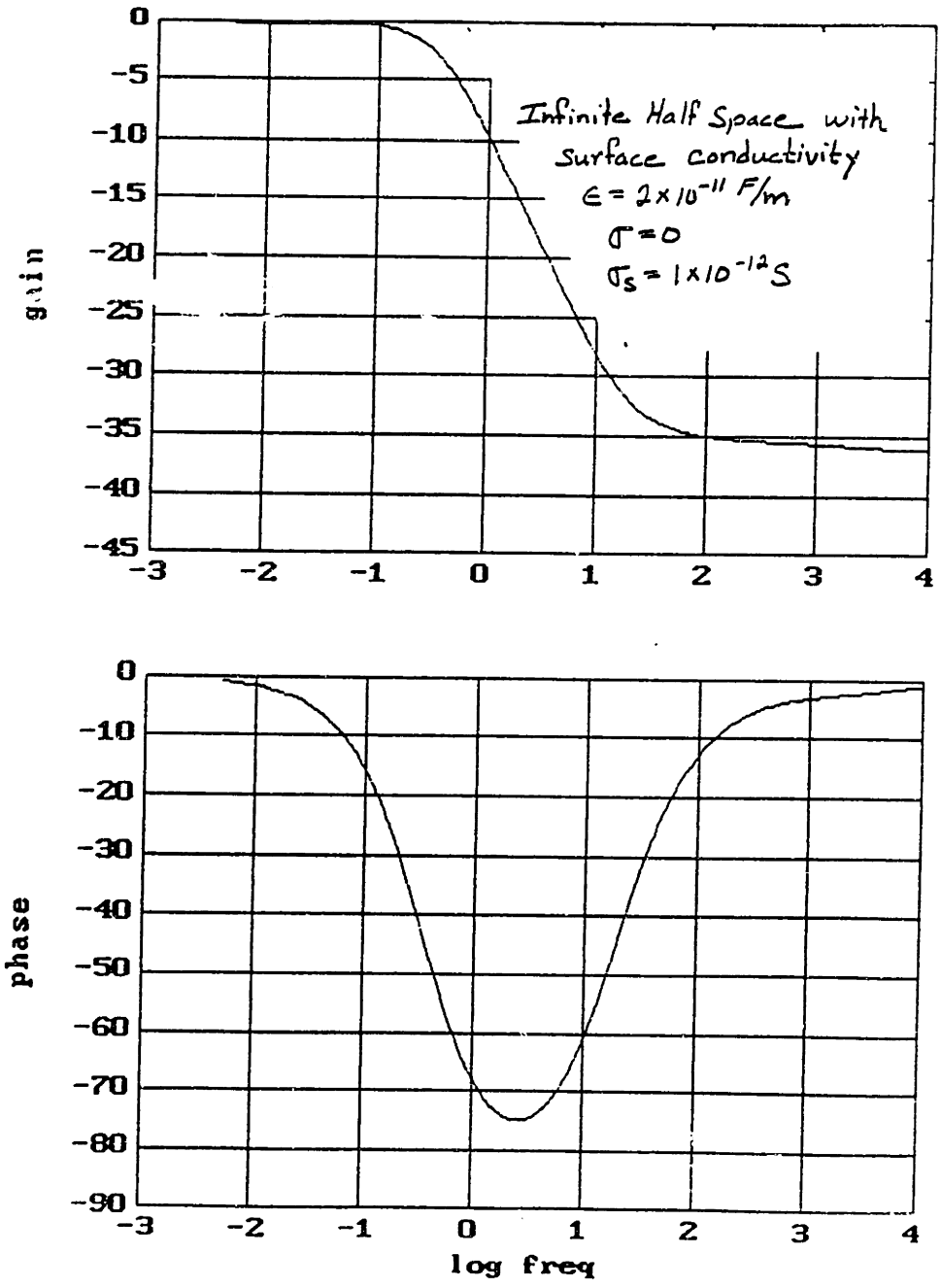

Figure 1.7: Predicted Response to Surface Conductivity: Macro Sensor

Fig: two

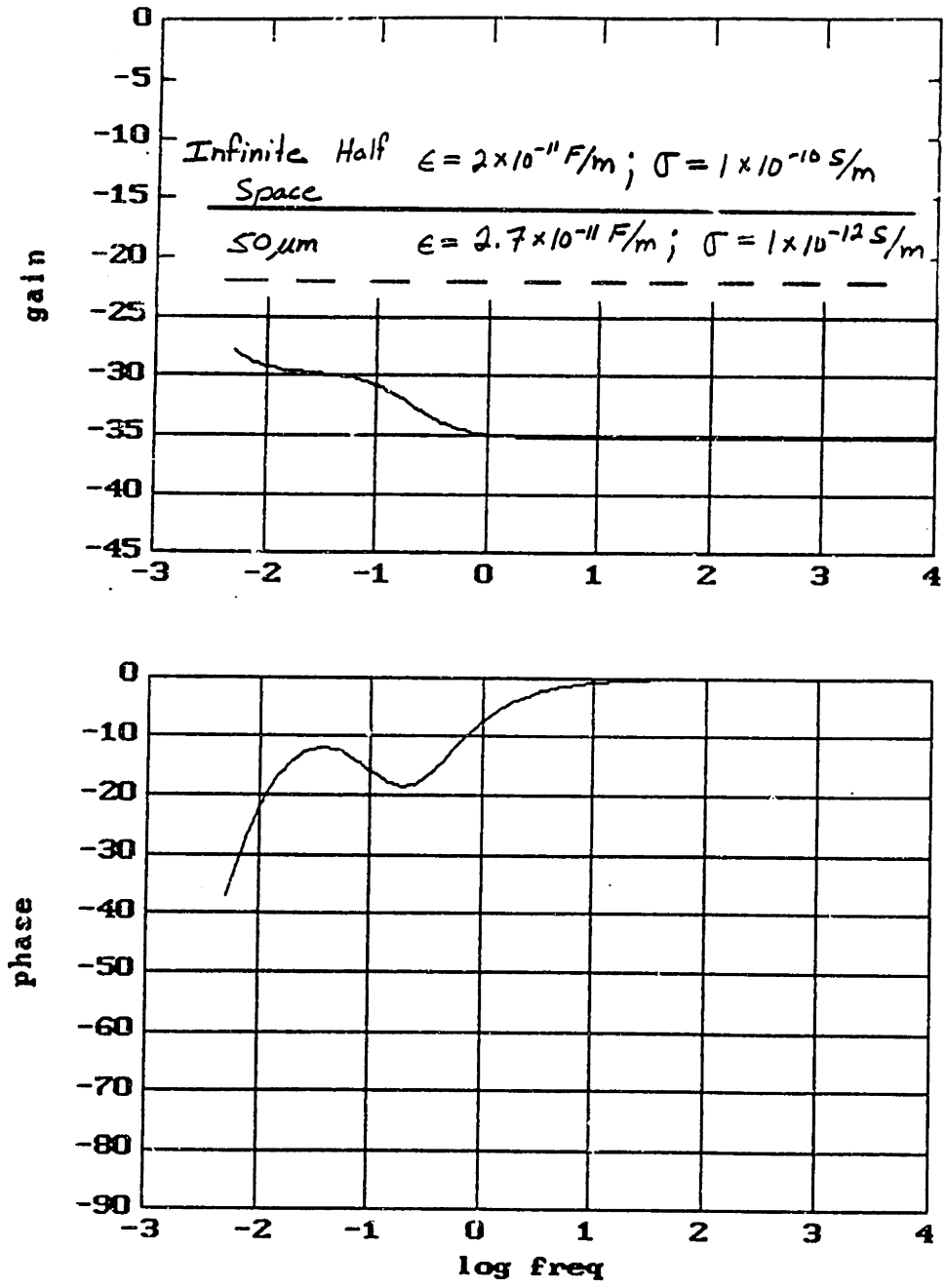

Figure 1.8: Predicted Response of Two Layers each with a Different Conductivity

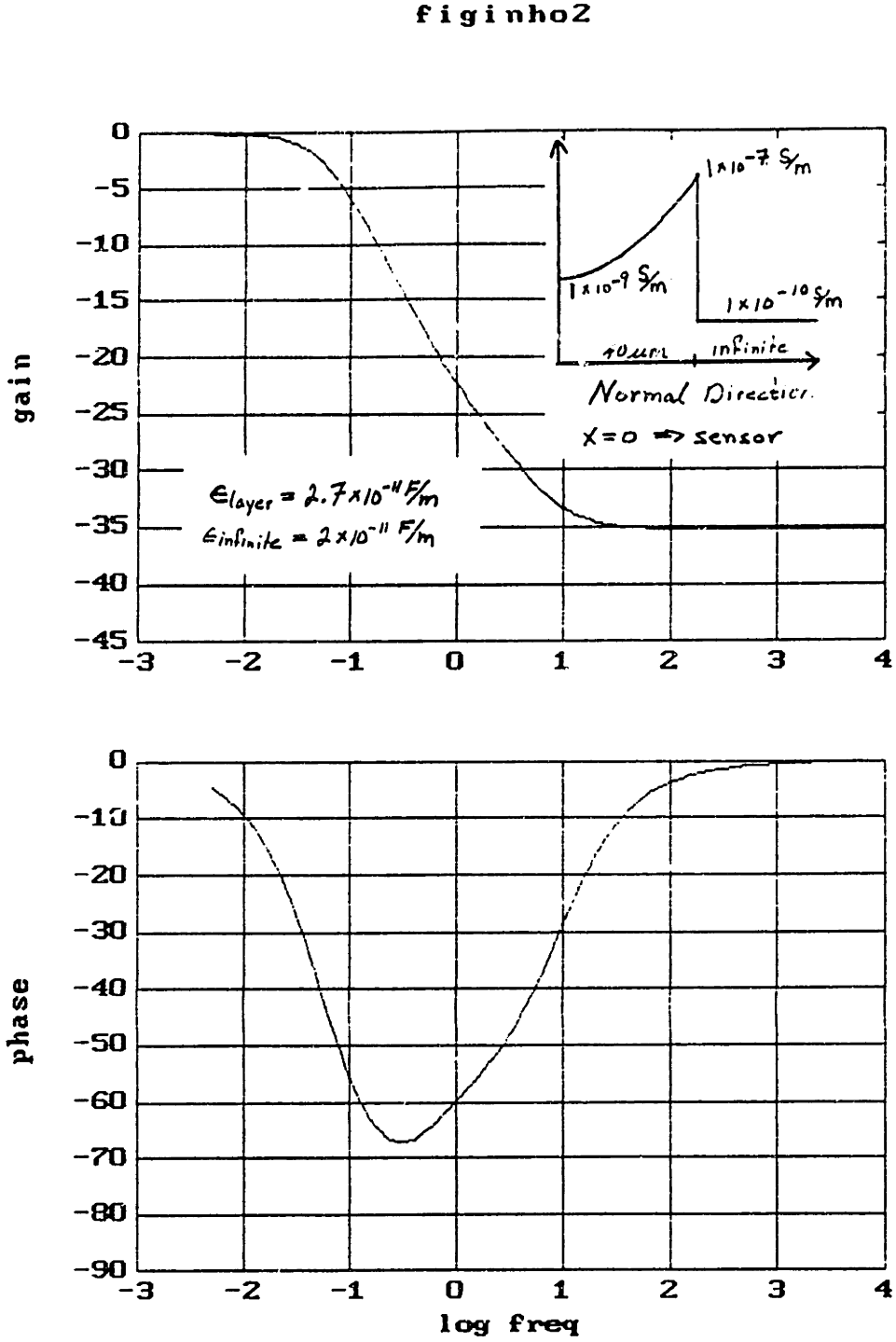

Figure 1.9: Response of Layer with Conductivity Profile

observed gain transitions are less than -20dB per decade, and phase responses are very "broad". Such a response cannot be attributed to a medium with uniform bulk properties. The only possiblilites are that it has spatially varying properties, or that it is dispersive. The problem of identifying the correct mechanism is often resolved from knowledge about the medium being measured. If it is known to be uniform in structure, then it is likely that dielectric dispersions are responsible for the non bulk-like response. The interpretation of gain and phase responses for dispersive medium then becomes an entirely different problem. The model assumption that the permittivty and conductivity are frequency independent is no longer valid. However, using the model, the dispersion in ϵ and σ for a material can be found by estimating, from the gain and phase, the bulk permittivity and conductivity at each frequency. Once the dispersion of the complex permittivity has been estimated, an attempt can be made to match it to models of dispersion phenomena.

The continuum model is consequently very flexible. It is able to model surface effects at boundaries, many layers each with different dielectric properties, or any other configuration that can be expressed as a surface capacitance density (see appendix). In addition, using parameter estimation schemes developed by Zaretsky, properties such as the complex dielectric constant and thickness of a thin film can be deduced. A more detailed description of the sensor, the continuum model, and its capablilites can be found in the following report: *Modal Approach to Obtaining Continuum Properties from Interdigital Electrode Dielectrometry* LEES Report TR86-019 [25]. The continuum model will be used to interpret data taken with the macro sensor.

Microdielectrometry fits into a more general category of problems known as "imposed ω-k" sensing. It is a technique where the temporal information is determined by the frequency of the applied sinusoidal signal ω, and the spatial information determined by the periodicity $\lambda = 2\pi/k$ of the electrode structure. This suggests that information can be obtained by changing either the temporal or spatial frequency of the device. Control of the temporal frequency is important for looking at relaxation phenomena in the media adjacent to the electrodes. Control over the spatial wavelength, on the other hand, determines the depth to which the electric fields generated by the electrodes decay into the material being probed. Consequently, property gradients in materials can be measured using a strategy where measurements are taken at different spatial wavelengths [26]. This method could be used, for example, to determine whether a "smeared" gain and phase response is due to inhomogeneities or frequency dispersions in the material. This technique is not restricted to just electrical sensing. Analogs include a magnetoquasistatic device, a thermal device, and a mechanical one.

Chapter 2

Development and Qualification of Prototype Sensor

2.1 Hardware Development for Low Frequency Measurements

The main unit of the microdielectrometer is a micro-computer based box which can be located at relatively great distances (30 ft) from the buffer/interface electronics which drive the sensor [27]. It synthesizes the driven signal and performs the analysis on the buffered response of the sensor. This piece of equipment remains constant with the use of different length scale sensors. The buffer/interface electronics, on the other hand, must be located within a foot of the sensor and is tailored individually for the macro and micro versions of the sensor. It basically buffers the drive signal and allows for a high impedance measurement of the floating gate potential.

2.1.1 Development of Interface Circuitry

The macro sensor (λ =1mm) and one version of its interface electronics is commercially available from Micromet Instruments [27]. It was originally designed for dielectric measurements of materials heated to temperatures up to 500°C. To meet these high temperature requirements, the sensor is constructed of aluminum oxide and palladium silver alloy. The palladium forms the electrode structure and ground plane which sandwich a 250μm layer of insulating aluminum oxide ($\epsilon_0 = 9.8$). The electrodes are deposited on the aluminum oxide such that its width is essentially the same as the interelectrode spacing. This entire assembly is then mounted on another thicker piece of aluminum oxide for structural strength. There are currently two versions of the macro sensor that are basically identical except for electrode geometry (see Figures 3.1 and 3.2). The effects of these different electrode layouts will be discussed later in this chapter.

The "listening" electrode, as previously described, is connected to the floating gate of a CFT, and the potential measured by using a feedback circuit utilizing an FET which is matched to the charge flow transistor (see Figure 2.1). In constructing

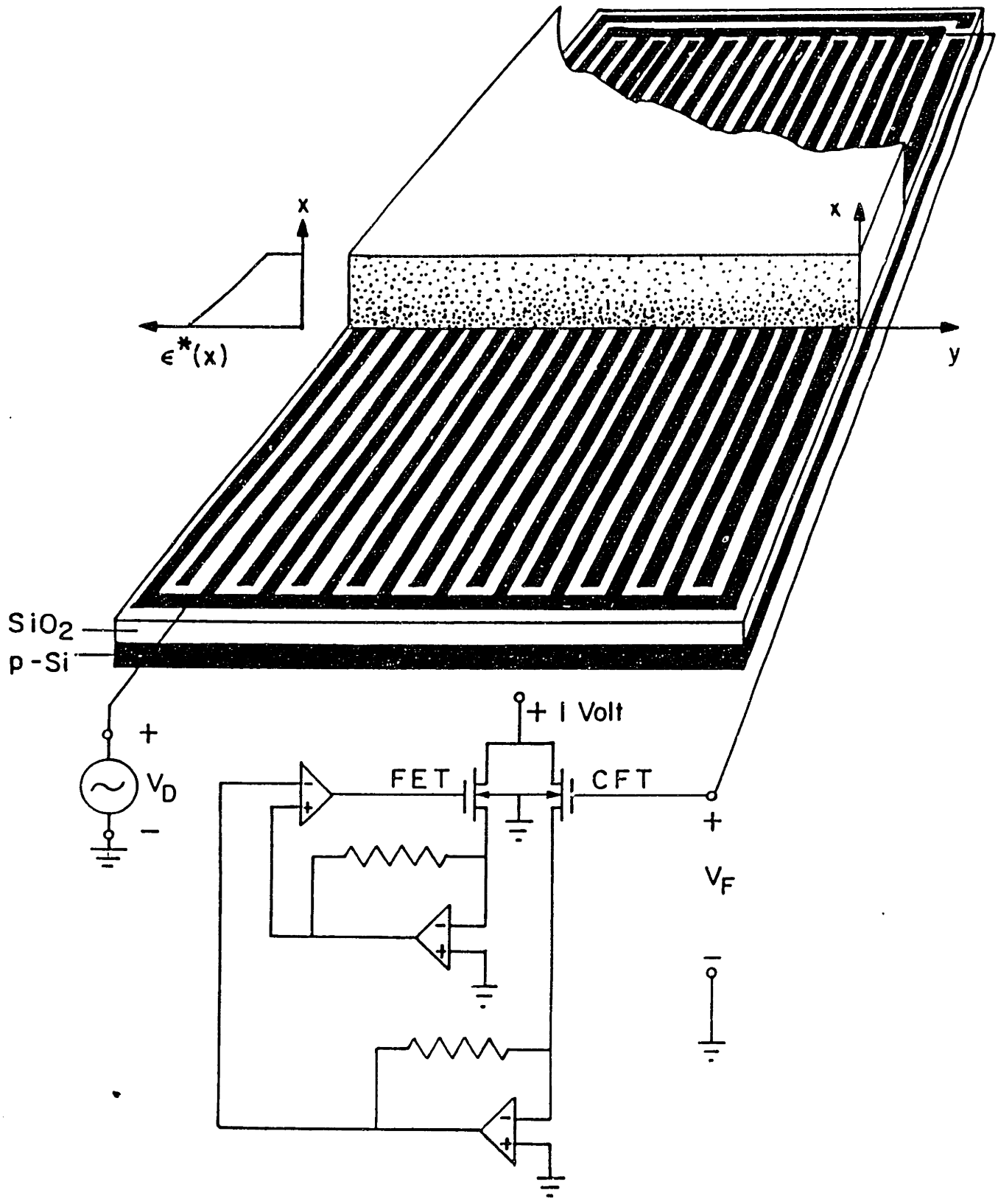

Figure 2.1: Feedback Circuit to Measure Floating Potential (reprinted from [25])

the micro sensor, these two transistors are microfabricated side by side upon the same substrate as the electrodes. Hence, they should have the same characteristics and respond to environmental changes in similar ways so that such effects can be ignored. The macro sensor, on the other hand, due to its high temperature operating requirements and fabrication limitations, makes placing a pair of transistors on the electrode substrate impractical. Thus, some other strategy is required where all the electronics are separate from the macro sensor.

The interface "box" that is commercially available for the macro sensor is limited to operating between 1 Hz and 10 kHz. Measurements taken below 1 Hz with this interface box produces erroneous data. Frequency responses taken in air, for example, exhibit positive phase excursions and a gain that begins to decrease at frequencies below a hertz. This is clearly not a response attributable to air. For an insulator such as air, zero phase and a flat gain are expected because only a capacitance should be reflected in the frequency response. This anomalous behavior is due to the electronics and is attributed to leakage currents coupling from the ground plane node to the floating gate node in the interface box. Figure 2.2 presents data over the entire frequency range of the microdielectrometer with a chip in air using the commercially available interface box.

The commercially available interface box does not use the high impedance measurement strategy which incorporates a matched set of transistors. The leakage current between the floating and ground nodes is due to conduction at low frequencies through two zener diodes which make up an integral part of the measurement circuit. This current, which begins to dominate the frequency response below 1 Hz, makes it difficult to detect charge relaxation effects in transformer oil which are not visible until much lower frequencies. It may be possible to accomodate these effects in the model by including a conductive component in the load capacitance (Y_l complex) of the pi network, but it would represent an extra process that would have to be modeled without contributing any information to the measurement of the desired material. Thus, the development of a new interface box capable of operating at the lower frequencies, free of the effects due to leakage currents, became a high priority objective. The key to successful measurements at these frequencies then depends upon the ability to make a high impedance measurement.

A prototype interface box was developed with help from Micromet Instruments. This new interface circuitry incorporates the matched transistors of the micro sensor which allows the high impedance measurement strategy to be utilized. To use the transistors of the micro sensor, its driven and listening electrodes were shorted and the listening electrode of the macro sensor connected to the driven electrode node on the micro sensor. To short the electrodes of the micro sensor, a sharp instrument was used to scratch the electrode surface. This effectively allows the listening electrode of the macro sensor to be connected directly to the charge flow transistor on the micro sensor. Once this is accomplished, a feedback circuit similar to the one in the micro sensor interface box can be used to measure the potential of the floating electrode for the macro sensor.

The potential problem with this strategy involves practical considerations such as leakage currents through the substrate of the circuit board between the floating

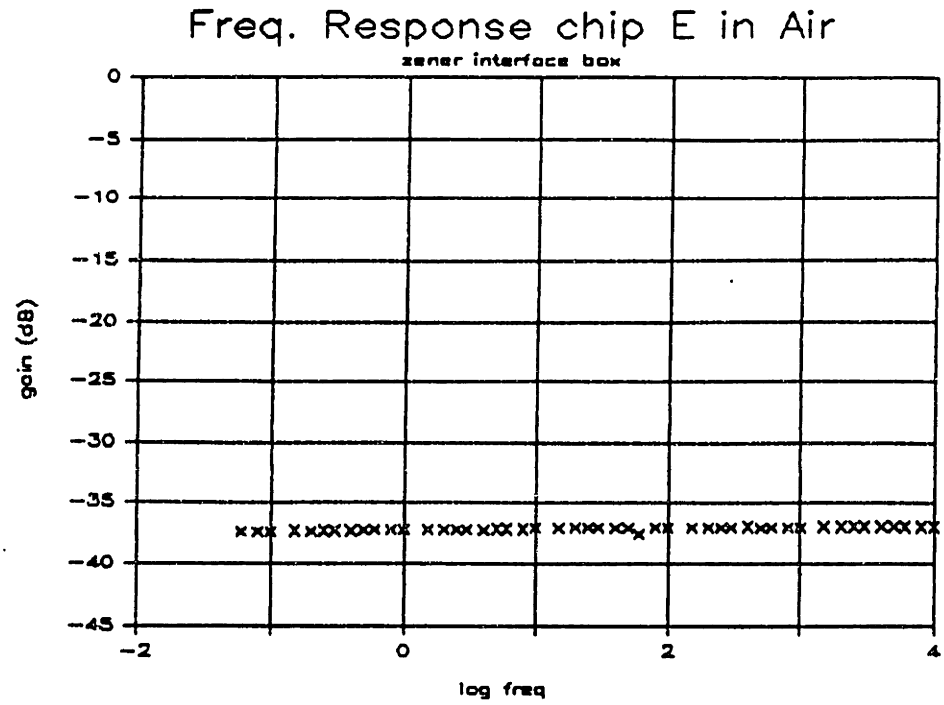

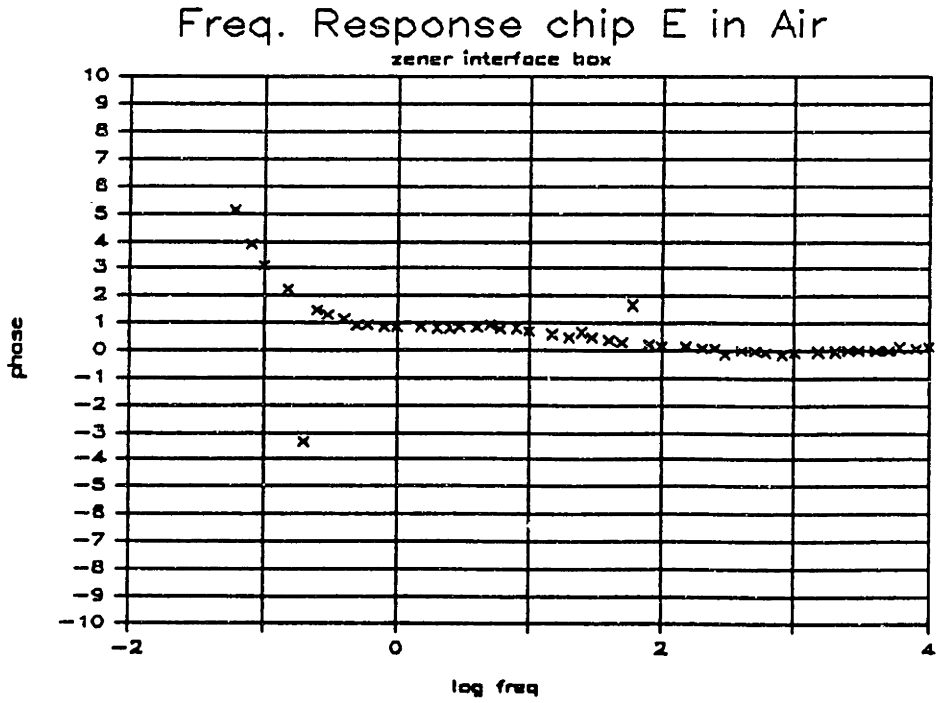

Figure 2.2: Effect of Leakage Current from Floating to Ground Node

and ground nodes, and stray capacitances due to leads that must be used to bring the signal from the macro sensor to the micro fabricated transistors now located in the interface box. This was not a problem with the micro sensor because the transistors were on the electrode plane and were designed with short leads that were well isolated. The first macro sensor interface circuit that was assembled, for example, was done on a normal printed circuit board. The circuit did not perform as desired at low frequencies because of leakage currents through, or along the surface of, the substrate material. Subsequent circuits were assembled on substrates that were known to be very insulating (such as teflon). Measurements taken with these interface boxes for macro sensors in air behaved satisfactorily from .005 Hz to 10 kHz.

Another potential problem to be aware of is that the matched transistors on the micro sensor are sensitive and can be damaged by static electrical discharges. When this occurs, measurements become completely meaningless and the shorted micro-sensor in the interface box must be replaced. Awareness of these practical considerations and precautions can facillitate the use of the macro sensor in a proper mode of operation and provide insight as to when it has failed.

2.1.2 Offset Voltage

Another feature of the microdielectrometer is its ability to extract the relative d.c. offset of the floating to the driven electrode. This is possible through the signal processing that is performed on the received signal when extracting the gain and phase. This offset can be due to the accumulation of charge on the floating electrode, or electro-chemical processes that affect the d.c. potential at the electrode interface. In any case, when the magnitude of the d.c. potential is above a few hundred millivolts, or if the offset is changing fairly rapidly (more than 5 millivolts from measurement to measurement), then the gain and phase measurements are suspect. A high constant offset will give a high frequency gain value that will be slightly different from a zero offset high frequency measurement. The reason for this effect is not clear, but it has been suggested that it might be caused by the mismatching of the transistors due to having an operating point that differs from the design value. Changing the operating point, however, does not seem to affect the phase information. If the offset is changing rapidly from measurement to measurement, then the gain and phase curves can become somewhat distorted. When this happens, repeated measurements should be taken until the offset has settled and reached some reasonable value. If the offset becomes too high (greater than a 1 volt), the measurements can become altogether meaningless.

One of the consequences of using a high impedance measurement is that once charge accumulates on the floating electrode, it takes a very long time for it to discharge. It would be convenient if the offset could be reset by the user. This is possible when using the macro sensor because the floating and driven nodes (i.e. before the matched transistors) are accessible in the interface box. Shorting these two nodes briefly is sufficient for removing charge accumulated on the floating electrode. The micro sensor, however, can not be reset in this manner because the

relevant nodes are micro-fabricated on the electrode substrate and are consequently inaccessible. The ability to reset the offset is important to maintaining a high confidence level when making measurements, and in cases where the sensor "fails" due to the excessive offset, it becomes a necessity.

2.2 Predicted Responses vs. Data

In this section, the predicted responses of the model are tested against the high frequency data obtained from both versions of the macro sensor. In the process of interpreting the data, the effects of the physical parameters of the sensor are explored and the model expanded and calibrated to allow accurate predictions of the behavior of either version of the macro sensor.

2.2.1 The Load Capacitance

Once the physical parameters describing the macro sensor have been entered into the model, the only missing piece of information necessary for predicting sensor responses is the appropriate load capacitance Y_l. The load capacitance primarily reflects a capacitor placed across the floating and ground node used to bring the gain into a certain operating range when taking measurements in air. It also incorporates any other capacitances between these two nodes such as the coupling that may occur between the leads bringing the signal to the interface box. Consequently, this value can be hard to evaluate and is generally determined by chosing a value which allows the model to predict the actual gain that is measured by the sensor in air. A typical capacitance might be C=2200 pF corresponding to a normalized dimensionless value of 57 ($Y_l = C/[\epsilon_{ox}(meanderlength)/2]$). The meander length used to normalize the load capacitance is a measurement of the total distance over which interelectrode coupling occurs. For the comb structure macro sensor, the meander length is approximately 100 cm; and for the "spine" electrode structure sensor, the meander length is approximately 85 cm. As pointed out before, the meander length is not used to determine the load capacitance used in the model, but is a good check to determine if the values used are reasonable.

2.2.2 Modeling Issues

Once the load capacitance was chosen to obtain a match in predicted response to actual response for the macro sensor in air, a correlation was attempted using these parameters for the predicted to actual high frequency response of the sensor in oil. Initial tests were done at high frequency (10 kHz) to allow measurement of only the capacitive coupling. Using the known physical dimensions and properties of the macro sensor, the model predicted a greater change in the high frequency gain in going from air to oil than was actually observed. In other words, the sensitivity of the macro sensor was less than predicted.

The sensitivity of the macro sensor is determined by the relative coupling of fields through the media being measured and coupling of fields through the oxide layer. In an extreme situation where most of the interelectrode admittance (Y_{12}) is due to coupling of the electric field through the insulating oxide layer, the device becomes insensitive to the properties of the material above simply because very little of the coupling is occuring through this region. Consequently, changing the permittivity of the adjacent material in such a scenario has very little effect upon the gain of the device. In terms of the Y parameters, the change in gain of measuring one material compared to another is determined by the sensitivity of Y_{12} to the permittivity of that material. Y_{12} can be thought of as two capacitances in parallel, one reflecting the coupling through the media above (C_{above}), and the other reflecting the coupling through the oxide layer below (C_{below}). The sensitivity of Y_{12} to changes in the permittivity of the material above is determined by the percentage change in C_{above} and C_{below}, and also by their relative magnitudes. It is reasonable to assume that C_{above} will change much more than C_{below} because the oxide layer below is partially shielded by the electrode structure to changes above. Thus, if it is assumed that changes in the total interelectrode coupling (Y_{12}) are due essentially to changes in C_{above}, then the larger C_{below} becomes, the less sensitive the overall capacitance is to changes in C_{above}. In other words, the percentage change of $X + \Delta x$ due to Δx is greater than the percentage change in $X + \Delta x + K$ where the larger K is, the smaller the overall effect that Δx has upon the total. The assumption is that K is not a function of x, which in the context of this problem is the same as saying that changes in C_{above} have no effect upon C_{below}. Strictly speaking, this is not true. Changes in the field distribution above will manifest themselves in the field distribution below through the matching of boundary conditions in the interelectrode regions. However the approximation should be a reasonable one. Although the argument presented is not analytically useful, it does provide some insight into the factors affecting the sensitivity of the macro sensor.

Consequently, to reduce the sensitivity predicted by the model, a higher C_{below} is needed. To understand how the physical parameters affect this admittance, it is helpful to refer to Figure 1.4. Increasing the oxide layer thickness and increasing the permittivity of the oxide layer have the effect of enhancing the coupling that occurs through the oxide layer. The effects of increasing the permittivity of the oxide layer will clearly increase the capacitive coupling through that region. Increasing the thickness of the oxide layer allows for better coupling of the electric field between the electrodes through the oxide layer because the ground plane has a decreasing influence upon the field distribution. If the ground plane were very close to the electrodes, then most of the coupling in the oxide layer would be electrode to ground and the interelectrode capacitance would be very small. Changing these parameters is assumed to have a relatively small effect upon the sensitivity of C_{above} to the material above. Thus, the decrease in the sensitivity of the sensor is due to the proportionately smaller contribution of the capacitance above, which reflects the properties of the material being measured, when the capacitance through the oxide layer below is increased.

Decreasing the interelectrode spacing in the model also has the effect of decreas-

ing the predicted sensitivity of the device when the permittivity below is greater than the permittivity above. In this case, the coupling through the oxide layer below must increase significantly more than the sensitiviy of C_{above} to the material above. It is, in this case, less obvious as to why the sensitivity of Y_{12} should change. All three parameters have been found through modeling work to directly affect the sensitivity of the macro sensor to changes in the permittivity of the measured medium.

The predicted change in the gain when comparing high frequency measurements of air to oil decreases when these physical parameters are altered as described. Thus, it is possible to match the sensitivity exhibited by the macro sensor with the predicted response of the model by changing one or a combination of these physical parameters. In addition, many different physical configurations have been found which are able to match the actual response of the sensor. The high frequency gain response of a macro sensor with the "spine" electrode structure to bulk phenomenon is tabulated in Table 2.1. This data is compared with predicted responses generated from actual physical parameters, and parameters compensated to match the high frequency gain response in both air and oil. Then, using the compensated parameters, the permittivity of an epoxy resin is estimated from its high frequency gain and compared to the micro sensor measurement of $9.6\epsilon_0$. The predictions using the compensated parameters are quite good. Thus, the problem becomes a question of why the predicted admittances are incorrect and how to develop a physically reasonable method to compensate for these errors. Changing known physical parameters isn't acceptable. Altering the thickness of the insulating oxide layer, for example, can affect the macro sensors response to surface conduction processes (see Chapter 2.3). However, the influence of these phsyical parameters on the calculated model admittances does suggest other possible explanations.

The same continuum model is used to characterize both the micro and macro sensors with appropriate inputs for the physical parameters. The modeling of the two different interdigitated electrode geometry macro sensors is done in exactly the same manner. However, the actual outputs of these two macro sensors are somewhat different and neither one's response is accurately predicted by the model using the actual physical parameters which are the same for both sensors. The macro sensor with the comb structure geometry (Figure 1.2) is closer to the model's predicted response and will be analyzed first.

An indicator of what the problem might be can be found from looking at the micro sensor's behavior, which is predicted very accurately by the model. The primary difference between the comb structure macro sensor and the micro sensor is the difference in the electrode surface area (normalized to each sensors wavelength) and the measurement electronics used for each sensor. The dimensions of the micro sensor are roughly 2 mm by 3 mm with the electrodes running the longer dimension and 2 cm by 2 cm for the macro sensor. This translates to an area of 40λ by 60λ for the micro sensor and an area of 20λ by 20λ for the macro sensor. Hence, the macro sensor has proportionately much less surface area where the electrodes are parallel and interdigitated. Thus, the fringing of fields at the edges would have a proportionately greater effect upon the macro sensor than the micro sensor.

High Frequency (10 kHz) Macro Sensor (spine electrode structure)

Measurements of Air, Oil, and Epoxy Resin

Data: (g = 20 log G, all measurements have zero phase)

	Air	Oil	Epoxy
g =	-37.1 dB	-35.6 dB	-29.63 dB
ϵ =	ϵ_0	$2.2\,\epsilon_0$	$9.6\,\epsilon_0$

(ϵ known for air and oil; ϵ_{epoxy} from micro sensor)

Predicted Model Responses

1) Actual Physical Parameters

oxide layer thickness: $\frac{\lambda}{4h} = 0.88$,

interelectrode spacing: $a = 0.2\,\lambda$,

oxide layer permittivity: $\epsilon_{ox} = 8.68 \times 10^{-11}$

Predicted Permittivities:

$\epsilon_{air} = \epsilon_0$; $\epsilon_{oil} = 1.7\epsilon_0$; $\epsilon_{epoxy} = 7.36\,\epsilon_0$

2) $\frac{\lambda}{4h} = 0.60$, $a = 0.2\,\lambda$, $\epsilon_{ox} = 8.68 \times 10^{-11}$

Predicted Permittivities:

$\epsilon_{air} = \epsilon_0$; $\epsilon_{oil} = 2.2\epsilon_0$; $\epsilon_{epoxy} = 9.8\,\epsilon_0$

3) $\frac{\lambda}{4h} = 0.85$, $a = 0.1\,\lambda$, $\epsilon_{ox} = 8.68 \times 10^{-11}$

Predicted Permittivities.

$\epsilon_{air} = \epsilon_0$; $\epsilon_{oil} = 2.2\epsilon_0$, $\epsilon_{epoxy} = 9.6\,\epsilon_0$

4) $\frac{\lambda}{4h} = 0.80$, $a = 0.2\,\lambda$, $\epsilon_{ox} = 1.11 \times 10^{-10}$

Predicted Permittivities:

$\epsilon_{air} = \epsilon_0$; $\epsilon_{oil} = 2.2\epsilon_0$; $\epsilon_{epoxy} = 9.8\,\epsilon_0$

Table 2.1: Changes in Predicted Response as Parameters are Varied

The analysis performed in developing the model assumes an infinite interdigitated electrode structure. Consequently, the lesser dimension of the macro sensor, which increases the importance of fringing effects at the edges, may account for some of the discrepancy between predicted and measured response.

The difference in the measurement circuitry between the micro and macro sensors may also help explain the model's inaccuracy. One of the consequences of moving the pair of matched transistors from the sensor's electrode substrate to the interface box was the increase in the length of the leads for the floating, driven, and ground signals between the sensor and the interface box. Hence, there is a contribution to the Y parameters due to the capacitance associated with these wires. In all the measurements that are presented, the wires from the sensor to the interface box are unshielded and kept relatively far apart (on the order of 5 cm) with a total length of around 30 cm.

A test for the significance of these capacitances can be performed by simply twisting a pair of signal wires to maximize the capacitive coupling between the two. It was found that there were no appreciable changes in the sensitivity of the sensor when twisting either the driven and ground signal wire, or the floating and ground signal wire. These correspond, respectively, to Y_{11} - the driven electrode to ground capacitance, and Y_l - the floating electrode to ground capacitance. In each case, the changes in these quantities are very small compared to the original load capacitance and thus have negligible effects upon the gain. The sensitivity is determined solely by how much Y_{12} changes when measuring materials of different permittivities. Thus, twisting the floating and driven electrodes has an enormous effect upon the high frequency gain response of the sensor. This capacitive coupling can be considered as part of C_{below} because it is independent of the properties of the measured material. Thus, the overall effect of changes in the coupling above, reflected by C_{above}, is diminished. This corresponds to a smaller change in the high frequency gain for a given change in the permittivity of the adjacent material.

These experiments suggest that an additional Y parameter be added in parallel with Y_{12} to reflect any interelectrode coupling that is not a function of the permittivity of the measured material (see Figure 2.3). Incorporating this extra admittance allows the use of the actual physical parameters of the sensor and still enable the model to predict the behavior of the macro sensor. This is done by taking a measurement in air and a measurement in oil ($\epsilon = 2.2\epsilon_0$) and solving for for the compensating capacitance (x) and the load capacitance (Y_l) in the following equations:

$$G^{air} = \frac{Y_{12}^{air} + x}{Y_{11}^{air} + Y_{12}^{air} + Y_l} \tag{2.1}$$

$$G^{oil} = \frac{Y_{12}^{oil} + x}{Y_{11}^{oil} + Y_{12}^{oil} + Y_l} \tag{2.2}$$

Typical measurements made by both versions of the macro sensor are tabulated in Table 2.2 along with the model generated Y parameters for each scenario and resultant calculation of the load capacitance and the compensation capacitance. It

Compensation Capacitance (x) for Comb and Spine Electrode Structure Macro Sensors

Data: (High frequency gain in air, oil, epoxy resin; zero phase)

A) ⇒ Comb electrode structure macro sensor

$$\frac{\lambda}{4h} = 0.88 \; ; \; a = 0.25\lambda \; ; \; \epsilon_{ox} = 8.68 \times 10^{-11}$$

B) ⇒ Spine electrode structure macro sensor

$$\frac{\lambda}{4h} = 0.88 \; ; \; a = 0.20\lambda \; ; \; \epsilon_{ox} = 8.68 \times 10^{-11}$$

	air	oil	epoxy resin
A)	-42.9 dB	-41.0 dB	-33.5 dB
B)	-37.1 dB	-35.6 dB	-29.6 dB

Precicted Parameters in Air and Oil

A) Air: $Y_{11} = 1.43$; $Y_{12} = 0.38$

Oil: $Y_{11} = 1.45$; $Y_{12} = 0.48$

B) Air: $Y_{11} = 1.53$; $Y_{12} = 0.50$

Oil: $Y_{11} = 1.54$; $Y_{12} = 0.63$

Calculate Compensation Capacitance (x) and Load Capacitance Y_1 using Equations 2.1 and 2.2.

A) $x = 0.0485$; $Y_1 = 57.93$

B) $x = 0.157$; $Y_1 = 45.08$

Estimated Permittivities with and without Compensation

A) $x=0, Y_1 = 51.37$

$e_{air} = e_0$; $e_{oil} = 2e_0$; $e_{epoxy} = 9.1e_0$

$x=0.0485$; $Y_1 = 57.93$

$e_{air} = e_0$; $e_{oil} = 2.2e_0$; $e_{epoxy} = 9.9e_0$

B) $x=0, Y_1 = 40.3$

$e_{air} = e_0$; $e_{oil} = 1.7e_0$; $e_{epoxy} = 7.36e_0$

$x=0.175, Y_1 = 45.08$

$e_{air} = e_0$; $e_{oil} = 2.2e_0$; $e_{epoxy} = 9.4e_0$

Table 2.2: Macro Sensor Performance: Version 1 vs. Version 2

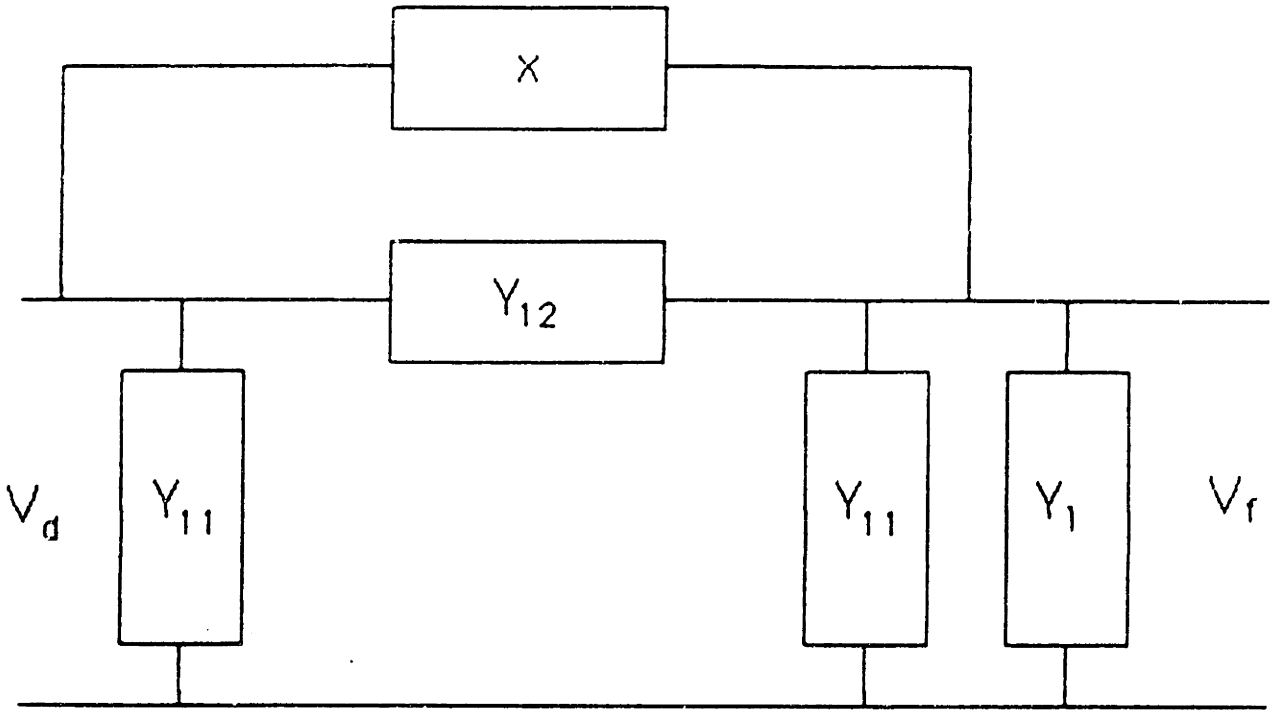

Figure 2.3: Modified Pi Network

was found that the comb structure macro sensor required a smaller compensation capacitance x than the the spine structure macro sensor. It is not obvious why this should be so except that the comb structure macro sensor more closely matches the assumptions made in developing the model. The bus down the middle of the spine structure sensor creates more corners which are not accounted for in the model. Since the sensors are otherwise identical, it is reasonable to attribute the difference in responses to the extra fringing produced by the second sensor.

A rough calculation can be done to determine the capacitance due to the leads for the driven and floating signals. The capacitance of two parallel wires in free space with radius $R = 0.5$mm, separated by a distance $l = 5$cm, and length $d = 30$cm is given by [28]

$$C = \frac{\pi \epsilon_0 d}{ln(l/R)} \tag{2.3}$$

which gives a capacitance of 1.8×10^{-12} Farads. This calculation would be an upper bound on the value of this capacitance because the wires, in general, are much farther apart and are not parallel. To compare this value to the compensation capacitance x, it is necessary to normalize it in the same manner as the load capacitance ($C_n = C/[\epsilon_{ox} meanderlength/2]$). This gives a value of 0.042, which is comparable to the compensation capacitance x calculated for the comb structure macro sensor.

An attempt was also made to shield the leads of the driven and floating electrode signals from each other by placing a grounded shell around each of these wires. This

grounded shell increased the electrode to ground capacitance which changed the gain levels measured, but had basically no effect upon the sensitivity of the sensor. This experiment would seem to indicate that the capacitive contribution of the leads to the interelectrode capacitance is negligible when they are kept far apart. If this is true, then it might be an indication that the fringing fields are responsible for the compensation capacitance that is needed in the model. However, it is difficult to predict what the effects should be when the coupling of the driven and floating electrodes to ground is increased, so that this test may not be very conclusive.

The final test of the model's ability to predict the high frequency gain as a function of permittivity is a comparison of predicted to measured gain for an epoxy compound with a permittivity of $\epsilon = 9.6\epsilon_0$. Table 4.2 indicates that use of the comensation capacitance x allows for accurate prediction of either sensor's response to the epoxy.

Thus, in this section, a method has been developed to compensate for lead capacitances and other stray capacitances which affect the interelectrode coupling. In addition, the geometrical effects of the sensor configuration have been explored.

2.3 Optimization of Sensor Design

If a comparison is made of the micro sensor's and macro sensor's high frequency gain response in going from air to oil, it is found that the micro sensor experiences a much larger change in its high frequency gain. It is, in other words, more sensitive to permittivity changes than the macro sensor. This result is reasonable upon examination of the oxide layer thickness and permittivity in each case. The interelectrode spacing in both cases amount to a quarter wavelength. However, the permittivity of the oxide layer, and the normalized oxide layer thickness (h/λ) is much smaller for the micro sensor than the macro sensor. Thus, the micro sensor has proportionately much less coupling through its insulating layer than the macro sensor. This accounts for the micro sensor's higher sensitivity.

Consequently, the way to improve the sensitivity of the macro sensor to permittivity changes is to decrease the thickness and permittivity of its insulating oxide layer. The limiting factors will be electric breakdown through this layer to ground, and whether it can maintain its insulating properties as thickness is decreased. In the Micromet design, the interelectrode spacing was apparently made to be a quarter wavelength for maximum symmetry, and to keep the overall interelectrode coupling at a reasonable level.

The key to maintaining optimum senstivity to charge relaxation phenomena is to use very insulating materials for the oxide layer. Basically, the goal is to make the oxide layer insulating enough so it is clear that any conduction processes observed are attributed to the medium being measured.

Another advantage of decreasing the oxide layer thickness is the resultant response to surface conductivities. The current version of the macro sensor has a "surface" response which resembles a "bulk" one. An optimized macro sensor, with a 50μm oxide layer thickness (all other parameters unchanged), has a predicted

response to a surface conductivity between its electrodes which is distinct from its predicted response to a bulk conductivity (See Figure 2.4). Its predicted response to a surface conductivity between the electrodes closely resembles the one generated for the micro sensor (see Figure 1.6). The response to surface conduction processes that are further removed from the electrode plane, however, become less and less "surface" like. Predicted responses are also plotted in 2.4 for surface conductivities that are 5μm and 10μm distant from the plane of the sensor. Thus, such an optimized sensor would be able to distinguish between a medium with a bulk conductivity, and surface conductivities on interfaces that are relatively close to the electrode plane.

An experimental sensor, made of the same materials as the other versions, was used to test these design criteria. The parameters of this sensor were identical to the other macro sensor versions except that its oxide layer was thinner by a factor of 2.5 (400μm). Its high frequency gain response in air was less than the others due to a smaller overall Y_{12} (smaller capacitive contribution from coupling through the oxide layer), and its sensitivity was higher as predicted by the model. The 400μm oxide layer was still not thin enough to make it sensitive to surface conduction phenomena. It's predicted response to surface conductivities was still very similar to its predicted bulk response.

The sensitivity of these sensors to changes in conductivity were the same. This has to be true because changes in the conductivity are only reflected by the scaling of the gain and phase curves with frequency. Thus, a sensor with much better sensitivity to permittivity changes can be designed using these guidelines.

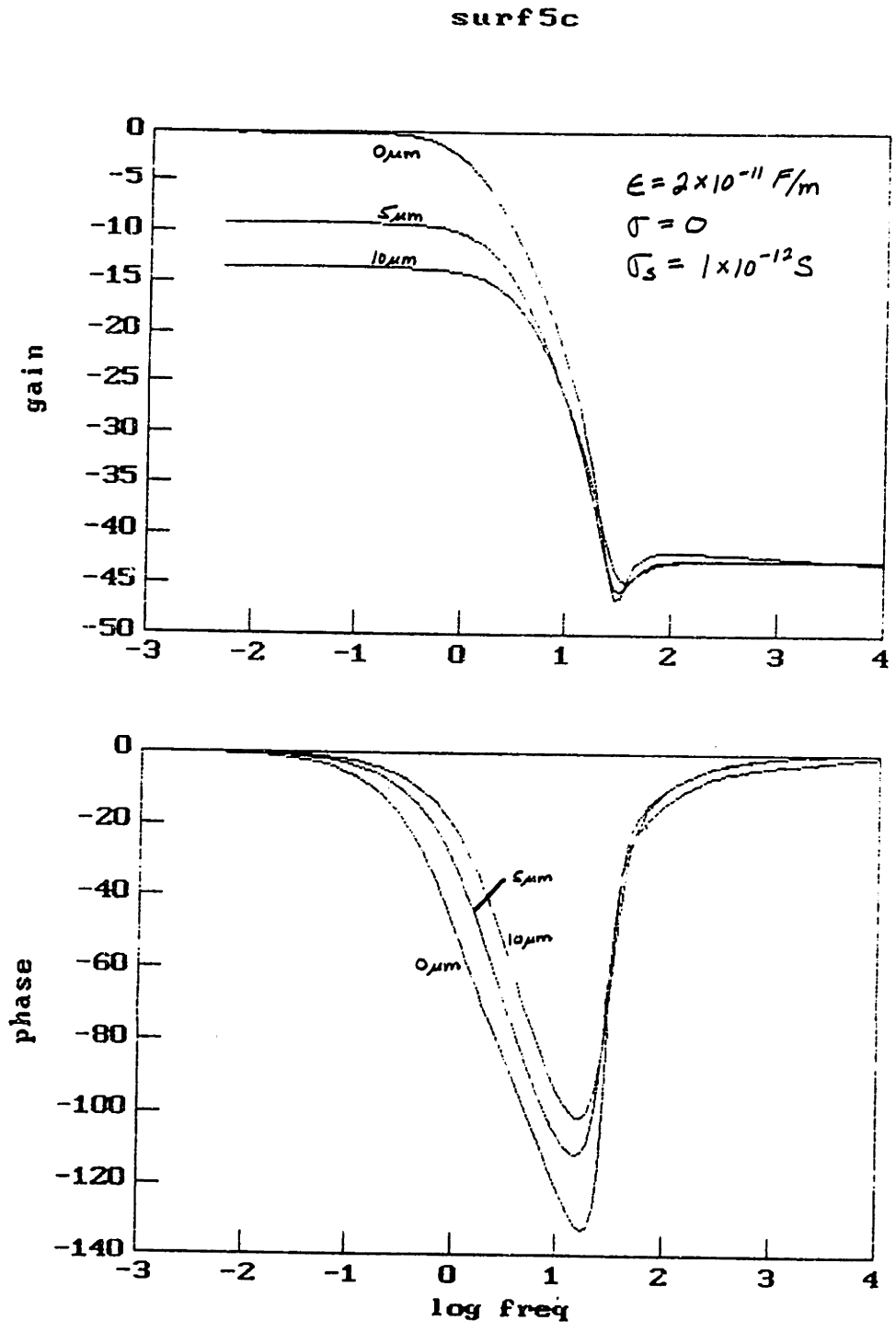

Figure 2.4: Predicted Macro Sensor (50μm Oxide Layer) Response to Surface Conduction Process at Electrode Interface; and at Interfaces 5μm and 10μm away

Chapter 3

Passivation of Sensor to Water

The addition of the compensation capacitance, x, to Y_{12} in the pi network has allowed for accurate predictions of the high frequency gain response (capacitive coupling only) of the macro sensor when measuring materials with different permittivities. The next step is to determine the sensor's response to a complex dielectric material over the entire frequency range of the device. As mentioned in the previous chapter, the frequency response (.005 Hz to 10 kHz) of the sensor in air gives a flat gain (≈ -40 dB) and zero phase, which matches the predictions of the model. It is gratifying that the model matches sensor readings in air, but it is for the most part, a rather uninteresting result. To test the model's ability to accurately predict responses at lower frequences, it becomes necessary to look at macro sensor readings of materials that are conducting enough to demonstrate the effects of charge relaxation upon the frequency response of the macro sensor. Transformer oil, which has a conductivity of approximately 1×10^{-12} mhos/m, is a prime candidate for such tests.

3.1 Effect of Water Contamination upon Frequency Response in Oil

It was discovered during initial tests of the macro sensor in oil that its frequency response was sensitive to moisture. Figure 3.1 shows the frequency response to oil with a moisture content of approximately 12 ppm (parts per million), and Figure 3.2 shows the frequency response to oil with a moisture content of approximately 50 ppm. The frequency response to the dry oil shows a relaxation process occuring at a much lower frequency than that indicated by the frequency response of the wet oil. In fact, if the conduction process is ohmic in nature, then an increase in the conductivity of the oil causes the gain and phase curves to shift to the right scaled proportionately in frequency (see Chapter 1.3.4). Thus, a comparison of Figure 3.1 and Figure 3.2 indicates that there is over an order of magnitude difference in the conductivity measured in each case. This was determined by the relative frequencies of their phase peaks, or projected phase peaks. However, it is known that the conductivity of transformer oil is relatively insensitive to moisture content.

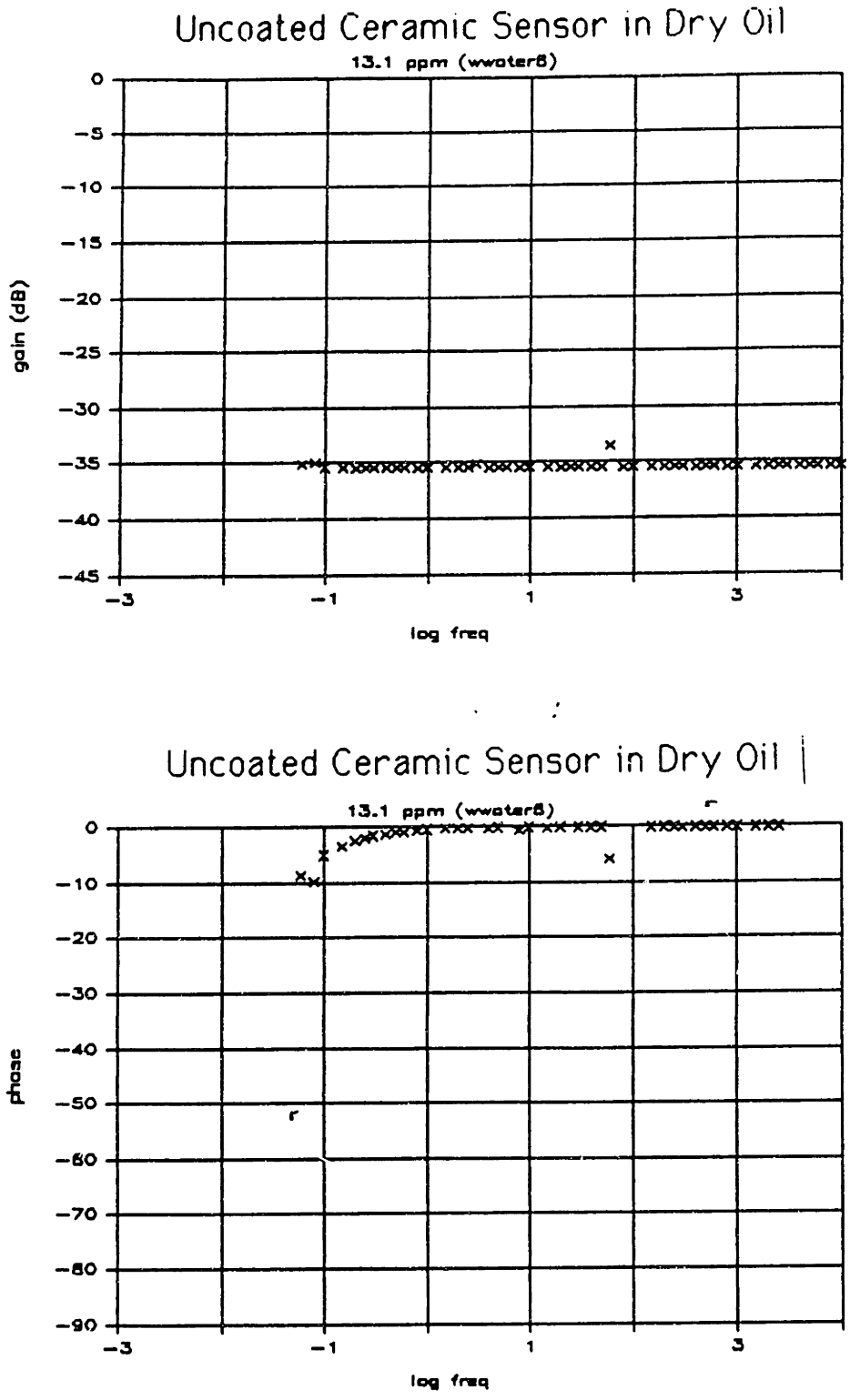

Figure 3.1: Uncoated Ceramic Sensor in Dry Oil (12 ppm)

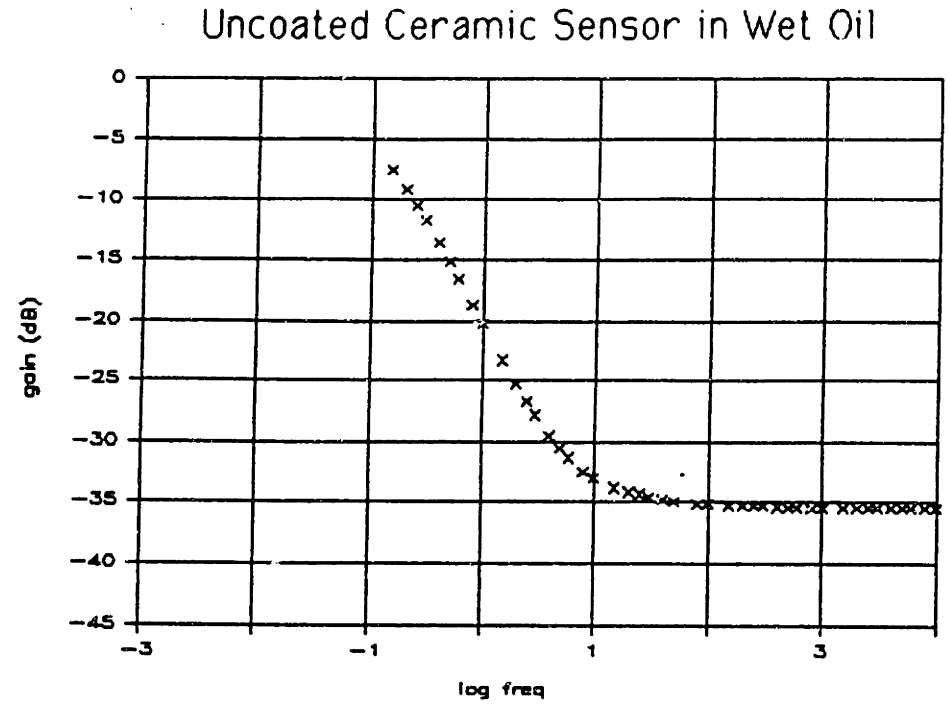

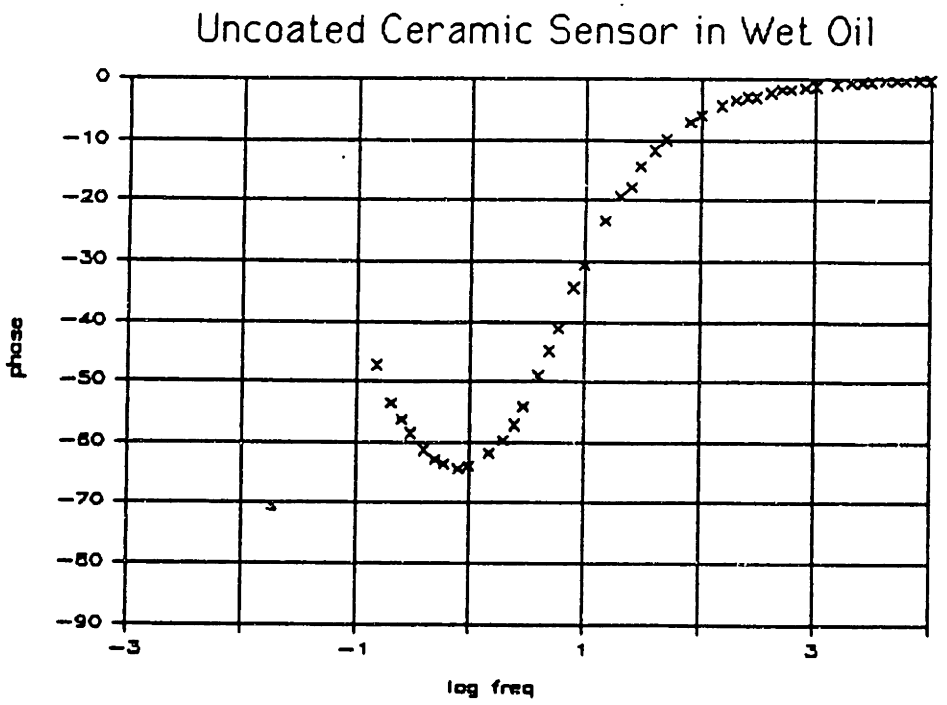

Figure 3.2: Uncoated Ceramic Sensor in Wet Oil (50 ppm)

Hence, the readings given by the macro sensor are faulty and are attributed to changes in the conductivity of the aluminum oxide as it absorbs water from the oil. Consequently, before accurate measurements of the bulk conductivity can be made, a method must be found for passivating the macro sensor to the effects of water.

3.2 Parylene Coatings for Water Passivation

Parylene is the generic name for members of a polymer series developed by Union Carbide Corporation. The basic member of the series, called parylene N, is poly-p-xylylene, a completely linear, highly crystalline material. Parylene C, the second member of the series commericially available, is produced from the same monomer modified only by the substitution of a chlorine atom for one of the aromatic hydrogens. Typical thermal, mechanical, electrical, and barrier properties are presented in Table 3.1.

Parylene C, which has the second smallest moisture vapor transmission coefficient, was chosen as the coating to apply to a macro sensor for passivation to water because of its ease of application. The coating process was performed by Paratronix Inc. [29] using a vapor deposition technique. They were able to deposit coating thicknesses down to about 5 μm. This was an acceptable thickness as good moisture insulation properties were desired with the thinnest possible coating. A thin coating is important because coupling through the parylene must be kept to a minimum to allow for maximum sensitivity to material beyond.

The macro sensors were coated with the leads previously attached to allow for a perfect seal. The first test of the effectiveness of the parylene coating was to look at the sensor's frequency response in air before and after exposure to water. If the frequency responses remain flat after this test, then the coating has performed satisfactorily. The next step was to test a parylene coated macro sensor's response in dry and wet oil to demonstrate the effectiveness of parylene in a transformer environment.

Figures 3.3 and 3.4 are the frequency responses of a macro sensor coated with a 5μm layer of parylene in dry and wet oil. The two sets of gain/phase curves have the same general shapes which is an indication that the relaxation mechanisms in each case are identical. The high frequency gains are the same, indicating that the permittivity has remained constant from the dry to wet oil. The frequency of the phase peaks are essentially unchanged indicating that the conductivities are also identical. Thus, the parylene coating seems to work quite well. The verification of the model's ability to predict bulk permittivities and conductivities from gain and phase responses will be explored in the next chapter.

3.3 Modeling of the Parylene Layer

To model the parylene layer, its thickness, conductivity, and permittivity must be known. The thickness was determined from the measurement of a witness strip that was coated along with the sensors. The electrical properties are specified in Table

PARYLENE TECHNICAL DATA

Paratronix

TYPICAL THERMAL AND MECHANICAL PROPERTIES

	Parylene N	Parylene C	Parylene D
Tensile Strength, psi.	6,500	10,000	11,000
Yield Strength, psi.	6,100	8,000	9,000
Elongation to Break, %	30	200	10
Yield Elongation, %	2.5	2.9	3
Density, g/cm.³	1.11	1.289	1.418
Coefficient of Friction			
Static	0.25	0.29	0.33
Dynamic	0.25	0.29	0.31
Water Absorption, 24 hours	0.06 (0.029")	0.01 (0.019")	—
Index of Refraction, no23°C.	1.661	1.639	1.669
Melting or Heat Distortion Temperature, °C.	405	290	> 350
Linear Coefficient of Expansion, (10^{-5}/°C.)	6.9	3.5	—
Thermal Conductivity, (10^{-4} cal./sec./cm.²-°C./cm.)	~3	—	—

Data recorded following appropriate ASTM method.

TYPICAL ELECTRICAL PROPERTIES

	Parylene N	Parylene C	Parylene D
Dielectric Strength, Short Time, volts/mil at 1 mil	7,000	5,600	5,500
Volume Resistivity, 23°C., 50% RH, ohm-cm.	1×10^{17}	6×10^{16}	2×10^{16}
Surface Resistivity, 23°C., 50% RH, ohms	10^{13}	10^{14}	5×10^{15}
Dielectric Constant			
60 Hz	2.65	3.15	2.84
10^3Hz	2.65	3.10	2.82
10^6Hz	2.65	2.95	2.80
Dissipation Factor			
60 Hz	0.0002	0.020	0.004
10^3Hz	0.0002	0.019	0.003
10^6Hz	0.0006	0.013	0.002

Data recorded following appropriate ASTM method.

TYPICAL BARRIER PROPERTIES

Parylene is qualified under Mil-I-46058C.

Polymer	Gas Permeability cm.³-mil/100 in.²-24 hours-atm. (23°C.) N_2	O_2	CO_2	H_2S	SO_2	Cl_2	Moisture Vapor Transmission, g.-mil/100 in.²-24 hours, 37°C.-90% RH
Parylene N	7.7	39.2	214	795	1,890	74	1.6
Parylene C	1.0	7.2	7.7	13	11	0.35	0.5
Parylene D	4.5	32	13	1.45	4.75	0.55	0.25

Data recorded following appropriate ASTM method.

Table 3.1: Typical Properties of Parylene

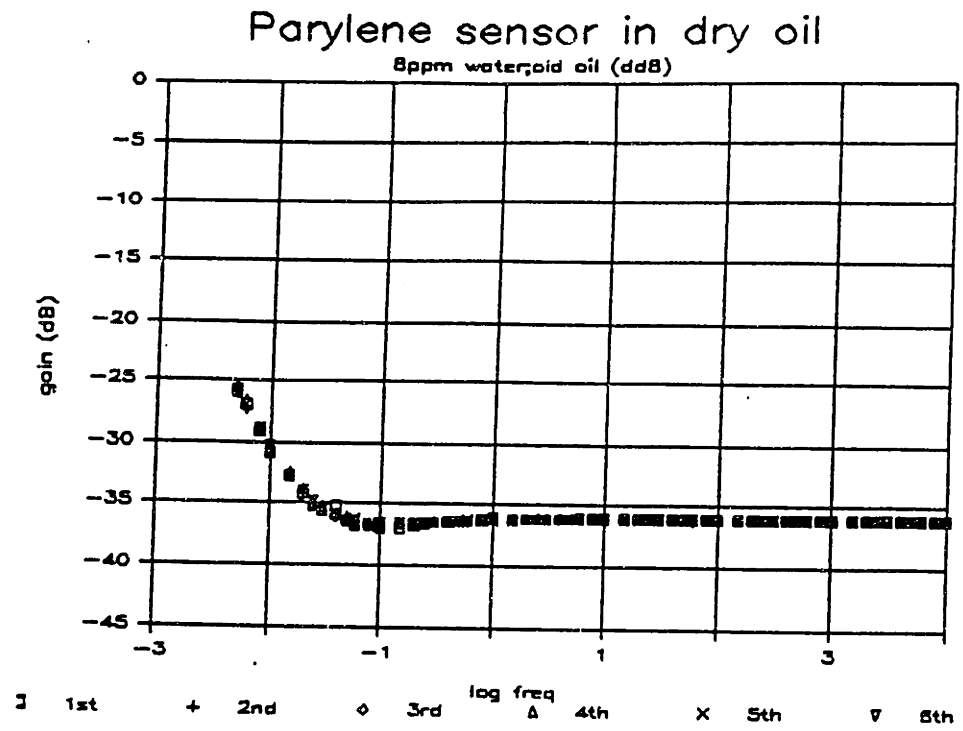

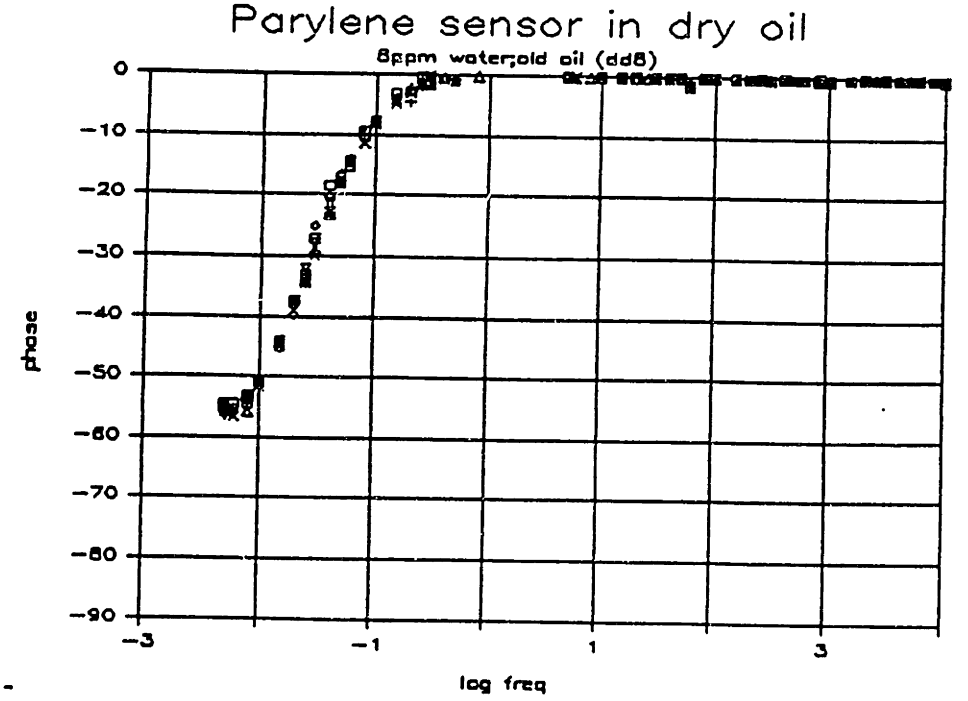

Figure 3.3: Parylene Coated Macro Sensor in Dry Oil (12ppm)

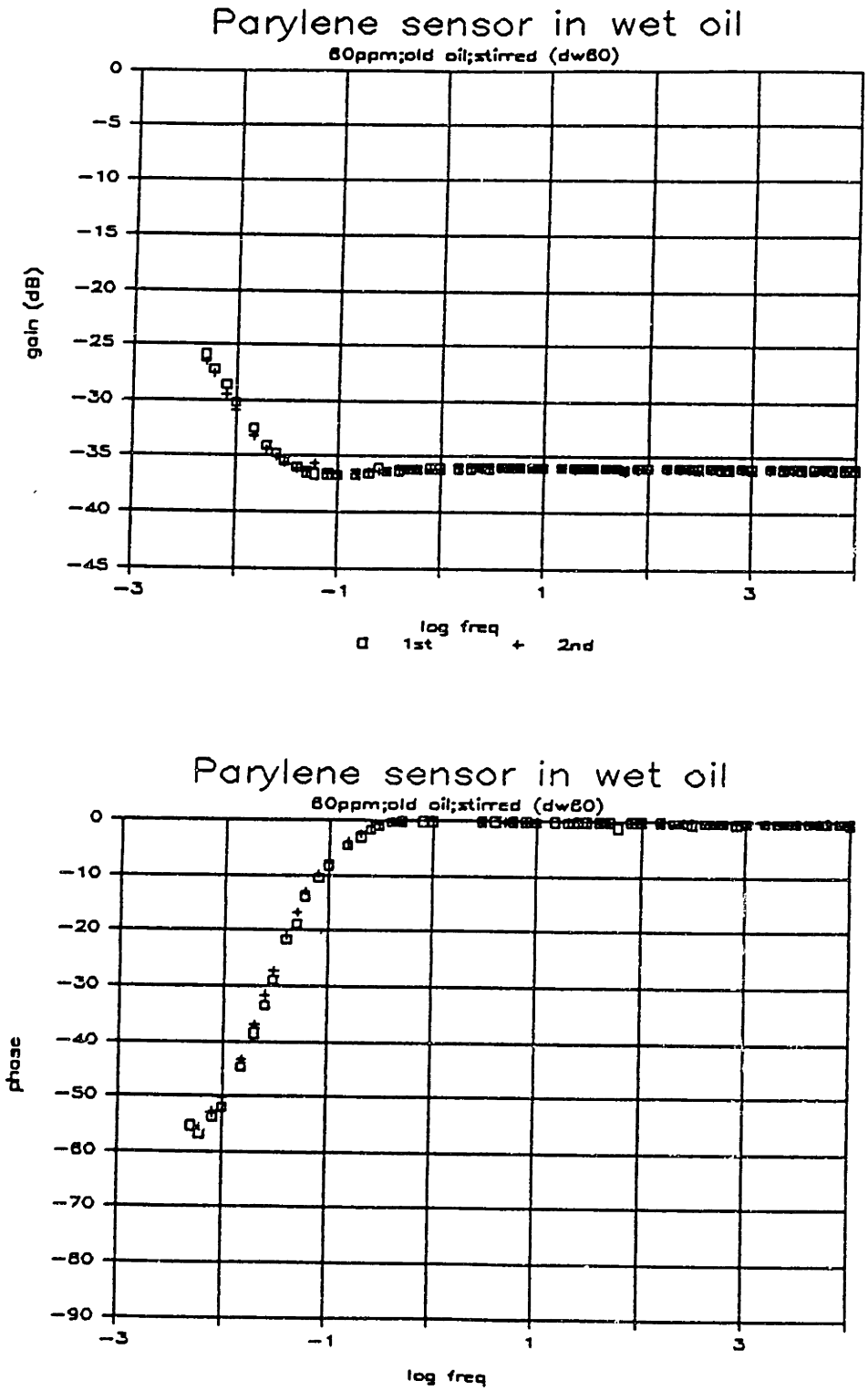

Figure 3.4: Parylene Coated Macro Sensor in Wet oil (57ppm)

3.1. Basically, the parylene is modeled as a 5μm thick, perfectly insulating media, with a permittivity of $3.1\epsilon_0$. Hence, its frequency response in air will have a flat gain with no phase, and the gain will be slightly higher than that of an uncoated macro sensor because the permittivity of parylene is greater than that of air. The response of a parylene coated macro sensor to a conducting media however, is quite different than that of an uncoated sensor. Figure 3.5 is the predicted response of a parylene coated macro sensor to very conducting transformer oil ($\epsilon = 2.2\epsilon_0$, $\sigma = 1 \times 10^{-10}$ mhos/m).

The shape of the gain and phase curves are similar to that of the predicted bulk response for an uncoated macro sensor. However, there are distinct differences. The gain curve, at low frequencies, does not approach unity gain. The value at which the gain levels off reflects the capacitance of the parylene layer when capped by a "perfect" conductor. This capacitance is a function of the permittivity and thickness of the parylene layer. A comparison of the phase curves shows that the angle at which the phase peaks for the parylene coated macro sensor is less than that of the uncoated one. Again, this peak value is a function of the thickness and permittivity of the parylene layer, and the permittivity of the oil.

Another effect of the parylene layer, which is highly insulating, is to further decrease the differences in response of the sensor to bulk conduction of an infinitie half space, and surface conduction at the parylene/infinite half space interface. This limitation will be demonstrated in the next chapter from experience with actual measurements.

Parylene has been shown to be very effective in passifying the macro sensor to moisture in transformer oil. It is also easily accounted for in the model and its predicted effects have been explored. The accuracy of the predicted responses for a parylene coated macro sensor will be explored in the next chapter when data on bulk measurements of the transformer oil using a parylene coated sensor are presented.

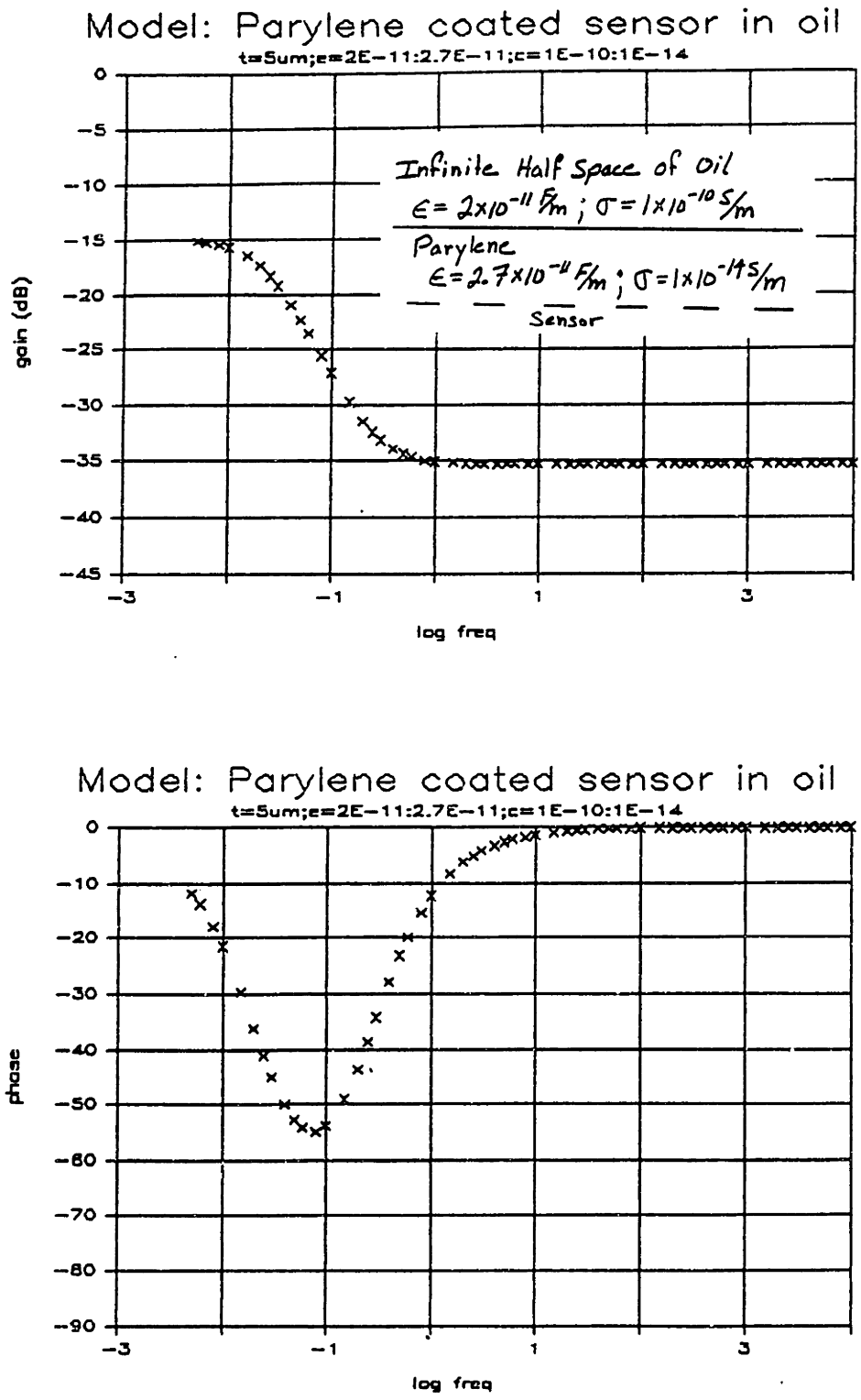

Figure 3.5: Predicted Response of Parylene Coated Sensor in Conducting Oil

Chapter 4

Measurement of Bulk Complex Permittivity with Passivated Sensor

In this chapter, measurements of various transformer oils are made with a parylene coated macro sensor, and the dielectric properties of the oil parameter estimated from the gain and phase frequency response. The parameter estimation strategies are briefly described and some of the limitations identified. Once the validity of the bulk dielectric measurements have been demonstrated, the effects of oxidation on the dielectric properties of the transformer oil are explored using a parylene coated macro sensor. Also, a study of the temperature dependence of the oil's conductivity is performed to allow normalization of readings taken at different temperatures. The chapter ends with a discussion of how a current version of the parylene coated macro sensor would best fit into an overall system designed to measure complex permittivity.

4.1 Parameter Estimation of Bulk Dielectric Properties

Up to this point, the model has been used to predict frequency responses of macro sensors with different physical configurations to materials with various complex dielectric properties. The ability to work backwards, by estimating properties of the measured media from the gain and phase response, is the mode in which most applications would operate. A parameter estimation scheme has been developed, by Zaretsky [25], where all known parameters are utilized, and the desired quantities found using a root searching routine based on one or more frequency measurements. The way in which such a parameter estimation routine works is to vary the desired parameters in the model until the predicted response matches the data input into the routine. It is assumed that the data used in the parameter estimation routine contains information about the desired parameter. For example, to parameter estimate the conductivity of a material, a data point with phase information would

be necessary. A high frequency data point reflecting only capacitive coupling would not allow for estimation of a conductivity. This is a consequence of the floating gate configuration used for microdielectric measurements.

The successful use of such estimation schemes requires that the model upon which the root searching is done must accurately reflect the situation for which parameters are to be estimated. In terms of the gain and phase curves, the shape of the measured frequency response must match that of the predicted one. This is a necessary condition for accurate parameter estimation, but not necessarily sufficient, as will be demonstrated shortly. If the shapes don't match, then the estimated quantity is a best fit of the data to an inaccurate model, which may produce meaningless results.

The final model consideration is one of uniqueness. If a predicted frequency response (gain and phase curves) matches data, then is it reasonable to conclude that the parameters in the model describing the measured material accurately reflect the actual physical situation. In Chapter 1.3.4, it was predicted that the frequency response of the macro sensor to a surface conductivity would be very similar to its response to a bulk conductivity. An example is presented where measurements were taken of a 240 μm thick polyethylene sheet using a parylene coated macro sensor in air. The discrete points in Figure 4.1 represent actual data, and the line, the predicted response from the model (which will be described shortly). This data looks very similar to Figure 3.5 except that the low frequency gain is less, and the phase peak shallower. This would indicate, according to that model (insulating layer with uniform permittivity bounded by an infinite half space of relatively conducting oil also with uniform properties), an insulating layer thicker than just the parylene coating, and some bulk conductivity for the polyethylene sheet. This is reasonable because one would not expect a perfect contact between the sensor and the polyethylene, and the resultant air gap would be a perfect insulator. Also, as far as the macro sensor is concerned, the polyethylene is thick enough to be considered an infinite half space.

The low frequency gain reflects the capacitance of the layer of parylene and air bounded by a perfect conductor. Thus, this gain is a function of the permittivity and thickness of each of those layers. Given that the permittivities of both the air and parylene are known as well as the thickness of the parylene, the thickness of the air can be determined using parameter estimation techniques. The thickness was parameter estimated to be 5 μm. A bulk conductivity of 2.5×10^{-8} mhos/m for the polyethylene is then estimated from the frequency at which the phase peak occurs, and its bulk permittivity of $2\epsilon_0$ is estimated from the high frequency gain. The predicted response from which these values were determined is plotted as the continuous curve in Figure 4.1. The shapes are very similar (except for the inexplicable tailing observed in the low frequency gain) and the conclusion that the properties of the polyethylene had been found might be made.

However, it is known that the conduction mechanism for polyethylene is attributed to a surface property and that the bulk of the polyethylene sheet is actually very insulating. Thus, the appropriate model to use would be a surface conductivity at the air-gap/polyethylene interface with the bulk of the polyethylene being very

fig:an3

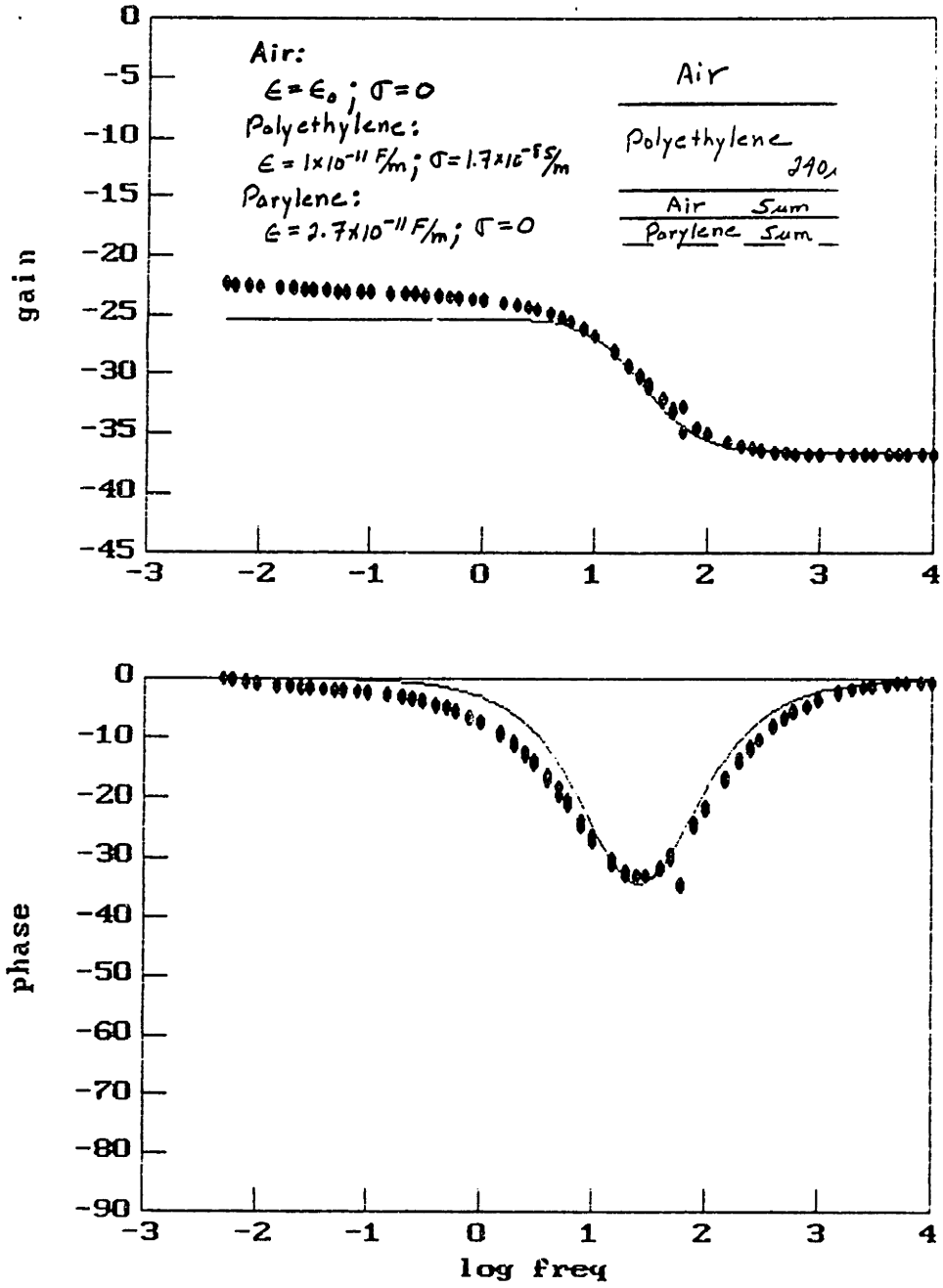

Figure 4.1: Frequency Response of Polyethylene Sheet: Data and Predicted Response

insulating. When such a model is used, a surface conductivity of 3×10^{-12} mhos, and the same bulk permittivity as before, gives a model prediction that is identical to the case with only a bulk conductivity. Thus, the only way, in this case, to choose the correct model from looking at just a temporal frequency response is from a priori knowledge of the characteristics of the polethylene sheet. This experiment also verfies the model's prediction that the macro sensor is unable to discriminate between surface and bulk conduction phenomena.

If a variable wavelength sensor were available, then the difference between the two situations could be easily distinguished by looking at the spatial variations of the conductivity. Or, if a macro sensor with a much thinner oxide layer were available, the surface response would be identifiable from its asymmetric phase curve, and greater than -20dB per decade gain transition. Hence, in the process of interpreting data, it is important to apply all the knowledge and intuition about the physical situation to insure that the modeling is reasonable, because it is possible to match data to predicted frequency responses generated from very different parameters.

4.2 Microdielectric Measurement of Transformer Oil

In this section, measurements of new and stressed transformer oils are taken with a parylene coated macro sensor and their complex properties estimated. The validity of these results is checked against conventional bridge measurements of these same oils. Then, the effect of temperature on the microdielectric measurements are explored and the inherent accuracy limitations of the macro sensor discussed.

4.2.1 New vs. Oxidized Oil

As a test of the macro sensor's ability to make bulk measurements, data of new transformer oil and oxidized transformer oil was taken and compared to conventional measurements (cell measurement using bridge circuit) of the same oil. Figure 4.2 presents macro sensor (parylene coated) measurements of transformer oil fresh from the barrel (multiple measurements are presented). Figure 4.3 shows the frequency response of a parylene coated macro sensor to oil that has oxidized while exposed to room air over a period of six months. From looking at the phase information, it is clear that the "old", or oxidized oil is much more conducting than the new oil. Also, both curves have the same shape as the predicted respone of a parylene coated macro sensor in conducting oil (see Figure 3.5). Parameter estimation of the data from the new oil gives a permittivity of $2.2\epsilon_0$ and a conductivity of 1.25×10^{-12} mhos/m, which is comparable to a conventional measurement of $2.2\epsilon_0$ for the permittivity and 1.35×10^{-12} mhos/m for the conductivity. The macro sensor measurements of the old oil result in estimated values of $2.2\epsilon_0$ for the permittivity, and a conductivity of 5×10^{-12} compared to the conventional measurements of $2.25\epsilon_0$ for the permittivity and 4×10^{-12} for the conductivity (all conventional bridge measurements were made

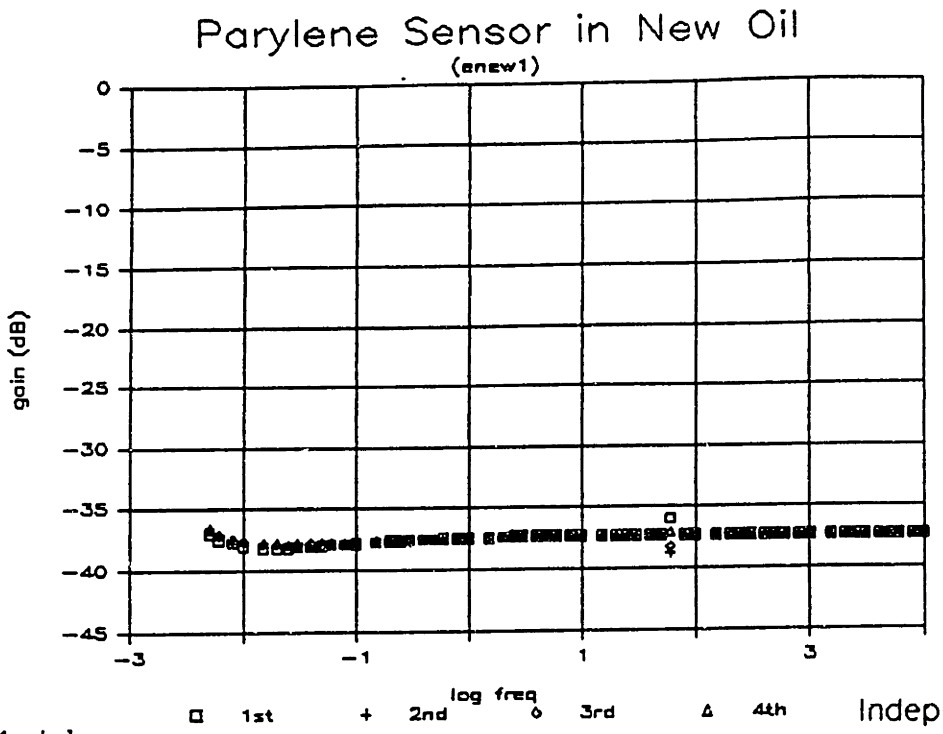

Model:
e=2.2
e=1.25E-12

Independent measurement.
ϵ=2.17
σ=1.35E-12

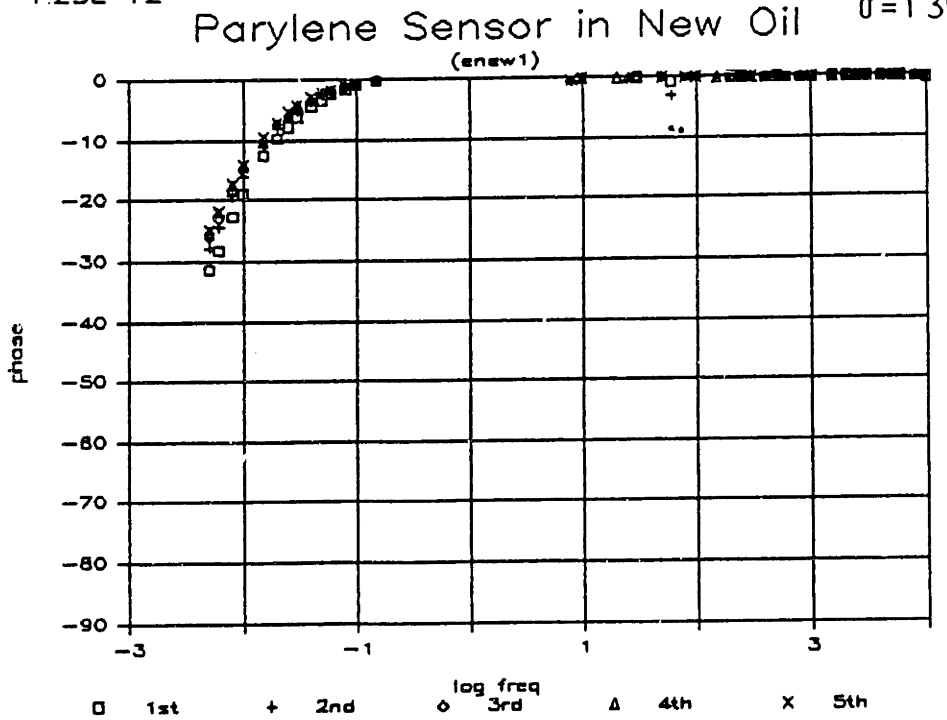

Figure 4.2: Measurement of New Oil with Parylene Coated Macro Sensor

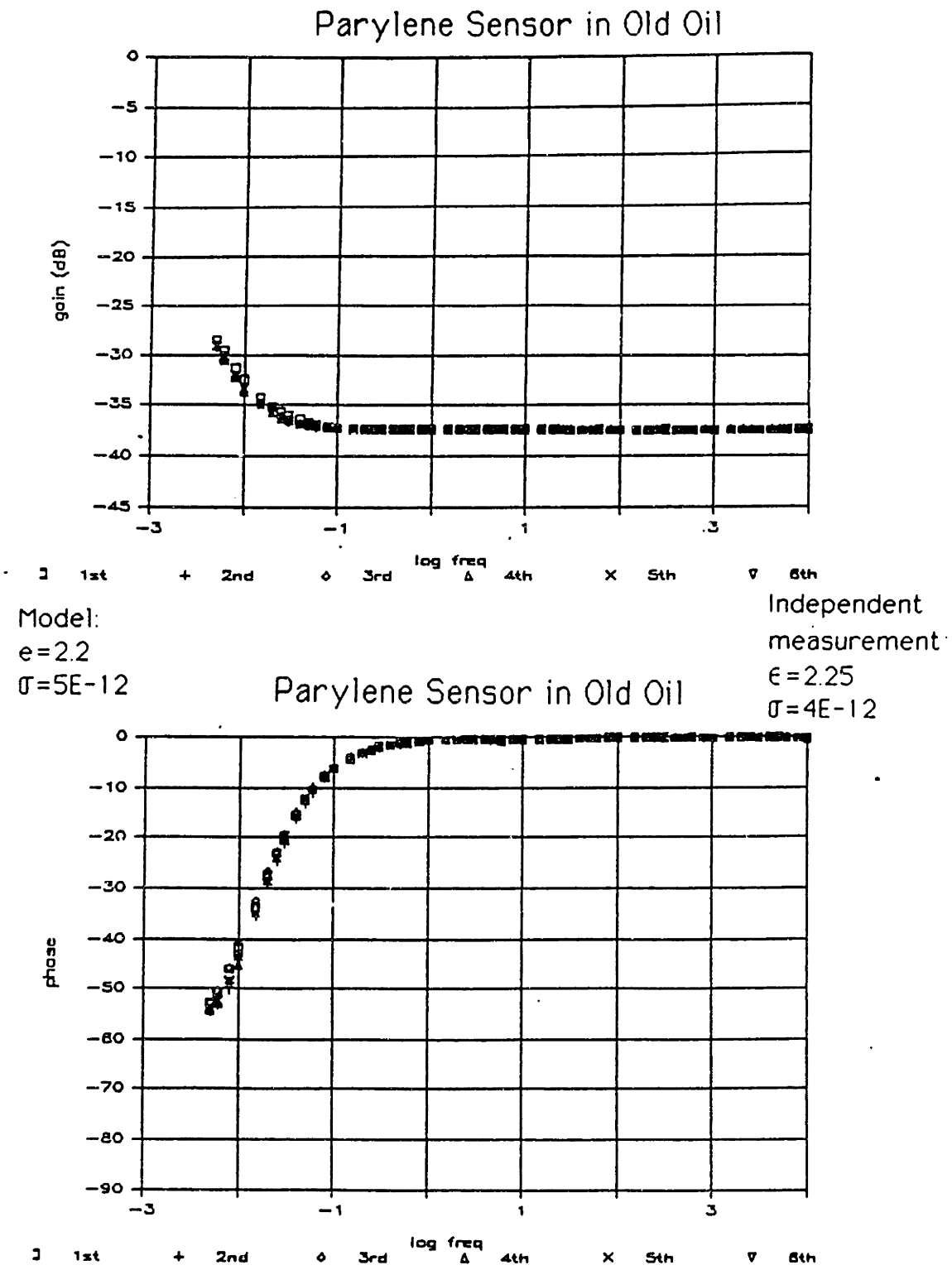

Figure 4.3: Measurement of Oxidized Oil with Parylene Coated Macro Sensor

by Bill Westphal, MIT). Thus, there is good agreement between the microdielectric measurements and the conventional measurements.

The next experiment explores the effects of oxidation upon the conductivity of the oil under more controlled conditions. A small quantity (100 ml) of oil was heated at $90°C$ for 72 hours while exposed to room air. The conductivity of the oil (measured using a parylene coated macro sensor) changed from 8×10^{-13} mhos/m to 4×10^{-11} mhos/m. The shapes of the gain and phase curves correspond to that of a bulk measurement with the curves remaining constant in shape, but shifting in frequency as the conductivity increased due to oxidation. No changes were observed in the permittivity of the oil at this level of oxidation. Hence, this experiment tends to confirm the reported results of other researchers from Chapter 1.2.2.

It has been demonstrated that the frequency response of the macro sensor can be adequately modeled, and that parameter estimation techniques give results that are comparable to conventional measurements. Also, oxidation experiments have further demonstrated the ability of the macro sensor to make accurate measurements and to detect changes in the transformer oil.

4.2.2 Temperature Compensation

It was found upon taking measurements of the transformer oil at different temperatures, that the conductivity would vary with the temperature. Hence, a method is needed to normalize conductivity readings taken at different temperatures so that meaningful comparisons can be made. This can be done using the Arhenius temperature dependence described in Chapter 1.2.2 (Equation 1.8). To verify that the conductivity has an Arhenius type temperature dependency, measurements of the conductivity for new oil were taken with a parylene coated macro sensor at various temperatures. The data is plotted in Figure 4.4 with log of the conductivity vs. inverse temperature in degrees Kelvin. The Arhenius temperature dependence is verified by the "straight" line result of the plot. The activation energy E_σ was found to be 2.8 kcal/mole which is less than that reported for a typical transformer oil in Chapter 1.2. The corresponding σ_0 was 2.1×10^{-8} mhos/m. The frequency responses from which these data points were extrapolated are illustrated in Figures 4.5 through Figures 4.8. It is important to notice that these plots have a bulk type response as seen by a parylene coated macro sensor. Once the bulk nature of the response is verified, the conductivities were estimated from the position of the phase peaks. From the low frequency gain response, where the oil has become a conductor, the thickness of the parylene layer can be deduced and agrees with the 5μm measurement reported in Chapter 3.

Once these values have been determined, subsequent measurements can be made at different temperatures, and σ_0 compared instead of the absolute conductivity. In addition, over longer time scales, measurements can be made to determine if the activation energy, E_σ, has changed.

Thus, when microdielectric measurements are made of the transformer oil, it is important that the temperature also be measured. Thus, comparisons of measurements can be made of data taken at the same temperatures, or comparisons made of

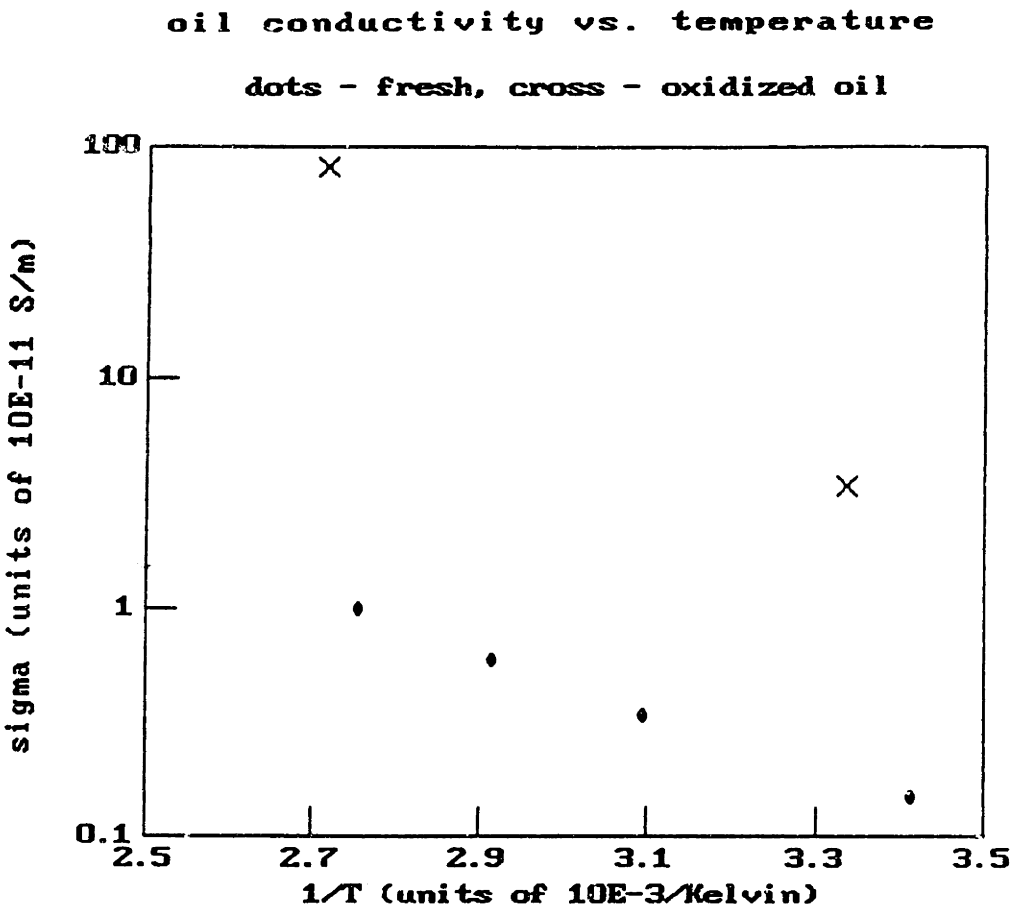

Figure 4.4: Log Conductivity vs. Inverse Temperature

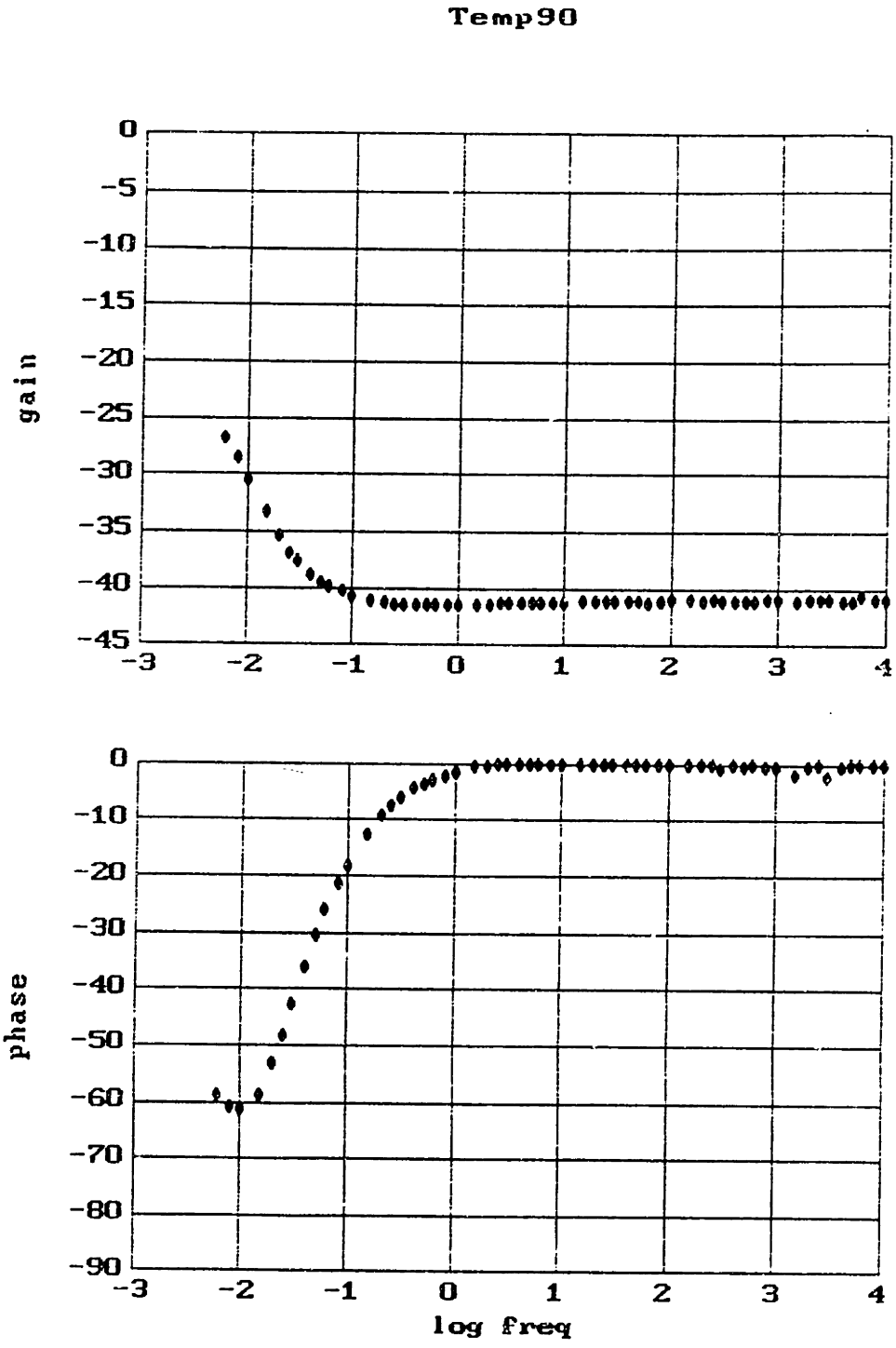

Figure 4.5: Frequency Response of New Oil at 90°C

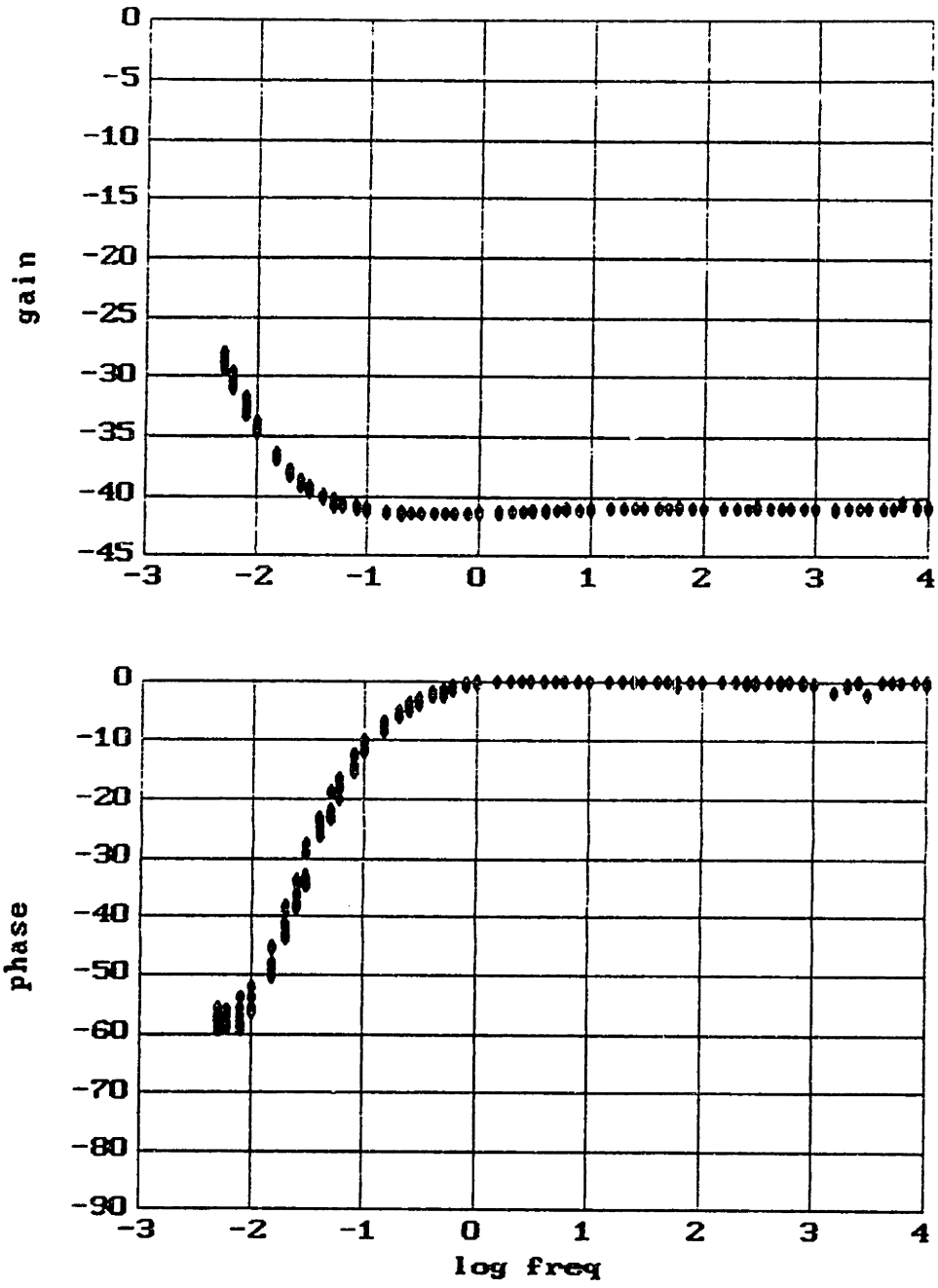

Figure 4.6: Frequency Response of New Oil at $70°C$

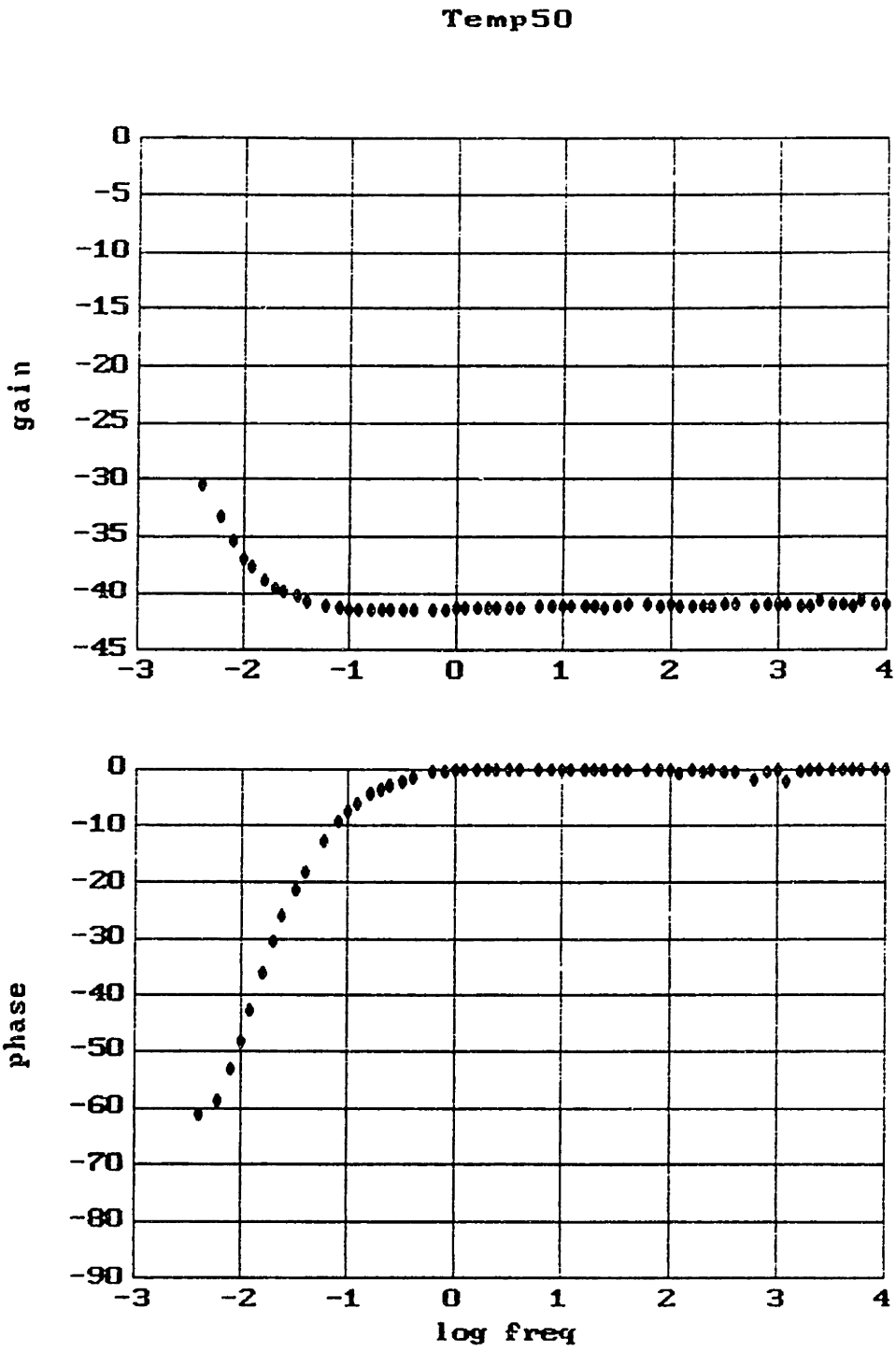

Figure 4.7: Frequency Response of New Oil at $50°C$

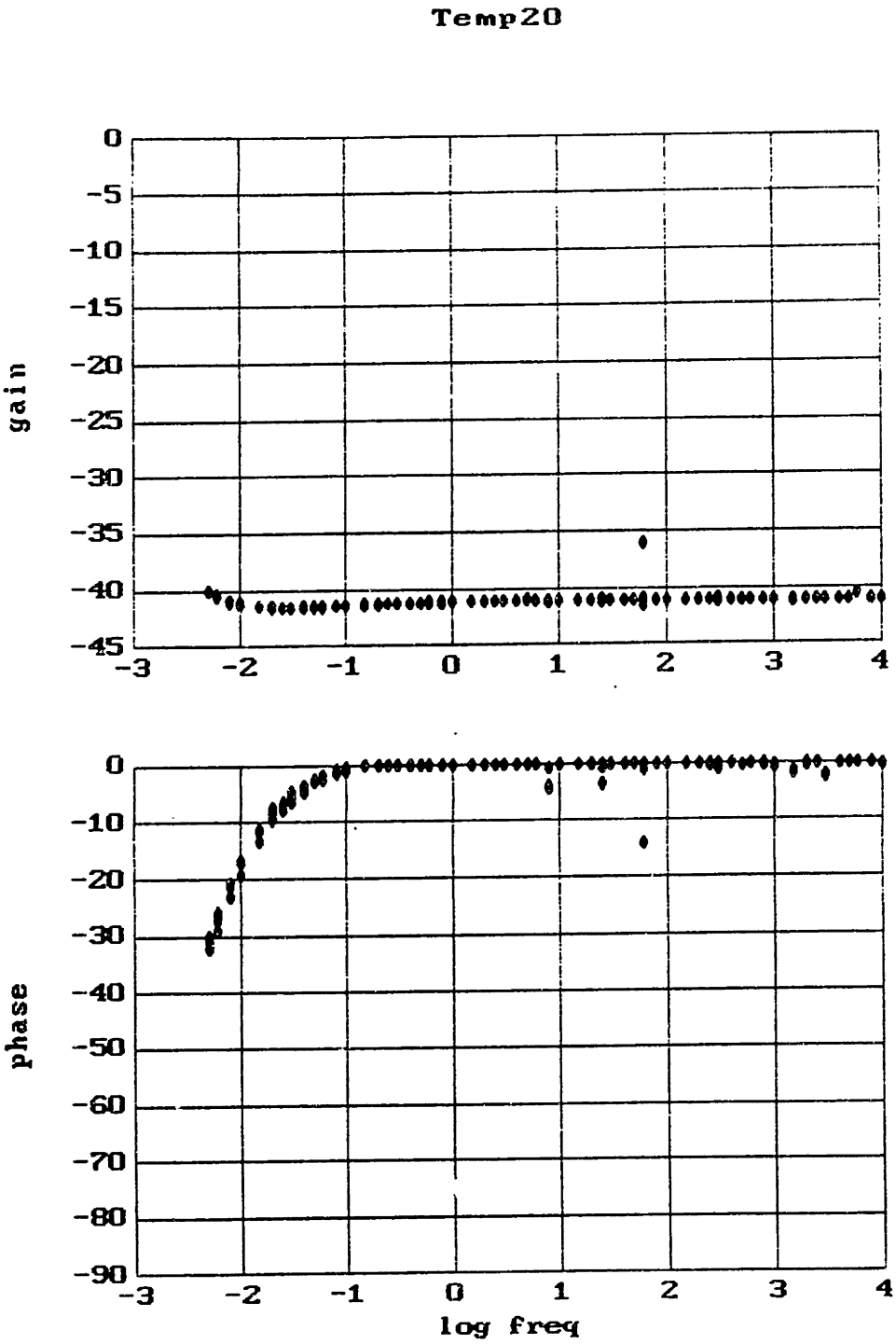

Figure 4.8: Frequency Response of New Oil at $20°C$

data taken at different temperatures after normalization using the Arhenius equation.

4.2.3 Accuracy of Macro Sensor Measurements

One of the limitations of the macro sensor encountered in running these last set of experiments was the relative insensitivity of the macro sensor to changes in permittivity. Changes in the high frequency gain in going from air (ϵ_0) to oil ($2.2\epsilon_0$), for example, amount to about 1.5 dB. Thus, changes of 0.1 dB correspond to a relatively large change in the parameter estimated permittivity. The result is that fluxuations in gain measurements due to offset changes make it difficult to take really accurate measurements. A 0.1 dB uncertainty (plus or minus) in the gain reading corresponds to an accuracy of plus or minus $0.1\epsilon_0$ in parameter estimating the permittivity of transformer oil. Thus, the macro sensor is not really optimized for making accurate permittivity measurements (see discussion in Chapter 2).

The limiting factor for parameter estimating conductivity is due to the discreteness of the frequency measurements. Readings can only be made at powers of ten times the following frequencies: 1, 1.5, 2.0, 2.5, 3, 4, 5, 6, 8, 10. Thus, without a continuous measurement of the phase, there is a small uncertainty when parameter estimating the conductivity from this discrete information. This error, however, is believed to be very small, and should be a neglibigle factor.

Consequently, the optimum configuration for measuring complex permittivity of transformer oil in a transformer environment, given the state of the current hardware, is to use both a micro sensor and a macro sensor in close proximity within the transformer or an oil circulation loop. The micro sensor, which has temperature sensing circuitry, would be used to take temperature readings. It would also be used for permittivity measurements because its geometry makes it much more sensitive to changes in this property (plus or minus 0.01 ϵ_0). The macro sensor would be used to take conductivity measurements, which the micro sensor has difficulty doing under certain operating conditions (i.e. very insulating, dry, oil at low frequencies). Using these two sensors in concert would then give optimal measurements of both the permittivity and conductivity of the oil. Also, the use of two sensors would allow for some cross checking of their operation which may be useful for diagnostic purposes.

Chapter 5

Detection of Moisture Absorption by Transformer Insulation through Dielectric Measurements

In this chapter, the importance of the electrical properties of the solid, electrical grade paper insulation is described. The effects of water upon the electrical properties of cellulose, and the types of failure that can result from overly high moisture content, is explored. The moisture content of both air and oil impregnated paper is found to have an enormous effect upon the conductivity of the cellulose, which makes the macro sensor very attractive as a potential device for moisture measurements of the paper insulation. The macro sensor is well suited for such measurements because of its planar, interdigitated electrode structure which allows for direct exposure of the paper to the oil, and its 1 mm wavelength enables sensing to a depth of 330 μm, which means that measurements encompass the bulk of the 100 μm thick paper.

5.1 Cellulose Based Solid Insulation

Pressboard is a dense, compressed fibrous sheet material composed of cotton and/or other vegetable fibers. It is used because of its low cost and desirable mechanical, chemical, and electrical properties. It has excellent mechanical strength and flexibility, and large sheets can be made to uniform thicknesses. Its chemical stability gives it long life, and it has excellent electrical properties when properly dried. Also, high dielectric breakdown strength can be obtained by oil impregnation. Consequently, it is ideal for use in a transformer.

5.1.1 Use of Paper Insulation in Transformers

Pressboard is used for the insulation of individual turns, the low voltage windings from the core, between the low and high voltage windings, and between coils and coil yokes [30]. Unfortunately, pressboard has a high affinity for moisture, and will

absorb any water that is available from the surrounding environment. Once enough moisture has peneterated the insulation of the coils, short circuits between turns are likely to occur. This in turn, can lead to the overall failure of the transformer. Thus, it is important that the moisture content in the transformer insulation be kept low to maintain the integrity and effectiveness of the cellulose insulation. Moisture removal from the insulation is first performed during the construction and commissioning of the transformer. The process is carefully monitored to prevent over drying which can cause unnecessary aging of the pressboard insulation. Once thoroughly dried, the transformer oil is blanketed with dry nitrogen and sealed against the environment (older transformers may not be as carefully sealed or sealed at all against the outside). However, even with these careful precautions, moisture levels will always slowly increase due to leakage, or oxidation of the oil and paper. Hence, once the transformer is in operation, it is important to be able to monitor the moisture content of the insulation so that moisture removal can be performed when necessary.

5.1.2 Moisture in Transformer Insulation

In a multi-component system of oil, paper, and air, the equilibrium water content of each component corresponds, for practical purposes, to having equal relative water saturation. Thus, in a closed system at equilibrium and constant temperature, the relative humidity of the air might be 30%, corresponding to a moisture content in the oil of 30% of 55 parts per million (saturation level), and moisture content in the paper of 30% of its saturated level of 17% water by weight. It has been shown that the water content of paper and various oils are directly proportional to the relative humidity of the air with which they are in equilibrium. The solubility of water in oil was found to increase with both temperature and degree of oxidation or contamination. The amount of water absorbed by the paper insulation, however, was found to be independent of temperature for a given relative humidity [31].

Even though the weight of oil contained in a transformer is about four times the weight of the cellulose insulation, the oil holds only about 0.1% of the total water in the transformer. Hence, even though temperature cycles can cause large fluxuations in the water content of the oil, their effects on the cellulose insulation would be barely perceptible. Thus, measurement of the parts per million water content of the oil can be misleading as an indicator of the water content in the solid insulation. A method is needed to measure the water content of the paper directly.

5.2 Techniques for Monitoring Moisture in Solid Insulation

One method of monitoring the moisture content of the pressboard is to measure its dielectric properties. Both the permittivity and conductivity of the pressboard have been shown to be sensitive to moisture. Rushall showed using bridge measurements that the loss tangent of oil impregnated pressboard changed from 0.007

for 1% moisture content (by weight) to around 2 for 10% moisture content [32]. He reported a change in permittivity of the oil impregnated paper from $3.8\epsilon_0$ to $18\epsilon_0$ over the same range of moisture contents. These measurements were taken at room temperature, and became progressively worse as temperature was increased. Breakdown, an indication of impending failure, was first encountered at 5% moisture level by weight (corresponding to approximately 35% of the saturation level) at a temperature of 90°C, and at 6% moisture levels at a temperature of 50°C. Thus, these values can be considered the maximum amounts of moisture that can be tolerated in the transformer insulation before failure becomes likely.

5.2.1 Resistance Measurement of Paper Probe vs. Moisture Content

From Rushall's measurements, it is apparent that the conductivity of oil impregnated pressboard changes by orders of magnitude as water is absorbed. Thus, the conductivity should make an excellent indicator for moisture in cellulose insulation. A system was developed by Stannett to measure moisture in insulation using such a strategy [31]. He used a paper probe in lieu of taking direct measurements of the insulation on the windings. Gold electrodes were vacuum evaporated on to each side in a grid pattern to allow easy moisture transference. To accurately reflect the moisture content of the winding insulation, the test probe would be installed in, or around, the windings. Transformers already in service could be fitted with a sensing element either in, or near the top of the tank where it would be immersed in hot oil rising from the windings.

Stannett performed a battery of tests upon his sensor under laboratory conditions to calibrate the device. He found that the resistance of unimpregnated paper ranged from 1×10^{12} ohms to 1×10^{7} ohms for paper in equilibrium with air at 5% to 45% relative humidity. The calibration curve was found to be linear when the log of the conductivity was plotted against the relative humidity of the air with which the paper was in equilibrium. He also found that the calibration curve for oil impregnated paper was basically the same. The insulation resistance in this case ranged from 1×10^{11} ohms to 1×10^{7} ohms for oil impregnated paper in equilibrium with air at 8% to 57% relative humidity. Again, the curve was linear when the log of the conductivity was plotted vs. relative humidity. Using these curves for calibration purposes, probes were actually tested in three operating transformers with some success [31].

5.2.2 Moisture Measurements with the Macro Sensor

The macro sensor, with paper held in place over the plane of the electrodes, would be able to make resistivity measurements, and in addition, also be able to measure the permittivity of the oil impregnated paper. The sensor that Stannett developed could be a very useful instrument, but is limited in its capabilities. The resistance that he measures includes contact resistances, and perhaps other factors that cannot be sorted out. The advantage of dielectrometry lies in its ability to sort out responses

to more complicated systems. It is able, for example, to recognize and account for imperfect contact between the paper and the electrodes, thus allowing for a much more accurate estimate of the dielectric properties of the paper insulation. If the goal was just to measure the water content of the pressboard, Stannett's device would be perfectly adequate and in no way inferior because to measure the moisture content of paper using a macro sensor, a calibration table must also be used. If, on the other hand, the complex permittivity of the paper is to be studied, then it is clear that the macro sensor has significant advantages over Stannet's paper probe.

If the conduction process in the oil impregnated paper is ohmic, then the gain/phase frequency response of the system will have a universal shape with some gain transition and phase excursion, reflecting the relaxation of charge, which shifts in frequency as the conductivity changes. This is a special case of a general class of universal responses that have a "power law" dependence [33]. To get the largest possible phase peak and gain transition as the charge in the paper relaxes, the paper must be held as closely as possible to the electrode plane of the macro sensor. A containment apparatus was developed to hold the paper in place against the sensor while still allowing for free exchange of water between the oil and the paper. The apparatus is illustrated in Figure 5.1. The paper is clamped at the edges between a "window" and a solid back piece with the sensor in the middle. To provide good contact, the sensor is pushed up against the paper using a spring loaded rod through the bottom of the apparatus. The contact between the paper and the electrode plane that is made in this way is not perfect, but is quite adequate.

Experiments with oil impregnated paper using this containment system were performed in a chamber filled with transformer oil. The response of the sensor to paper in oil with 28 parts per million water is shown in Figure 5.2. The two phase excursions and their corresponding gain transitions indicate that two different charge relaxation processes are occuring. The transition occuring at the higher frequencies is attributed to the relaxation of charge in the oil impregnated paper. The transition occuring at lower frequencies is attributed to the relaxation of charge in the transformer oil between the paper and the parylene. Once the paper becomes conducting, it shorts out the macro sensor's response to anything else beyond, and the only other media between the paper and the parylene, which is conducting, is the oil. A reasonable model for this system might be an infinite half space of oil ($\epsilon = 2.2\epsilon_0$, $\sigma = 1 \times 10^{-12}$ mhos/m), a layer of 84μm paper ($\epsilon = 2.2\epsilon_0$, $\sigma = 1 \times 10^{-8}$ mhos/m), a 45 μm oil gap between the paper and the parylene, and a 5μ layer of parylene $\epsilon = 3.1\epsilon_0$, $\sigma = 0$). The predicted response of this system is illustrated in Figure 5.3 and is very similar to the data. The major differences lie in the broader phase excursion and deeper phase peak due to the relaxation of charge in the paper. This is an indication that the conduction process in the paper is either not ohmic in nature, or has some spatial dependence. However, a best fit of the data to a model, where the conduction in the paper has been assumed to be ohmic, can be made by matching the position of the estimated phase peak to the data. A conductivity 4×10^{-8} mhos/m was estimated for the paper in this manner.

This value was determined, by shifting the phase peak of the predicted response in Figure 5.3 by a factor of 4 in frequency to match the phase peak due to the paper

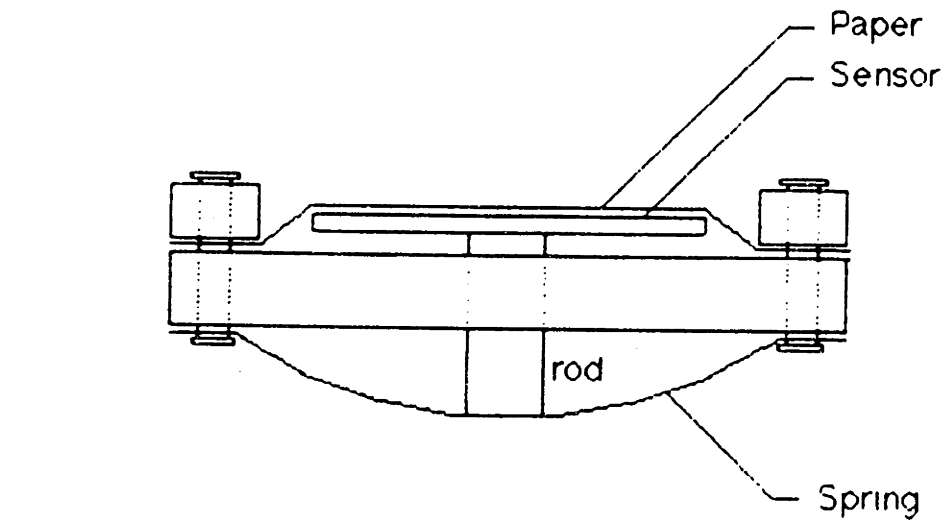

Figure 5.1: Paper Containment Apparatus

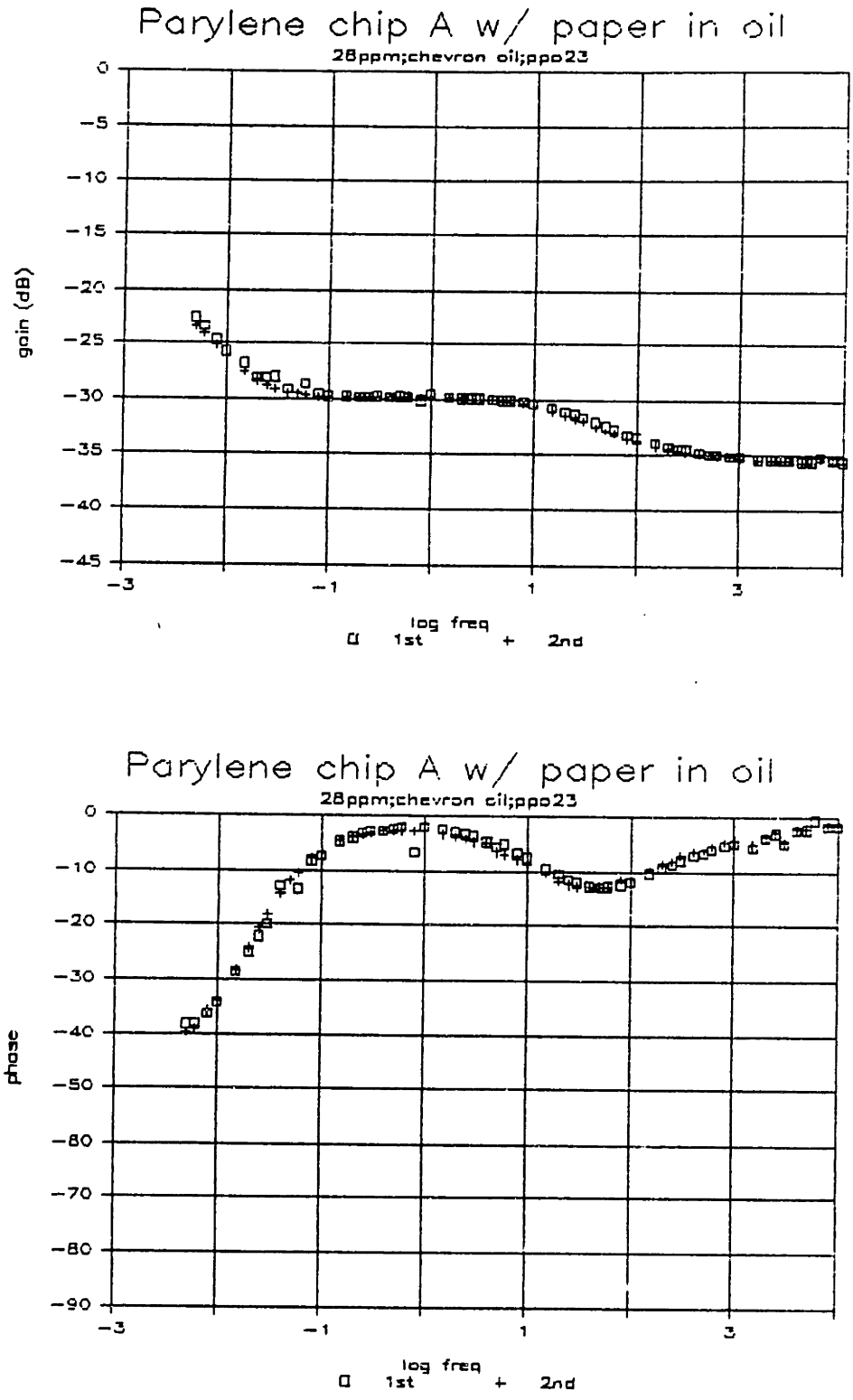

Figure 5.2: Paper in Oil with 28 ppm Water

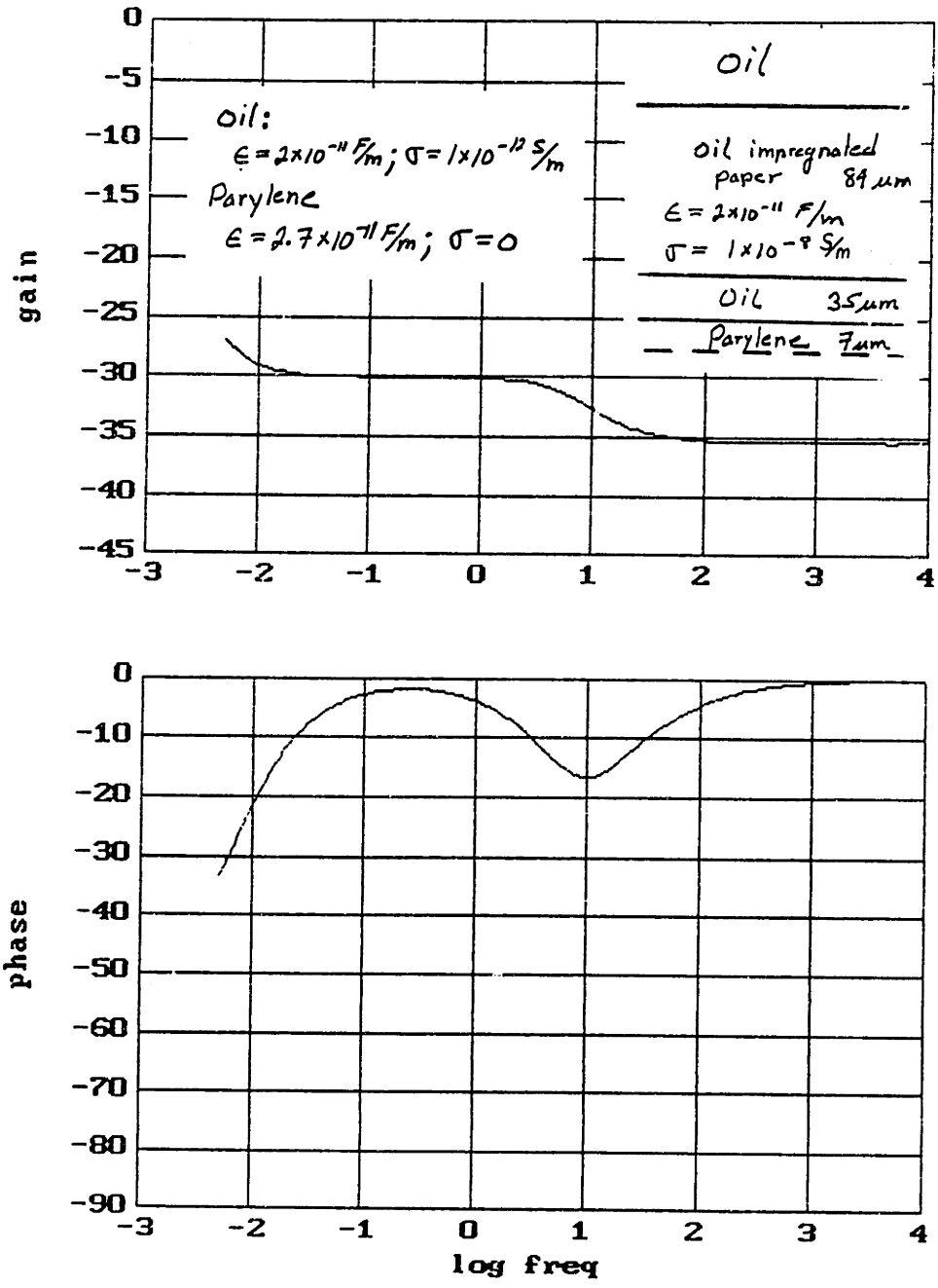

Figure 5.3: Predicted Response of Oil Impregnated Paper

in Figure 5.2. This correlates to a factor of 4 increase in the predicted conductivity of the paper (from 1×10^{-8} to 4×10^{-8} mhos/m). Changing this conductivity in the model does not, however, affect the phase information attributed to the relaxation of charge in the oil between the parylene and the paper. To determine the conductivity associated with the charge relaxation in this oil layer, the conductivity which determined the low frequency phase response of Figure 5.3 is scaled up by a factor of 2 to shift the phase information at the lower frequencies so that it matches the phase of the data. This results in a conductivity of 2×10^{-12} mhos/m for the conductivity of the oil layer between the parylene and the paper. Again, changing this value does not affect the part of the response due to the paper. However, if the conductivity of the paper and the oil become close enough, then a superposition of the two curves results and they can no longer be treated independently. When this occurs, interpretation of the data becomes much more difficult. These observations were made based upon experience with the model, and verified using parameter estimation routines. The shifting of curves in frequency with conductivity becomes trickier for more complicated systems, such as the multi-layered one just analyzed.

The conductivity calculated for the oil between the parylene and the paper is, however, much greater than that observed with a plain parylene coated sensor for the same oil. It is not clear as to why the presence of paper would enhances the conductivity attributed to this oil. Further data, which will be presented shortly, verifies that the conduction process reflected by the phase information at the lower frequencies is not affected by moisture, and thus can not be attributed to the paper insulation.

The values for the permittivy and oil gap thickness used to generate the predicted response of the oil impregnated paper, illustrated in Figure 5.3, was estimated from two different gain curve segments. To estimate the permittivity of the oil impregnated paper, the thickness of the oil gap between the parylene and the oil must first be determined. This thickness can be estimated from the level gain value that is reached after the relaxation of charge in the paper. Essentially, at these frequencies, the paper has become a conductor, and the capacitance of the parylene and oil capped by a "perfect" conductor is specified by their permittivities and the thickness of each layer. An oil gap 35 μm thick was estimated from this information. Once the thickness of this oil layer is known, the permittivity of the paper was estimated, from the high frequency gain, to be approximately $2.2\epsilon_0$.

The oil used in the experiment just described was essentially brand new with a moisture saturation level of around 60 parts per million water at room temperature. Thus, assuming the paper was in equilibrium with the oil (17 ppm water), the paper in the experiment was essentially 28% saturated, corresponding to the previously estimated conductivity of 4×10^{-7} mhos/m. A calibration table can be made in this manner by gathering this information at various moisture contents of the oil.

To increase the moisture in the system, wet nitrogen was bubbled through the oil in the chamber. To decrease the moisture in the system, the chamber would be evacuated. The frequency response of the macro sensor to the oil impregnated paper was taken and the moisture content of the oil determined from a sample. It is assumed that the oil is in equilibrium with the paper when the macro sensor

measurements are taken, and that the saturation level of the oil used in these tests remains constant. Also, all measurements were taken at constant temperature. Figure 5.4 is a plot of the frequency of the phase peak for relaxation of charge in the paper vs. the moisture content of the oil. Given that the assumptions about the oil are accurate (60 ppm water for saturation at room temperature, and that moisture is in equilibrium with the paper), the relative moisture saturation of the paper can be deduced. Also, using the frequency at which the phase curve peaks (fp), the conductivity of the paper can be estimated. Hence, a calibration table of log conductivity vs. relative saturation of the paper can be made and is shown in Figure 5.4. The conductivity changes by close to three orders of magnitude in going from 20% to 80% moisture saturation. This is consistant with Stannett's resistance measurements. Also, the range of moisture levels measured by the macro sensor are in the same range of values reported by Rushall for likely electrical breakdown. Thus, the macro sensor should make a good instrument for measuring critical moisture levels in the paper insulation. The frequency responses, for the data points of the calibration tables, are illustrated in Figures 5.6 through 5.12. Notice that the phase information associated with the low frequency charge relaxation (where data is available) is the same from plot to plot. This indicates that the conductivity of the oil is insensitive to the water, which was also demonstrated in Chapter 3. Also, the shape of the curves associated with the relaxation of charge in the paper seems to be fairly universal as they shift in frequency. These characteristics are important because it indicates that the conduction process in the paper at different moisture contents remains the same.

In addition, a slight increase (less negative) of about 0.5 dB was obseved in the high frequency gain measurement in going from the driest to the wettest paper. This corresponds to an increase of $1.2\epsilon_0$ in the permittivity of the oil impregnated paper as the moisture content increases. This is reasonable because water is very polar ($80\epsilon_0$) in the range of frequencies used by the dielectrometer.

5.3 Dispersion in the Complex Permittivity of the Paper

If a more accurate picture of the conduction mechanism in the paper is desired, then the discrepancies between the data and the ohmic model must be addressed. It was indicated earlier that the two most likely explanations for the non bulk-like response of the paper was either a spatially dependent complex permittivity, or a dispersive complex permittivity. It is unlikely that the conductivity of the paper is space varying because the paper is uniform, and the moisture is given enough time to diffuse equally throughout the paper. Thus, a frequency dependent complex permittivity is likely, and can be estimated using the continuum model.

The physical configuration of an infinite half space of oil, followed by the paper, more oil, parylene, and the sensor, which was used to to estimate "ohmic" conductivity values for paper as function of moisture, can also be used to estimate dispersions in the paper (see Figure 5.3). The complex permittivity of the parylene

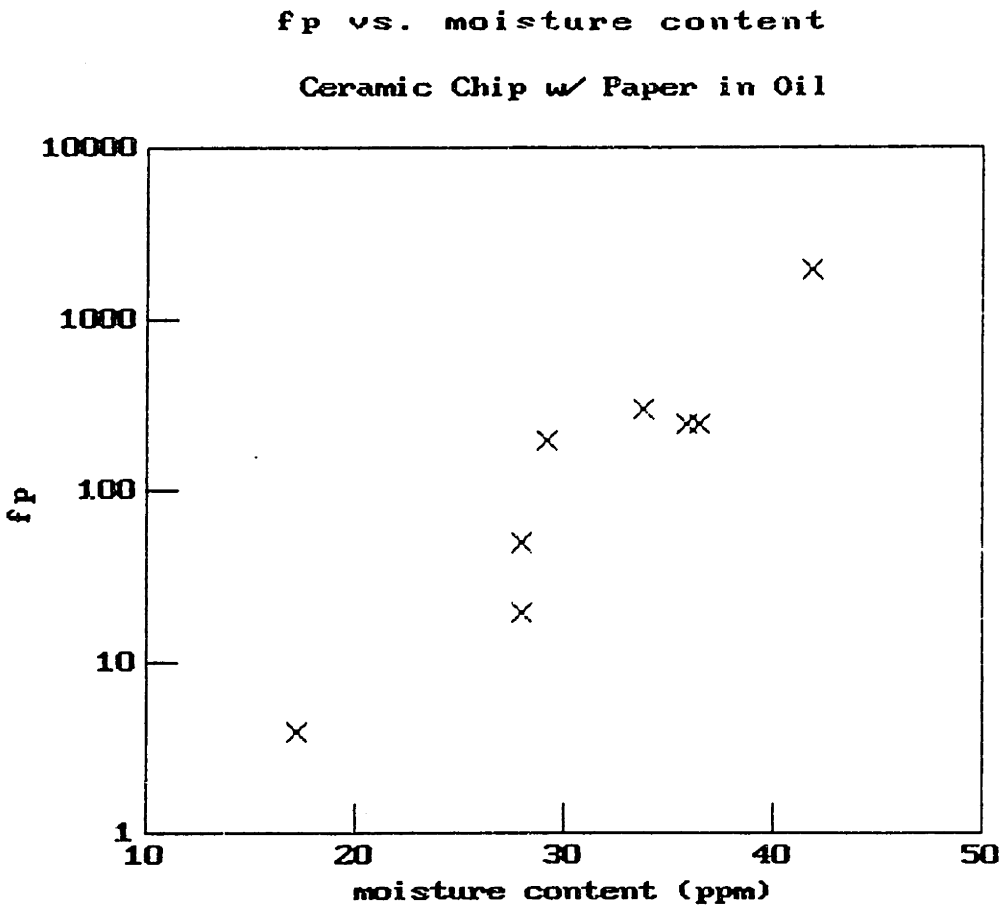

Figure 5.4: Log fp vs. Water content of Oil

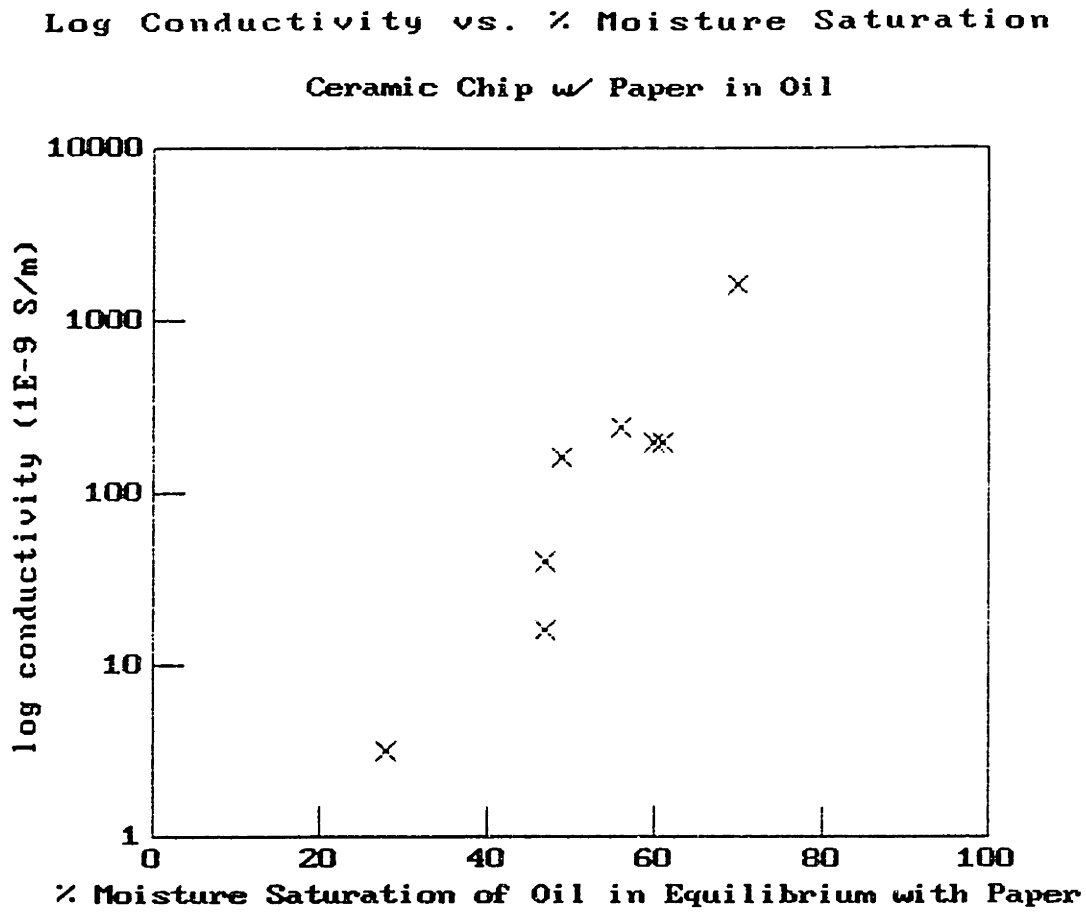

Figure 5.5: Log Conductivity vs. Relative Water Saturation of Oil impregnated Paper

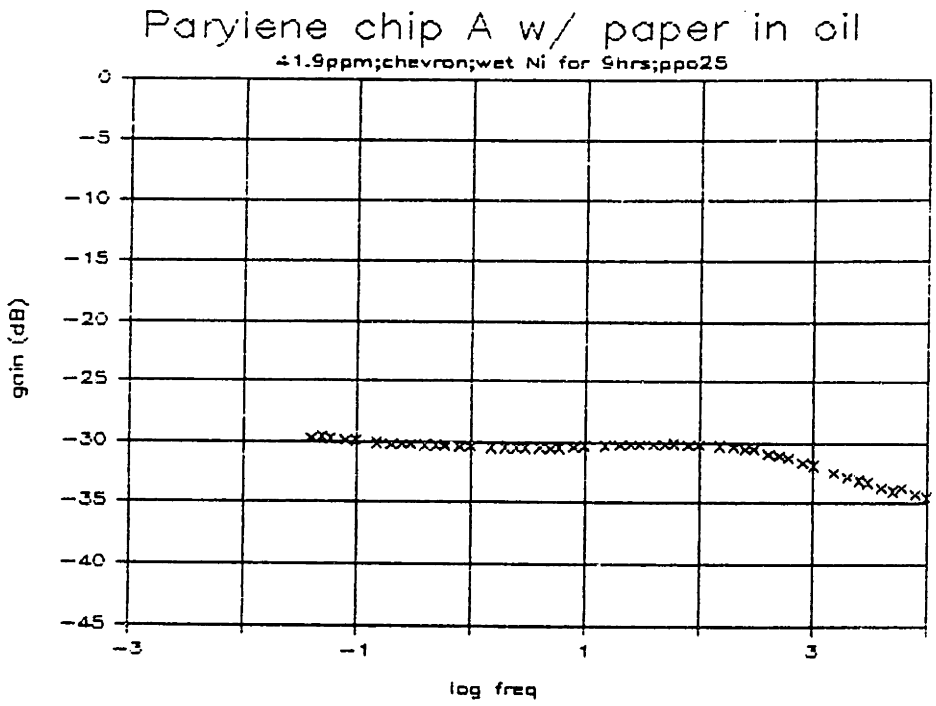

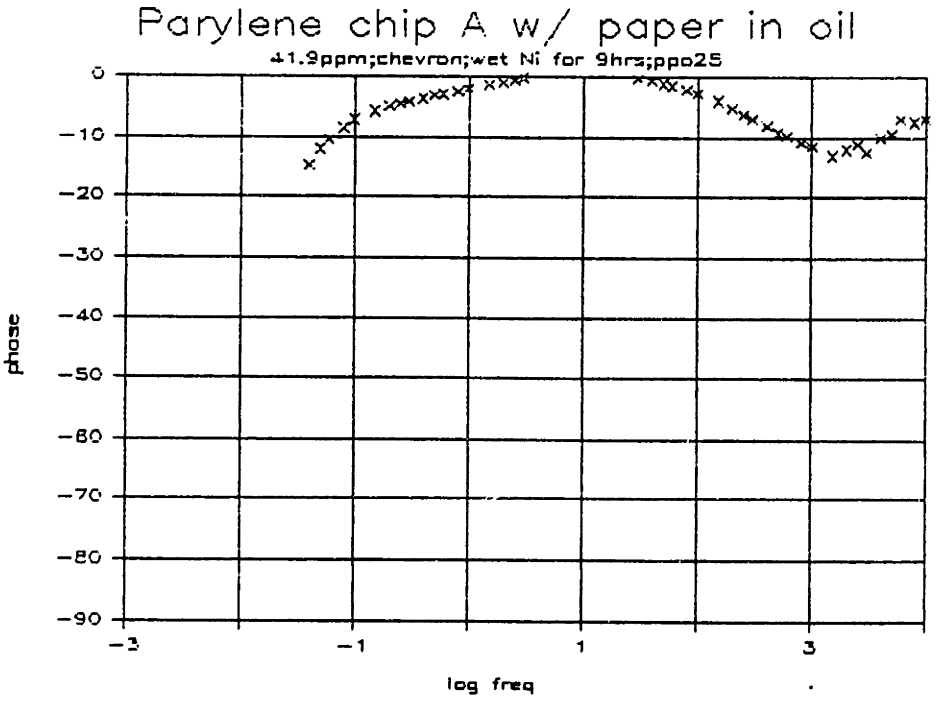

Figure 5.6: Paper in Oil with 41.9 ppm Water

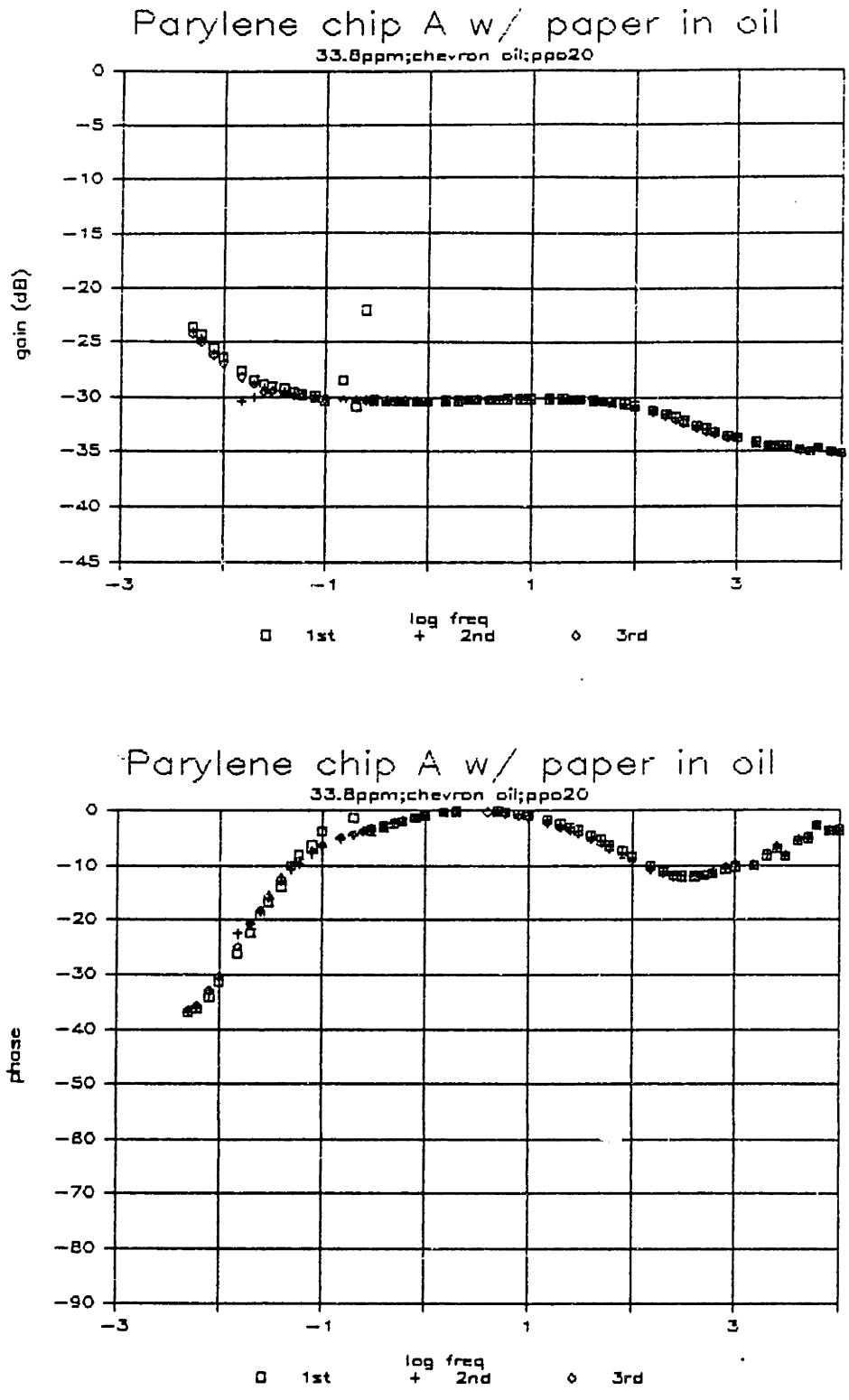

Figure 5.7: Paper in Oil with 33.8 ppm Water

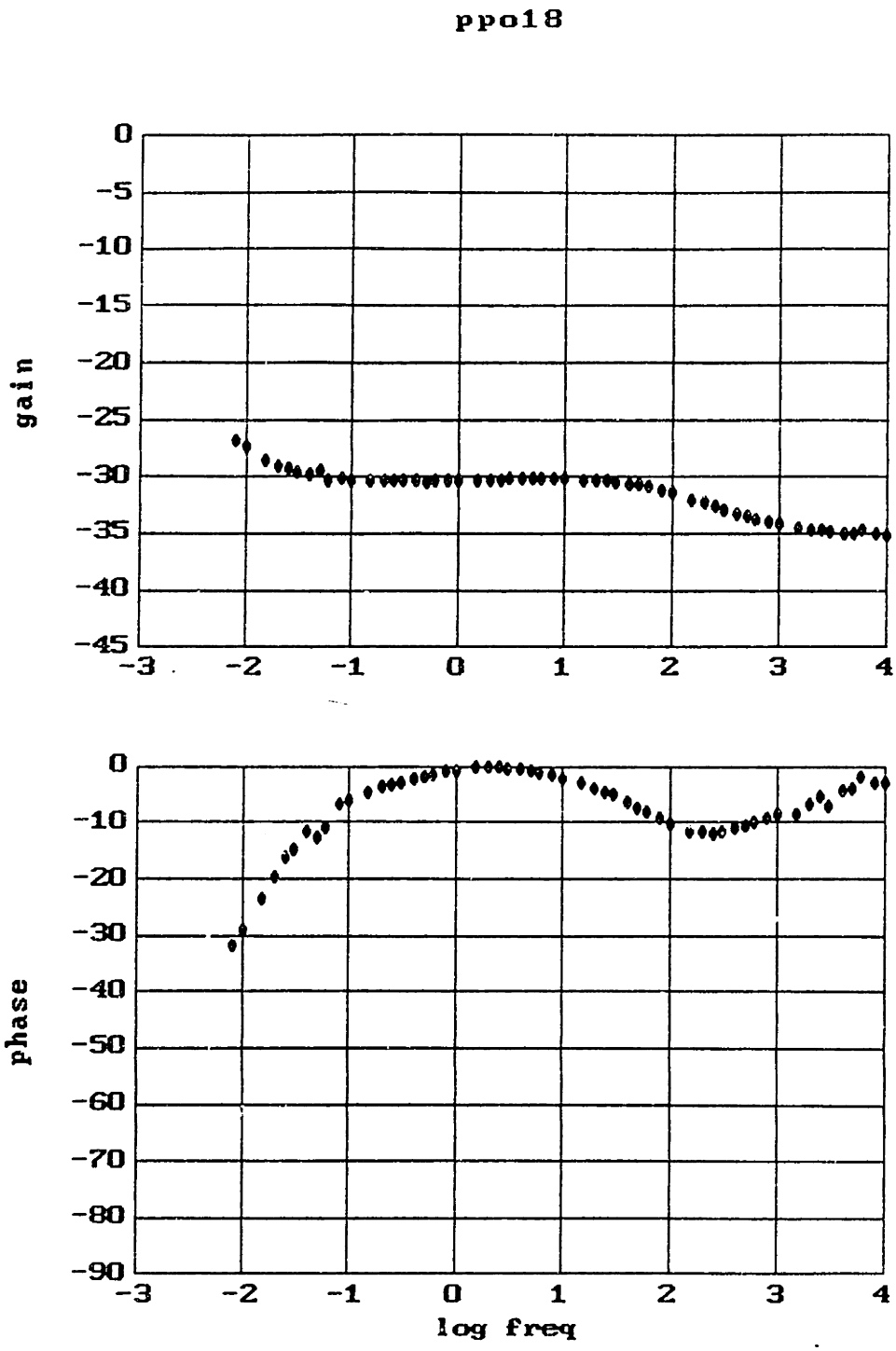

Figure 5.8: Paper in Oil with 36.5 ppm Water

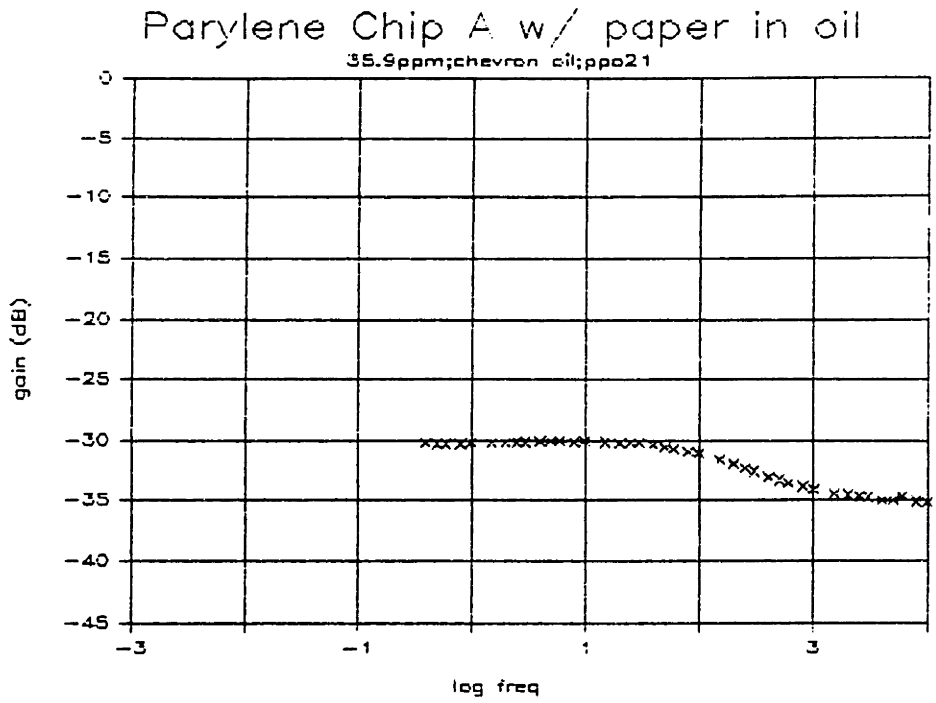

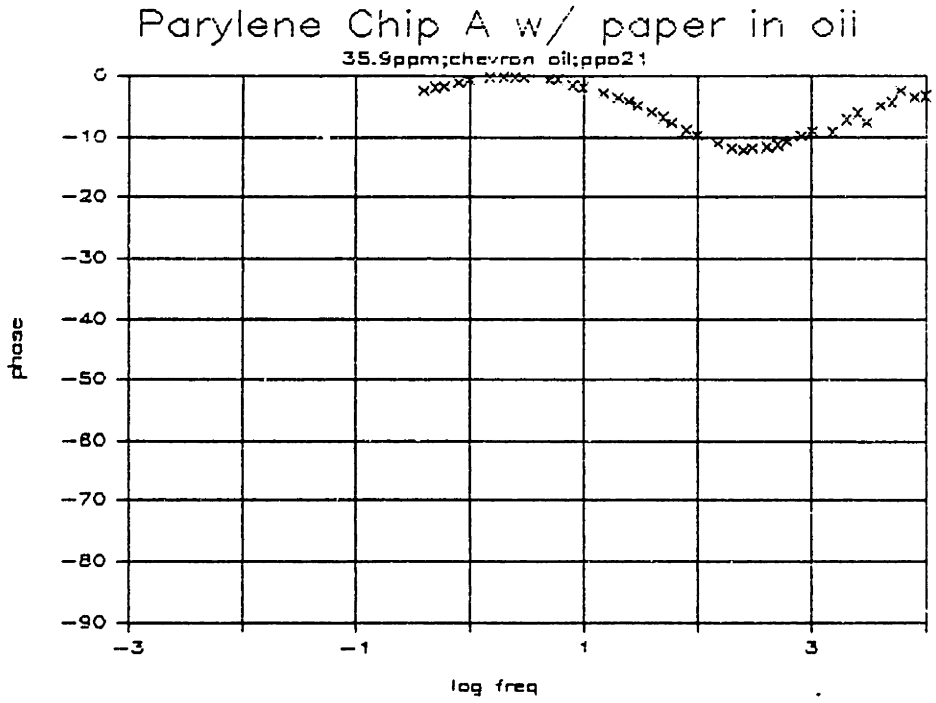

Figure 5.9: Paper in Oil with 35.9 ppm Water

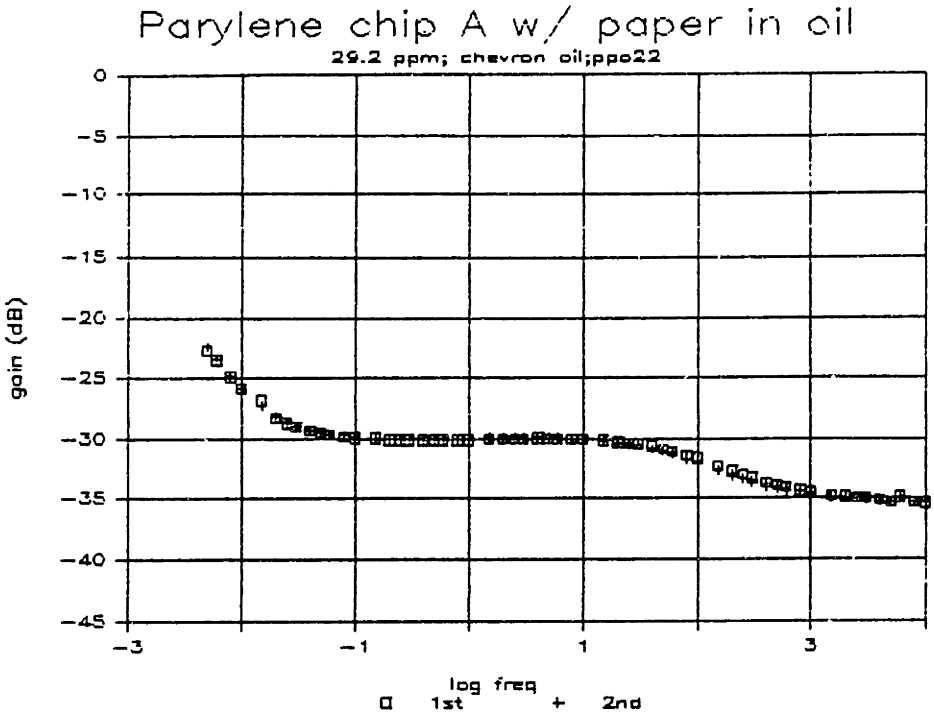

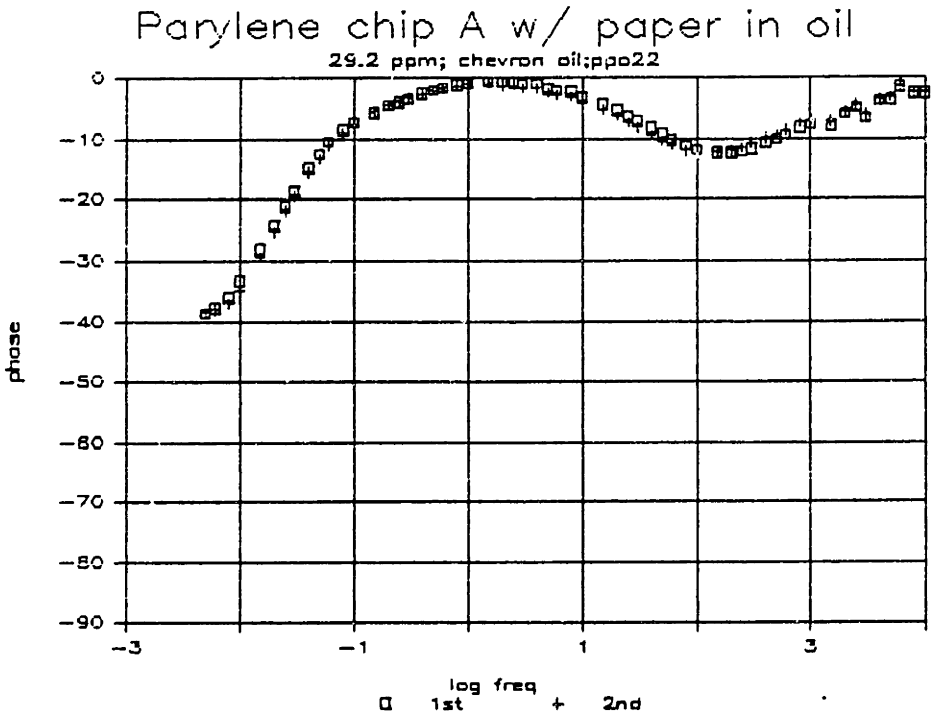

Figure 5.10: Paper in Oil with 29.2 ppm Water

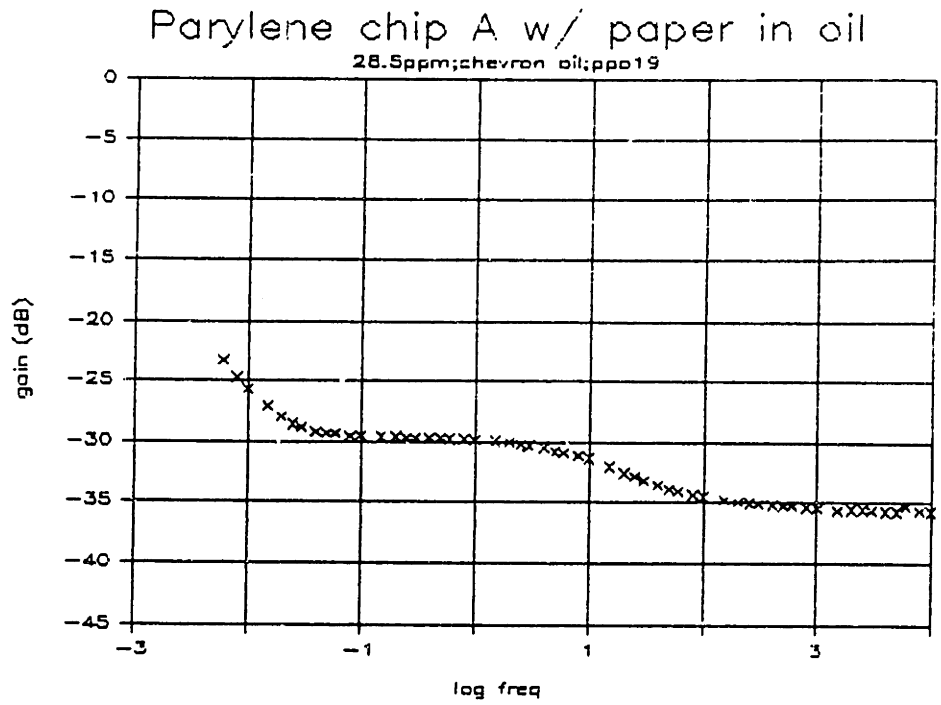

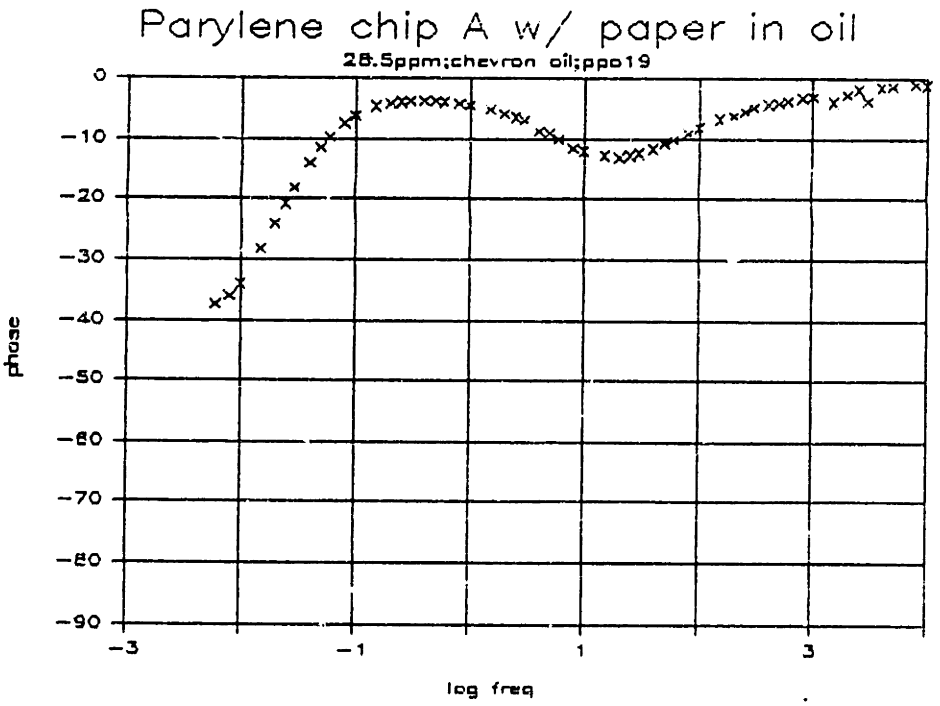

Figure 5.11: Paper in Oil with 28.5 ppm Water

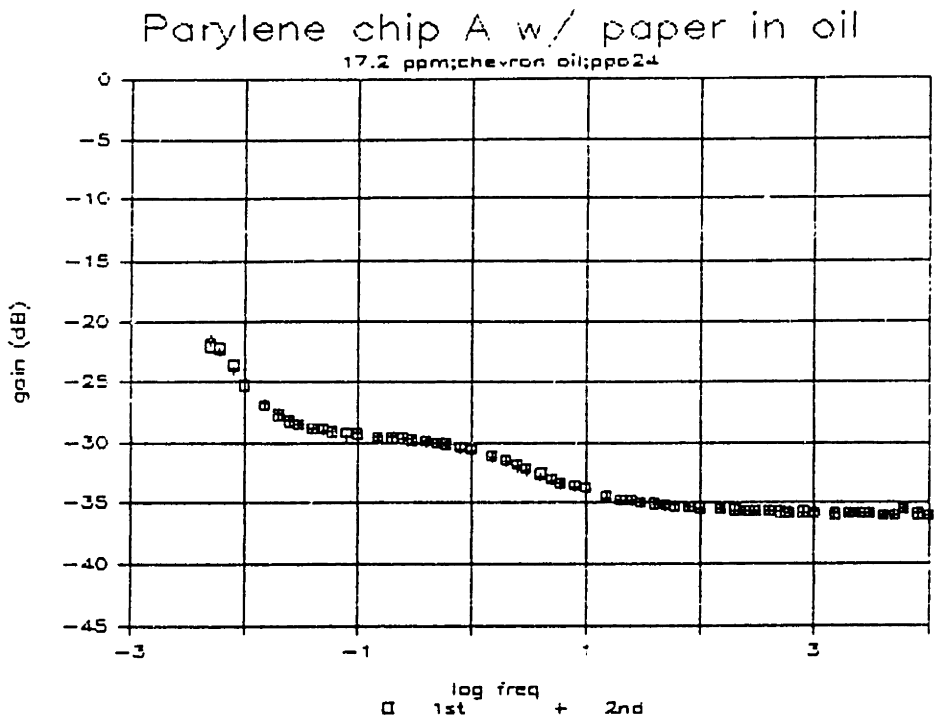

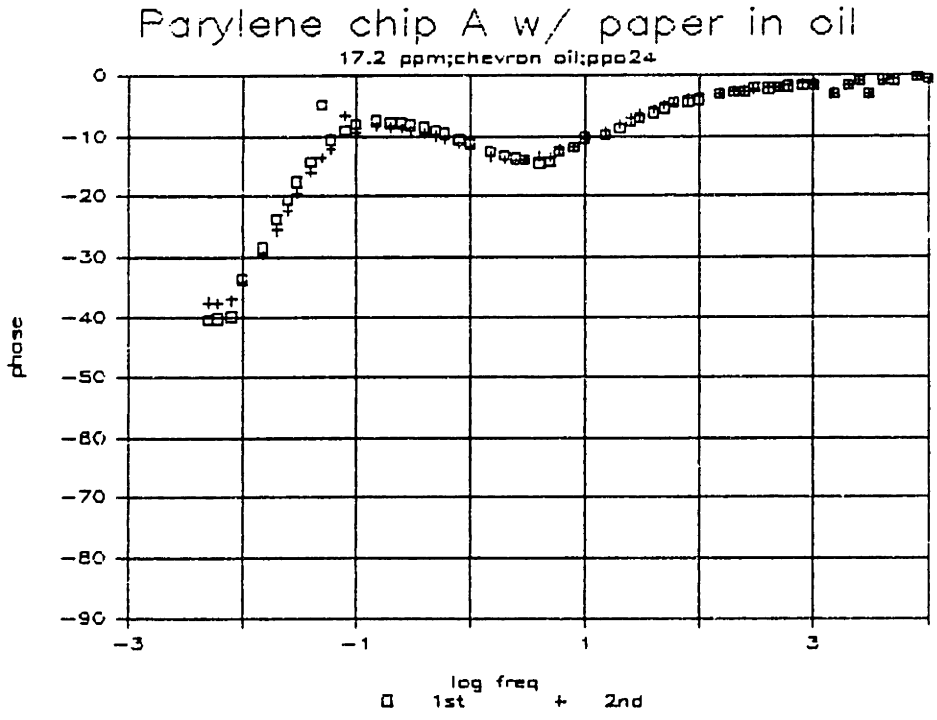

Figure 5.12: Paper in Oil with 17.2 ppm Water

is known, the permittivity of the oil is known, and its conductivity can be estimated from the phase response observed at low frequency. This phase information can be matched using bulk, non dispersive parameters so that the estimation of an ohmic conductivity for the oil is justified. Given these parameters, it is possible to estimate the complex permittivity of the paper at each frequency. Plots of log conductivity and permittivity vs. log frequency are shown in Figure 5.13. The dispersion is then expressed in an ϵ' (permittivity), ϵ'' ($\epsilon'' = \sigma/\omega$) representation where the non dispersive components, ϵ_∞ and σ_{ohmic}, have been subtracted out. The resulting plot is illustrated in Figure 5.14.

The dispersion observed in the paper is reminiscent of a debye dipole response. However, the slopes of the asymptotes for ϵ'' are incorrect. The debye model predicts a $1/\omega$ dependence, whereas the dispersion in the paper has approximately a $1/\omega^{1/2}$ dependence. Also, the debye model predicts a $1/\omega^2$ dependence for ϵ' above the frequency of maximum loss, and the paper exhibits a response closer to a $1/\omega^{1/2}$ dependence. The dispersion of the paper could be matched using a summation of debye responses corresponding to a distribution of relaxation times. This may be reasonable as it would not be difficult to imagine inhomogeneities, on both a macroscopic and microscopic level, which affect the relaxation times of dipoles.

There is, however, a simpler, more universal law described by Jonscher [33] which seems capable of matching the dispersion observed in the paper. The frequency dependence of many different dielectric solids, regardless of their physical and chemical natures, exhibit an ω^{n-1} dependence where n is between zero and one.

$$\epsilon(\omega) = B(iw)^{n-1} \tag{5.1}$$

which can be separated into a real and imaginary part:

$$\epsilon' = B(sin\frac{n\pi}{2})\omega^{n-1} \tag{5.2}$$

$$\epsilon'' = -i(Bcos\frac{n\pi}{2})\omega^{n-1} \tag{5.3}$$

Jonscher describes this "power law" as a universal mechanism for which the ratio of energy lost per cycle to energy stored per cycle is independent of frequency.

The power law dependence also satisfies the Kramer-Kronig transforms which relate ϵ' to ϵ'' according to the following transforms [33]:

$$\epsilon'(\omega) = \frac{1}{\pi}\int_{-\infty}^{\infty}\frac{\epsilon''(x)dx}{x-\omega} \tag{5.4}$$

and

$$\epsilon''(\omega) = \frac{-1}{\pi}\int_{-\infty}^{\infty}\frac{\epsilon'(x)dx}{x-\omega} \tag{5.5}$$

where both are principal valued integrals in the complex plane. Thus, if the frequency dependence of one quantity is known, then the frequency dependence of the other one can be found. One of the consequences of these transforms is that at "zero" frequency, the following relation results:

$$\epsilon'(0) = \frac{2}{\pi}\int_{-\infty}^{\infty}\epsilon''(\omega)d(ln\omega) \tag{5.6}$$

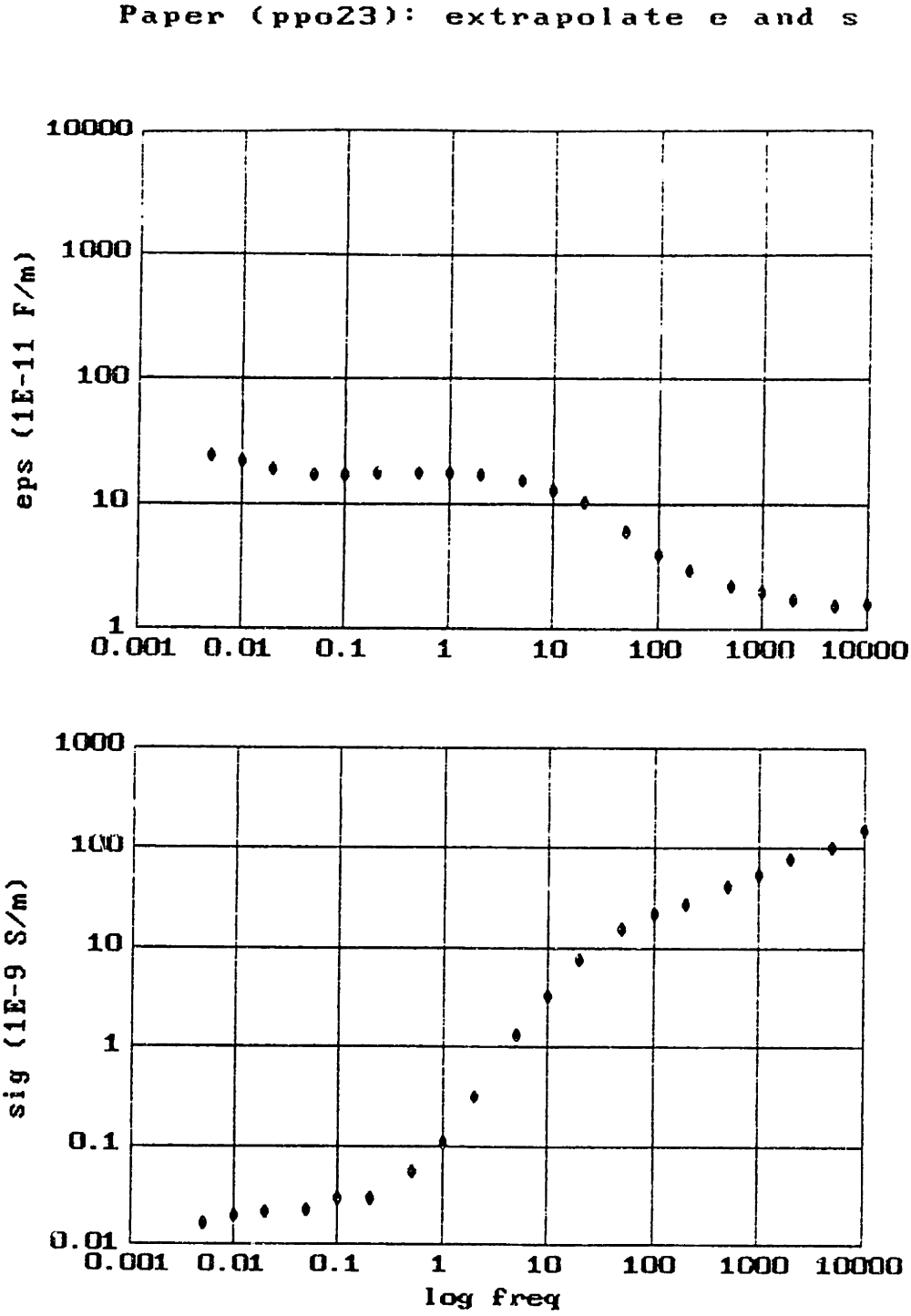

Figure 5.13: Complex Permittivity Dispersion Estimated from Data Presented in Figure 5.2

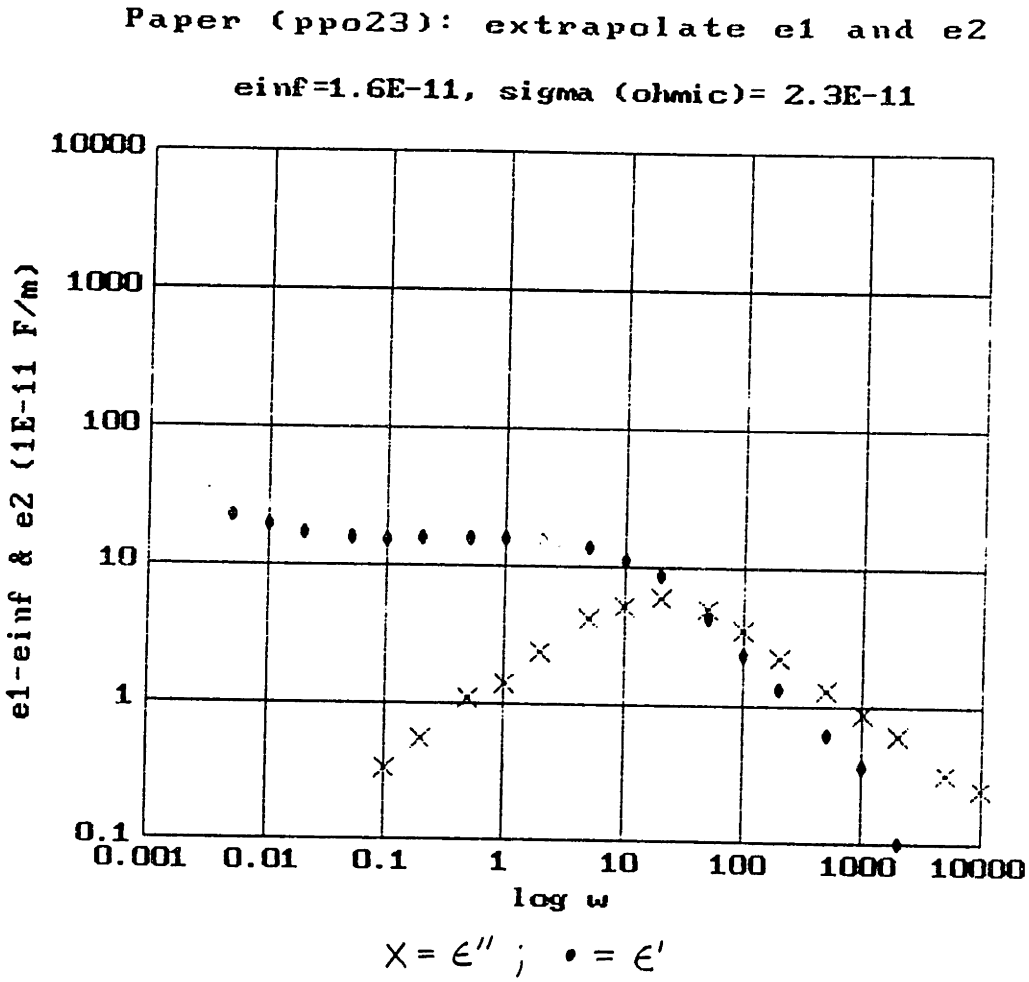

Figure 5.14: Plot of Log ϵ' and ϵ'' vs. Log Frequency (ω) for paper

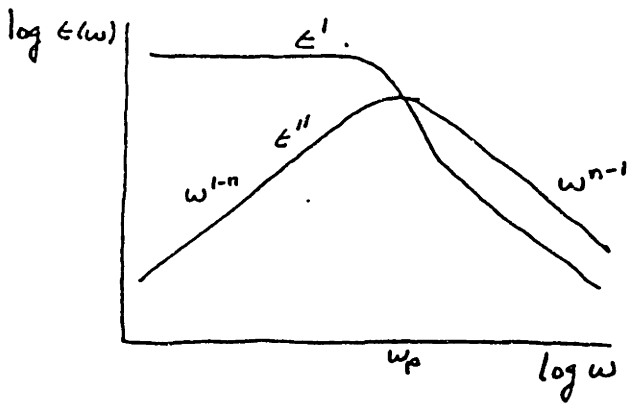

Figure 5.15: ϵ' and ϵ'' for Frequency Dependence of Equation 5.7

This is simple to check for the dielectric dispersion of the paper. The integral of ϵ'' can be thought of as the area under the "triangle" in Figure 5.14 with base extending from -1 (log 0.1) to 4 (log 10000) with height 6×10^{-11}F/m. This gives an area of approximately 1×10^{-10}F/m which matches the low frequency value of 1.6×10^{-10} found for ϵ' of the paper. Thus, the dispersion in the paper seems to satisfy at least one requirement of the Kramer-Kronig transforms. Also, the high frequency ($\omega > \omega_p$, where ω_p is the frequency for maximum loss) asymptotes for ϵ' and ϵ'' will have the same slope if the dispersion follows the power law. ϵ' and ϵ'' for the paper do not start out parallel for frequencies greater than ω_p, but it is possible that they do become parallel at slightly higher frequencies.

To match the dispersion of ϵ'' in the paper, two power laws, one above the peak loss frequency and one below, are combined in the following manner:

$$\epsilon'' \propto \frac{1}{(\omega/\omega_p)^{-m} + (\omega/\omega_p)^{1-n}} \tag{5.7}$$

where $n = m = 1/2$ for the paper. Thus, it is possible to shift the curves in frequency without altering their shapes by changing ω_p. Hence, the change in response of the paper with water content would be attributed to an ω_p which changes with varying moisture in the paper. ϵ' and ϵ'', with frequency dependence given by Equation 5.7, are illustrated in Figure 5.15 [33]. The physical interpretation for the power law involves the characterization of a class of charge species that are intermediate between dipoles and free carriers. Jonscher calls them "hopping" charge carriers.

These carriers spend most of their time in a localized site, and jump from site to site when they attain sufficient energy to overcome the potential barrier. Thus, charges traveling along an extended chain of sites can contribute to the loss factor, whereas charges that bounce back and forth between a localized set of sites contribute to the effective dipole moment. It is unclear what mechanisms in the paper would lead to this type of behavior. At this point, it would seem appropriate to look at various theories for conduction in oil impregnated paper.

5.4 Theory for Conduction Mechanism in Paper

A considerable amount of research has been done in an attempt to determine the conduction mechanisms in paper. However, there still seems to be a general consensus that the electrical properties of paper are not well understood. In this section, some of the theories for conduction in paper are reviewed.

Any theory describing the conduction mechanism in paper must be able to explain the orders of magnitude change in conductivity observed when moisture is absorbed. The bulk of the evidence available indicates that the conduction process is ionic in nature. Consequently, most of the theories that have been proposed center on explaining how ionic conduction in the paper might change by orders of magnitude as moisture is absorbed. There are bascially two ways in which the ionic conduction current in paper can change. There may be changes in the number of ions available for conduction; and there may be changes in the rate at which they move through the material under a given applied voltage (i.e. the mobility of the ions change). O'Sullivan [34] [35] measured the bulk mobility of various ions in cellulose film with high salt contents and calculated values of conductivity which were of the same order as his experiments. He found that the mobility of ions increased rapidly with moisture content. The mobility of hydrogen ions, for example, ranged from $3\times10^{-8}\text{cm}^2\text{volt/sec}$ at a moisture content of 10% of saturation to $8\times10^{-5}\text{cm}^2\text{volt/sec}$ at a moisture content of 40%.

O'Sullivan [36] suggests the following reasons as to how moisture affects the conductivity of cellulose films: (i) viscous hindrance to ionic movement in fine capillaries in the cellulose, (ii) the degree of absorption of the salt ions on the cellulose (conductance proportional to number of free ions), (iii) the degree of adsorption of water molecules on the cellulose, (iv) the effective dielectric constant of the medium, which determines the conductance of the salt, (v) the number of continuous conducting paths in the cellulose, or (vi) the frequency of forward continuation of discontinous conducting paths. From looking at theoretical and experimental temperature coefficients, O'Sullivan concluded that above 50%, the dominant factor is the viscous hindrance of ions along capillaries, and for moisture contents below 20%, the dominant factor is the frequency of forward continuation of discontinuous conducting paths. He discounts factor (ii) from unpublished data that he has indicating little to no adsorption of salt ions, factor (iii) because it is insufficient to account for the change in conductance, and factor (v) because it isn't able to account for changes in conductivity with temperature. O'Sullivan concedes, however, that factor (iv)

may be a reasonable explanation for the conduction phenomena observed in paper.

X-ray studies of paper show that its structure consists of crystalline regions interspersed with amorphouse cellulose. At high moisture contents, when the cellulose is swollen, the intercrystalline regions may be regarded as capillary channels filled with water and amorphous cellulose. The channels cause a viscous hindrance to the transport of hydrated ions. As the moisture content decreases, the cross sections of the channels also decrease, increasing the viscous hindrance to ion migration which results in a decrease in conductance. This would also explain the drastic change in ion mobilities observed. As the moisture content decreases even further, a transition may occur where the intercrystalline regions go from moisture filled channels to thin films of water on the crystallites and chains of amorphous cellulose. A further reduction might then produce breaks in the films. At moisture contents below 20%, O'Sullivan argues that the principal factor affecting the transport of ions appears to be due to ions being stopped at breaks in these water channels until they can be "repaired" by condensation of water molecules from the gas phase. Conduction at moisture levels between 20% and 50% can then be explained by a combination of these two theories.

Hearle [37] argued that the theory of conduction at low moisture contents proposed by O'Sullivan breaks down when one considers the effect of polarization, due to the separation of charges, that occurs when positive and negative ions move to opposite ends of a "broken" path. The development of this reverse field will, at some point, cancel the applied field and the forces associated with it. When this equilibrium condition is reached, ions in that path segment will no longer migrate to the ends. Hearle identifies some weaknesses in this theory, but does not dismiss it outright. He suggests, instead, that a better explanation might be that a small increase in the dielectric constant of the paper due to absorption of water causes a large increase in the dissociation of ion pairs. He did not, however, have sufficient data to conclusively support this theory. In fact, he states that both hypothesized conduction mechanisms probably have some effect, and that one can only try to determine whether one is predominant. Hearle believed, however, that the effect of dielectric constant rested on a surer theoretical foundation, and involved fewer arbitrary assumptions, than the effect of frequency of forward continuation of discontinuous paths. For higher moisture contents, Hearle is in agreement with O'Sullivan in that they both believe that viscous hindrance of ion migration is probably the governing mechanism.

The two theories for low moisture conduction, and the single theory for high moisture conduction in paper seem to encompass most of the ideas that were encountered in the literature review. A good summary of these theories and their variations are presented in Chapter 21 of the *Handbook of Physical and Mechanical Testing of Paper and Paperboard, Vol. 2*, edited by Richard E. Mark [38].

Unfortunately, none of these researchers attempt to give an actual dispersion relation for the complex permittivity of the paper. Consequently, it is not possible to test the data obtained with the macro sensor against any of these theories. Also, it is unclear whether or not the idea of "hopping" charge carriers, described by Jonscher, is consistant with these theories. Thus, the next step might be to

determine the plausibility of "hopping" charge carriers as the conduction mechanism in oil impregnated paper.

Chapter 6

High Frequency Measurements of Particles in Transformer Oil

It was indicated in Chapter 4, in the section on Zaretsky's parameter estimation strategies, that certain quantities could be estimated from the data if enough is known about the rest of the system. One such quantity that can be estimated is the thickness of films adjacent to the sensor. This estimation scheme takes advantage of the fact that the high frequency (i.e. lossless) gain response is a function of the thickness and permittivity of the film, and the permittivity of the infinite half space beyond. If the permittivity of the film is different from that of the infinite half space, then changes in the thickness of the film will be reflected in the high frequency gain. If the permittivities of the film and the oil are known, then the thickness can be estimated from the high frequency gain. In addition, the film thickness must be less than $\lambda/3$, or the sensor considers it to be an infinite half space.

In this chapter, the feasibility of applying this estimation strategy to the macro sensor for use as a particle detector is explored. First, some initial experiments are performed, with tightly controlled parameters, to study the feasibility of measuring the thickness of a layer of sedimented particles on a macro sensor. An uncoated sensor is used to maximize sensitivity to the dielectric constant of the adjacent layer, and because only high frequency measurements are needed, moisture absorption by the aluminum oxide is not a problem. Then, the problems that are encountered in trying to use the macro sensor as a general particle sensor are discussed.

6.1 Sedimentation of Monodisperse Particles

To study the feasibility of measuring sedimenting particles using a macro sensor, an experiment was designed with the goal of minimizing the number of variables in the problem. The particles used in the experiment were Potters Glass Beads (H-002) which were sifted to minimize dispersions in the particle sizes. The glass beads are spherical, approximately 41μm in diameter, and have a mass density of 4493 kg/m^3 [39]. The permittivity and loss tangent at 1 kHz are respectively $16.8\epsilon_0$ and 0.0013. Thus, the particles should be basically lossless at 10 kHz, which is important

because the thickness estimation scheme relies upon a lossless gain measurement. This information completely characterizes the particles for the purposes of these experiments.

The properties of the oil relevant to the sedimentation problem at room temperature are its mass density (870 kg/m^3) and its viscosity. The oil's viscosity of 0.0164 kg/ms was measured, at room temperature, using a viscometer. These properties of the oil, along with the size and mass density of the particles, determine the sedimentation rate of the particles in the oil. The equations governing the dynamics of this process are presented in the following section.

6.1.1 Equations Governing Particle Sedimentation

The equation governing the rate of sedimentation of particles in the oil is given by Stoke's drag force on a rigid sphere falling through a static fluid (MKS units).

$$6\pi\eta a U_0 = \frac{4}{3}\pi a^3(\rho_p - \rho_{oil})g \tag{6.1}$$

where η is the viscosity, U_0 the settling velocity of the particles, a the particle radius, ρ_p the mass density of the particles, ρ_{oil} the mass density of the oil, and g gravitational acceleration (9.8 m/s^2). It is a good approximation provided that viscosity dominates inertial effects in the fluid flow around the sedimenting particle. This corresponds to having a Reynolds number, $\rho U_0 2a/\eta$, less than one [40]. A settling velocity of 192 μm/s for the glass beads was determined by timing the movement of the front between clear oil and murky oil as the particles settled. The Reynolds number was found to be 0.42 using this velocity. Thus, the approximation should be a reasonable one. From Equation 6.1, the velocity U_0 is found to be:

$$U_0 = \frac{2}{9}\frac{a^2}{\eta}(\rho_p - \rho_{oil})g \tag{6.2}$$

The settling velocity calculated from Equation 6.2 is 211 μm/s which is in agreement with the observed value.

The other quantity that is of interest is the rate of rise of the accumulated layer at the bottom of the sedimentation chamber. This rate is determined by the settling velocity U_{bot}, the density of particles in the oil when well mixed p_0, and the density of particles in the accumulated layer p_m.

$$U_{bot} \approx \frac{p_0 U_0}{p_m} \tag{6.3}$$

where p_m is assumed to be much greater than p_0. Furthermore, the density of particles in the accumulated layer (p_m) can be expressed in terms of the voidage ϕ (the fraction of space in a unit cell that is not occupied by the particles) as

$$\phi = 1 - \frac{4}{3}p_m\pi a^3 \tag{6.4}$$

This allows Equation 6.3 to be rewritten in terms of the voidage ϕ:

$$U_{bot} \approx \left(\frac{p_0 U_0}{1-\phi}\right)\frac{4}{3}\pi a^3 \tag{6.5}$$

Thus, if the rate of rise of the accumulated layer could be measured, then its voidage could be determined. In the next section, a technique is presented for measuring the thickness of the sedimented layer using a macro sensor. The voidage that is calculated from the measured rate of rise of this layer is then shown to be consistant with the "effective" permittivity calculated for the oil/particle system.

6.1.2 Experimental Measurements of Sedimenting Particles

The expermimental setup is illustrated in Figure 6.1. The Macro sensor is placed at the bottom of a circular well that holds 150 ml of oil. An initial uniform particle density, p_0, of 1.83×10^{11} particles/m^3 was chosen to give a reasonable rate of rise for the layer accumulating on the macro sensor assuming a voidage of around 50%. For 150 ml of oil, this corresponds to 4.78 grams of the glass beads. To start the experiment, the particles are vigorously stirred to provide an even distribution of particles throughout the sedimentation cell. Macro sensor measurements are then taken every ten seconds at 10 kHz as the particles are allowed to settle. The phase response is essentially at zero, indicating that there are no losses in the system, and a plot of the high frequency gain vs. time is shown in Figure 6.2. Once the accumulated layer has reached a thickness greater than $\approx 330\mu$m ($\lambda/3$), the macro sensor can be considered as measuring an infinite half space. From the "saturated" high frequency gain of -35.05 dB, the average, or effective permittivity, of the oil/particle system is estimated to be $6.1\epsilon_0$. Once the effective permittivity of an "infinite" particle bed has been determined, it is possible to go back to the gain measurements taken before the response of the macro sensor was saturated and estimate the thickness at each time interval. The plot of estimated thicknesses vs. time is illustrated in Figure 6.3. The increase in thickness is linear in time. The slope of the line, 2.64μm/s, is the rate at which the particles rise as they accumulate. A voidage of 43% is calculated using Equation 6.5. In the next part, the voidage inferred from calculating an effective permittivity is shown to be consistant.

6.2 Effective Permittivity

Consider spheres with some permittivity ϵ_p embedded in a medium of permittivity ϵ. The effective permittivity is defined according to the following formula:

$$\vec{D} = \epsilon_{eff}\vec{E} \tag{6.6}$$

where $\vec{E}$ is the average macroscopic field excited in the medium, and $\vec{D}$ is the total electric displacement field. The displacement field is determined in part by the polarization of the medium:

$$\vec{D} = \epsilon\vec{E} + \vec{P} \tag{6.7}$$

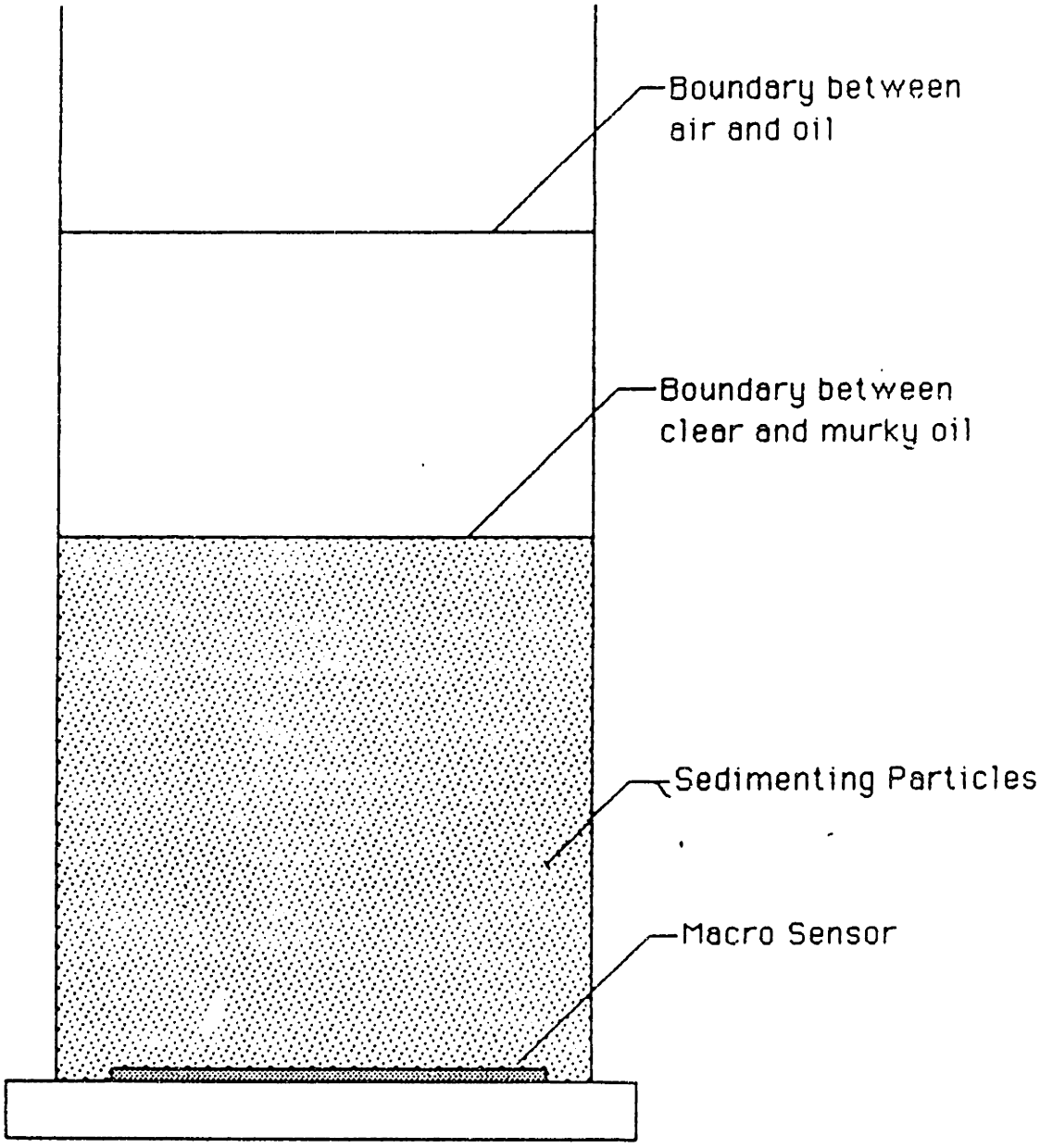

Figure 6.1: Sedimentation Cell with Macro Sensor at Bottom

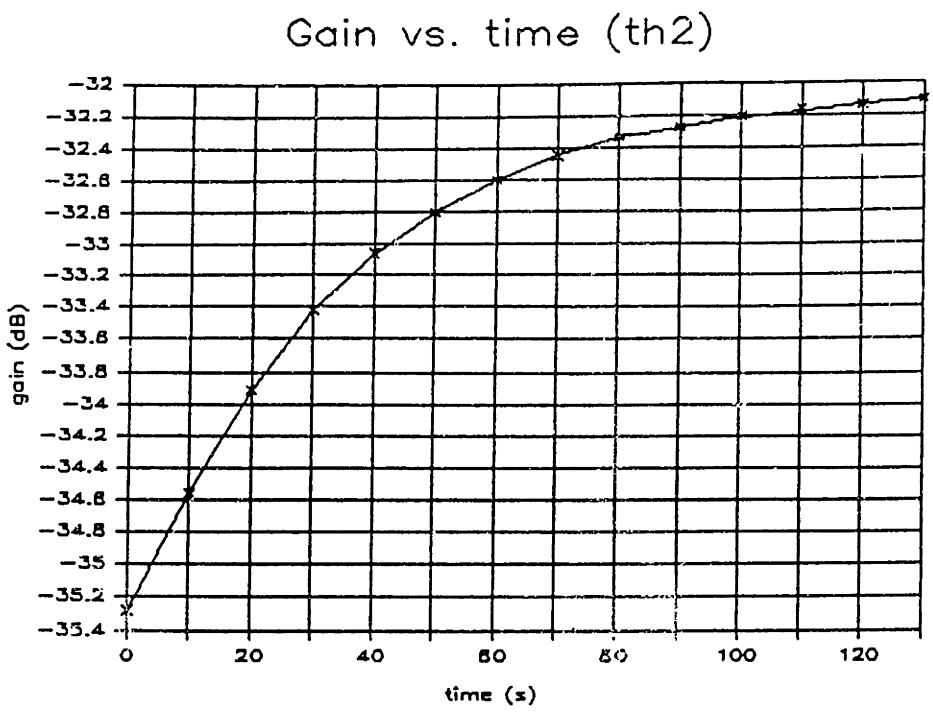

Figure 6.2: Gain at 10 kHz vs. time (seconds) as Particles Accumulate

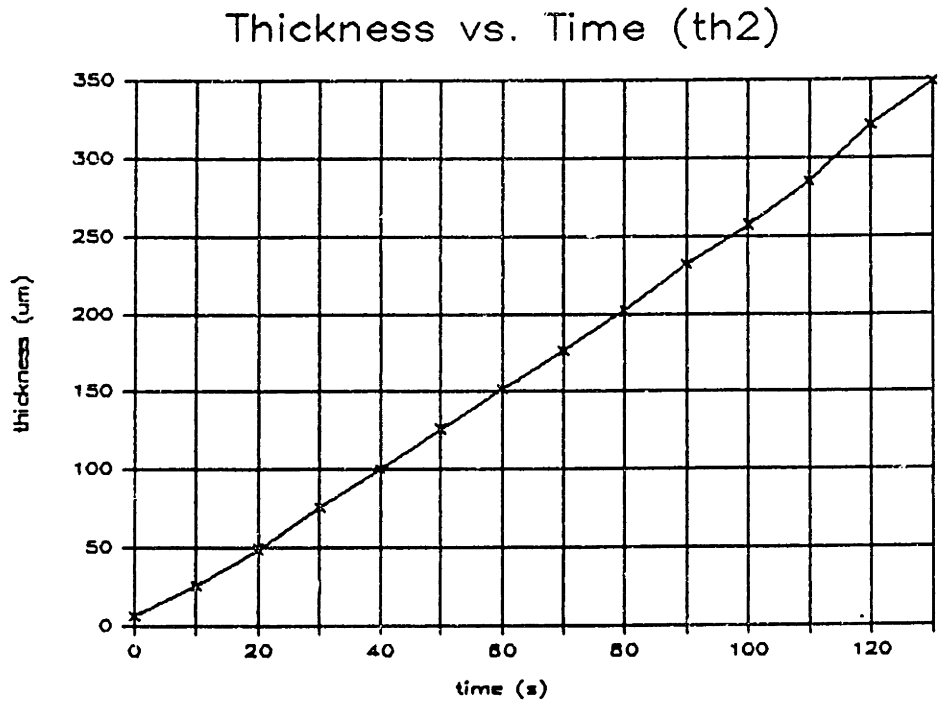

Figure 6.3: Estimated Thickness vs. Time

The polarization is determined by the dielectric properties, the volume fraction of the spheres, and the polarizability of each constituent. The induced dipole moment of a sphere is determined by the excitation electric field $\vec{E}_e$, where the average field and the excitation field differ by the depolarization field [41]:

$$\vec{E}_e = \vec{E} + \frac{\vec{P}}{3\epsilon} \tag{6.8}$$

The polarization per unit volume is given by the dipole moment for one sphere multiplied by the number of spheres per unit volume. The dipole moment for a single sphere is given by:

$$\vec{p} = 4\pi\epsilon a^3 \left(\frac{\epsilon_p - \epsilon}{\epsilon_p + 2\epsilon}\right)\vec{E}_e \tag{6.9}$$

Multiplying by the particle density of the bed, and rewriting in terms of the voidage gives:

$$\vec{P} = 3\epsilon(1-\phi)\left(\frac{\epsilon_p - \epsilon}{\epsilon_p + 2\epsilon}\right)\vec{E}_e \tag{6.10}$$

Substituting this equation into Equation 6.7, and replacing $\vec{E}_e$ with $\vec{E}$ using Equations 6.8 and 6.10, gives the following result (often referred to as the Lorentz sphere model) [42]:

$$\vec{D} = \frac{\epsilon[3\epsilon_p + 2\phi(\epsilon - \epsilon_p)]}{[3\epsilon + \phi(\epsilon_p - \epsilon)]}\vec{E} \tag{6.11}$$

Substituting in the parameters of the experiment ($\epsilon = 2.2\epsilon_0$, $\epsilon_p = 16.8\epsilon_0$, and $\phi = 0.43$), the effective permittivity is calculated to be $6.4\epsilon_0$. This is in reasonable agreement with the value of $6.1\epsilon_0$ that was estimated from the high frequency gain measurement of the macro sensor. Thus, the voidage which determines the effective permittivity, is consistant with the voidage found from the rate of rise of the sedimented layer.

6.3 Feasibility of Particle Detection in a Transformer

Under very special conditions, where all the properties of the particles and oil relevant to the problem are specified, it is possible to determine the density of particles in the oil from the rate of rise of the accumulating layer. However, in an actual transformer, the particles are probably non-spherical, and non uniform in size and mass density. Given these variables, it becomes basically impossible to estimate the density of particles in the oil even if the dielectric properties of the oil and particles are known. If the dielectric properties are also unknown, then the problem becomes even more hopeless. In addition, if the particles are very conducting, then a single monolayer would problably be sufficient to short out the sensor. A shorted sensor is unable to provide much information, except to indicate the presence of conducting contaminants in the oil. Thus, the use of a macro sensor in the transformer as a particle detector is most likely not practical.

Chapter 7

Dielectric Measurement of Particle Coatings as Degradation Products are Adsorbed from Transformer Oil

In this chapter, the feasibility of using particles placed on a parylene coated macro sensor to detect degradation products in the oil is explored. The strategy of looking for changes in the dielectric properties of a particle bed, immersed in some fluid, as targeted substances are adsorbed, was first explored by Fuchs (MIT). He used an uncoated macro sensor, operating at frequencies over 1 Hz, to develop a detector for liquid chromatographic applications [43]. His goal was to dielectrically detect changes in a bed of specially treated silica gell as the separated eluents passed through sequentially in time (separation process occurs in a column of particles designed specifically for that purpose). He used chromatographic grade acetonitrile as his liquid carrier and was trying to detect vitamin E acetate and Vitamin D_2 as they passed through the detector. Fuchs used a high pressure liquid chromatography pump to force the acetonitrile carrier through a particle bed packed on the surface of an uncoated macro sensor.

In the experiments to be presented in this chapter, the transformer oil is the liquid carrier for the degradation products that are to be dielectrically detected as they are adsorbed by the particle bed. Pumping the oil through a particle bed with a parylene coated macro sensor in the configuration used by Fuchs is inpractical because of the high pressures involved. The pressure necessary to pump transformer oil through a bed of particles is high enough to damage the parylene coating on a macro sensor, thereby exposing it to effects of moisture contamination. Thus, a somewhat different approach is used for the experiments to be presented.

The particles tested in this chapter include fuller's earth, which is used to clean transformer oil, and various types of liquid chromatographic grade silica gel, which is used for separation of eluents in liquid chromatography. Both are candidates because of their tendency to adsorb certain types of molecules onto their surfaces. The strategy is to expose the particles to the oil, and look for changes in the dielectric

response of the system as the properties of the oil are changed through oxidation. It is fairly certain that both types of particles will adsorb degradation products from the oil. The uncertainty in this strategy, due to the lack of understanding about the surface chemistry at the interface between the oil and the particles, lies in whether a change will be observed in the dielectric properties of the oil/particle mixture as degradation products are adsorbed. In addition, there is a lack of data regarding the types of products that are generated, outside of gasses, when the oil is degraded in various ways. This lack of information makes it difficult to approach the problem using physical insights. Basically, the approach taken here is to try various experiments and then analyze the results. In addition, because the dielectric properties of these particles are unknown, the interpretation of results becomes even more difficult. There is no a priori information from which to work from.

In the experiments to be presented in this chapter, the oil is degraded in two ways: it is oxidized, and its moisture content is increased. The oil is degraded through oxidation because it is simple to do, and more seems to be known about the effects of non gaseous by products of this degradation process than about others. The particles are also contaminated with water to determine if it dominates the response of the system. This is important because moisture content would be an uncontrolled factor when taking measurements in a transformer, and these experiments are aimed at measuring contaminants other than moisture. Finally, an attempt is made to interpret the results of these experiments.

7.1 Experimental Procedures

The first step in the experimental procedure was to degrade some oil. This was done by heating good oil at 100°C for approximately 6 hours while exposed to oxygen. Then, to determine if the particles adsorb degradation products, the oxidized oil is pumped through a bed of the particles, and dielectric measurements with the macro sensor were made of the oil before and after filtering. Changes in the color of the oil were also noted. The filtering apparatus is shown in Figure 7.1. It is very similar to the one used by Fuchs in his experiments except for the absence of a macro sensor. The oil is pumped through this bed with approximately 200 pounds per square inch pressure using a high pressure chromatography pump (courtesy of Waters Associates). If a particular type of particle adsorbs constituents from the oil which are associated with oxidation (i.e. it either reduces the conductivity of the oil, or changes its color), then further experiments are performed to determine if there is a change in its dielectric properties.

The first set of microdielectric measurements are made on the particles used to filter the oil. The particle/oil mixture, which resembles a paste, is removed from the filtering apparatus and smeared upon a parylene coated macro sensor. The paste is spread on thick enough to insure that the macro sensor sees it as an infinite half space. Microdielectric measurements are then made for comparsion to later data.

To use a particle bed directly with a macro sensor in transformer oil, a containment cell must be designed to hold the particles in place over the electrode plane

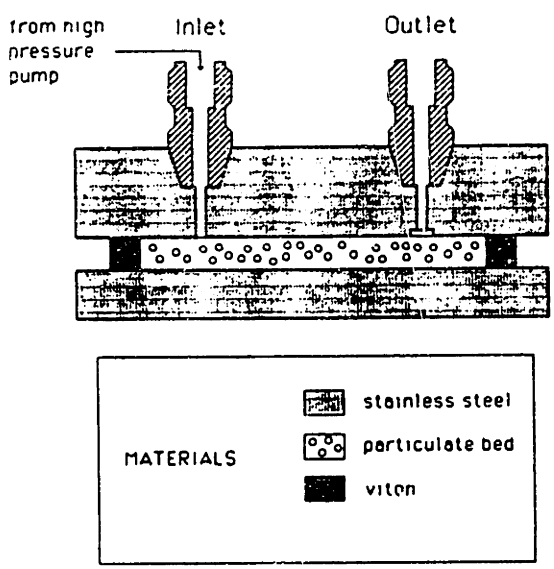

Figure 7.1: Particle Filtering Systen

of the macro sensor. A cell identical to the paper containment apparatus described in Chapter 5 (see Figure 5.1) is used with a teflon filter (Millipore - LCWP 090 25 10μm teflon filters) instead of paper to secure the particles between the sensor and the filter. The layer of particles is made thick enough so that it can be treated as an infinite half space. This containment cell, with a macro sensor packed with particles, is then placed in clean, and then contaminated oil and the gain and phase responses recorded. This strategy depends upon oil diffusing through the teflon and into the particles in a reasonable amount of time. Experiments to be presented indicate that this time is relatively short. Data is then compared between these measurements and the measurement of the particles used in the filtration experiment.

7.2 Fuller's Earth

Fuller's, or diatomaceous earth is a natural substance, resembling potters clay, which was discovered to adsorb impurities from oils. It is commonly used to reclaim oil that has been severely oxidized/degraded. Its effectiveness in this regard was confirmed upon flowing oxidized oil through a bed of fuller's earth. The conductivity of the filtered oil was a factor of 6 smaller than the oxidized oil (5×10^{-13}mhos/m, 3×10^{-12}mhos/m). Thus, the particles are clearly removing something from the oxidized oil which reduces its conductivity. It is important to note that it was demonstrated in Chapter 3 that removal of moisture from the transformer oil ba-

sically has no effect upon the conductivity of the oil. In addition, the color of the filtered oil was much lighter than that of the oxidized oil, also indicating the removal of substances from the oil.

Microdielectric measurements of the particles used to filter the oil showed essentially flat gain with no phase. Frequency scans of clean and oxidized oil with a fuller's earth "coated" macro sensor using the previously described confinement apparatus were also taken. The responses all had flat gain with essentially no phase. The responses of the fullers earth coated macro sensor in clean and oxidized oil are illustrated in Figures 7.2 and 7.3. It is clear that the oil has diffused through the teflon layer because the high frequency gain increased when the sensor was moved into the oil. Thus, the teflon filter should be adequate for these experiments. The essentially flat gain and zero phase observed in each case may be an indication that the fuller's earth has immobilized ions responsible for conduction in the oil. There is, however, a slight transition in the gain that is observed for the fuller's earth coated sensor in the oxidized oil along with what might be argued to be a slight phase excursion. If this truly reflects a relaxation process, it is much to faint a response to be accurately interpreted. Consequently, further tests with this material were suspended in light of the completely uninformative response obtained from initial experiments.

7.3 Silica Gel

The terms silica, silica gel, silicic acid, and porous glass all essentially refer to the same adsorbent which is prepared from sodium silicate [44]. The adsorptive properties of a silica depend on the hydroxyl chains attached to surface silicon atoms. Thus, solutes are adsorbed on silica through hydrogen bonding, with the hydroxyls usually serving as hydrogen donors. Polar molecules in general will be adsorbed, with amines and other bases preferentially retained (compared to other polar adsorbents) due to the mild acidity of the silica surface. The adsorptive properties of the silica can be modified by treating it in various ways. One set of particles to be tested, for example, was treated by reacting it with a monofunctional silane carrying an 18 carbon alkyl chain which, among other effects, passifies the silica to moisture. In the following sections, experimental results obtained from various sets of silica particles are presented and discussed.

7.3.1 Untreated Silica Gel

The liquid chromatographic grade silica gel (LiChrosorb Si 60) used in this set of experiments is untreated. The particles have low size dispersion and are nominally 10 μm in size. Again, these particles were used in a filter and the conductivity of oxidized oil was measured before and after filtering. Results very similar to those found for the fuller's earth were observed. The conductivity of the oxidized oil was 3×10^{-12} (same oil as previous experiment), and the conductivity of the filtered oil was approximately 6×10^{-13}. The color of the filtered oil was also significantly

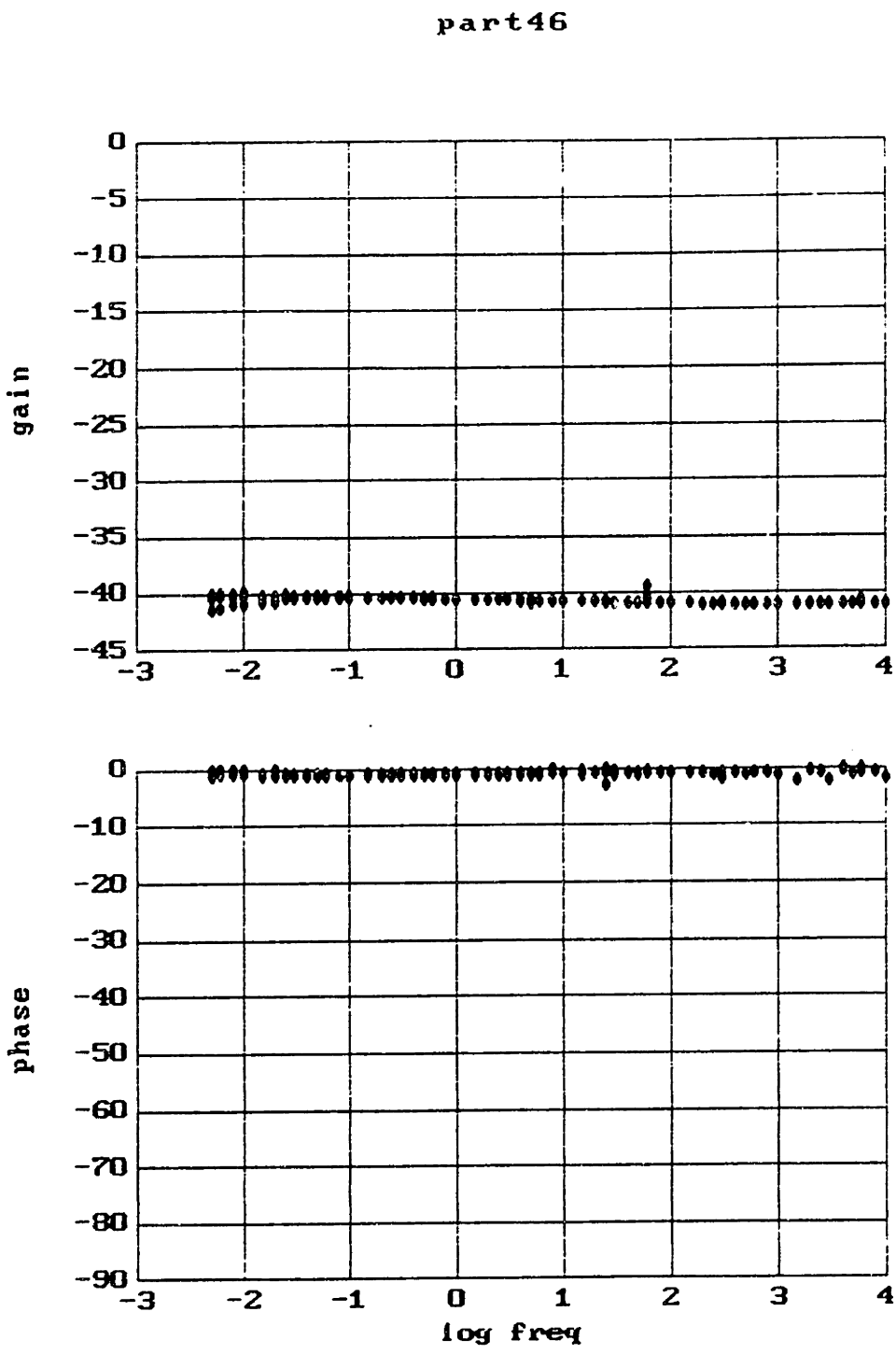

Figure 7.2: Macro Sensor with Fuller's Earth in Clean Oil

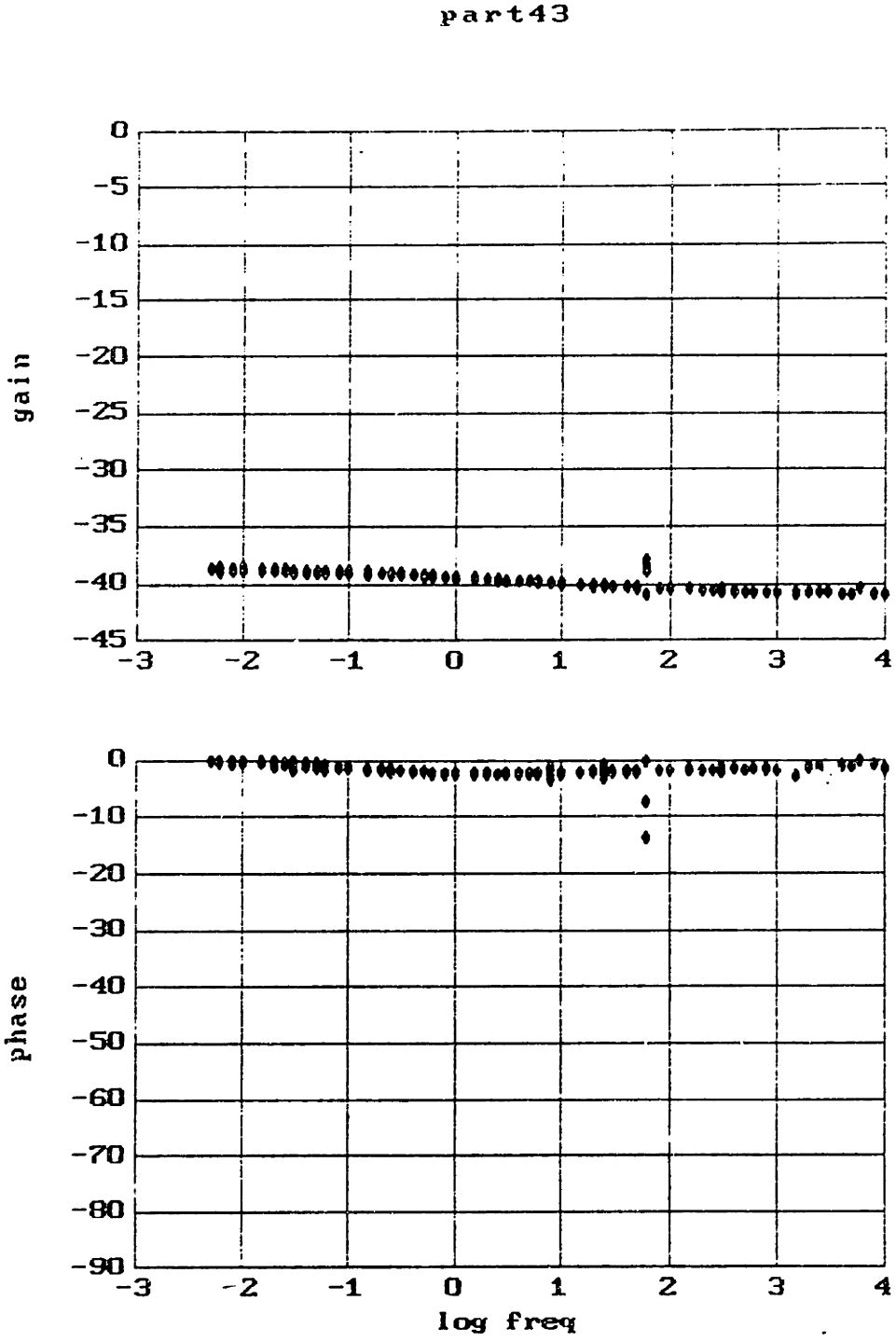

Figure 7.3: Macro Sensor with Fuller's Earth in Oxidized Oil

lighter in color than the oxidized oil. Thus, the silica gel seems to behave similarly to the fuller's earth in terms of its ability to "clean" the oil.

The macro sensor's response to the silica particles in both air and oil clearly indicate that relaxation processes are present. The response to the silica particles in room air is illustrated in Figure 7.4. The two phase excursions, and their corresponding gain transitions, are an indication that two different charge relaxation processes are occuring in the air/particle system. In addition, it was found upon placing the sensor in an evacuation chamber that both relaxation phenomena disappeared. The gain response, in this case, remained level at -43.3 dB with no phase. It was assumed, from this last set of data, that moisture was responsible for both relaxation phenomena observed in air.

The response of the particle packed macro sensor in oil with approximately 25 parts per million moisture is illustrated in Figure 7.5. The response in oil is very similar to the response in air. Two phase peaks are present, along with the corresponding gain transitions. Again, the response of the macro sensor, with previously dried particles, placed in clean, dry oil has a flat gain response of approximately -40 dB (compared to that of -43.3 dB in air) with no phase. Thus, moisture is also implicated as the dominant factor of the particle's response in oil. Consequently, these particles are not very useful for looking at other contaminants in the oil.

The frequency response of these particles does not appear to be that of a one dimensional heterogeneous system of ohmic material having frequency independent permittivity. Thus, the response in both the air and oil are attributed to dispersions in complex permittivity. The dispersions are apparently different for the measurements in air and oil because the phase responses observed are significantly dissimilar. The first attempt at finding a dispersive model might stem from the work presented in Chapter 6. Equation 6.11 can be generalized to characterize conductivities in both the particles and the media that they are embedded in by making the epsilon of each constituent complex: $\epsilon^* = \epsilon - \frac{j\sigma}{\omega}$. This generalized Lorentz sphere model would predict two different relaxation processes. One would be determined by the conductivity of the particles, and the other by the conductivity of the medium in which the particles are embedded. Figure 7.6 is the predicted response to an oil/particle system where the oil has a conductivity of 1×10^{-11} and the particles have a conductivity of 1×10^{-8}. A 40% voidage is used. Unfortunately, the predicted response using this model does not really resemble the data obtained in oil. Also, it becomes difficult to explain where the conduction processes are occuring in the measurements taken with the particles in the air. The air is an insulating medium, which means bulk conduction is possible only in the particles. Such a model would predict only a single phase peak attributed to the relaxation of charge in the particles. A second relaxation phenomena could be incorporated by including a surface conduction process on the particle surfaces in the Lorentz sphere model reflecting a film of adsorbed water (see appendix B). The relaxation of charge on the particle surface would generate its own phase peak as illustrated in Figure 7.7. Unfortunately, the shape of the predicted response does not quite match the data. However, it does predict two phase peaks if the particles have both a bulk and surface conductivity.

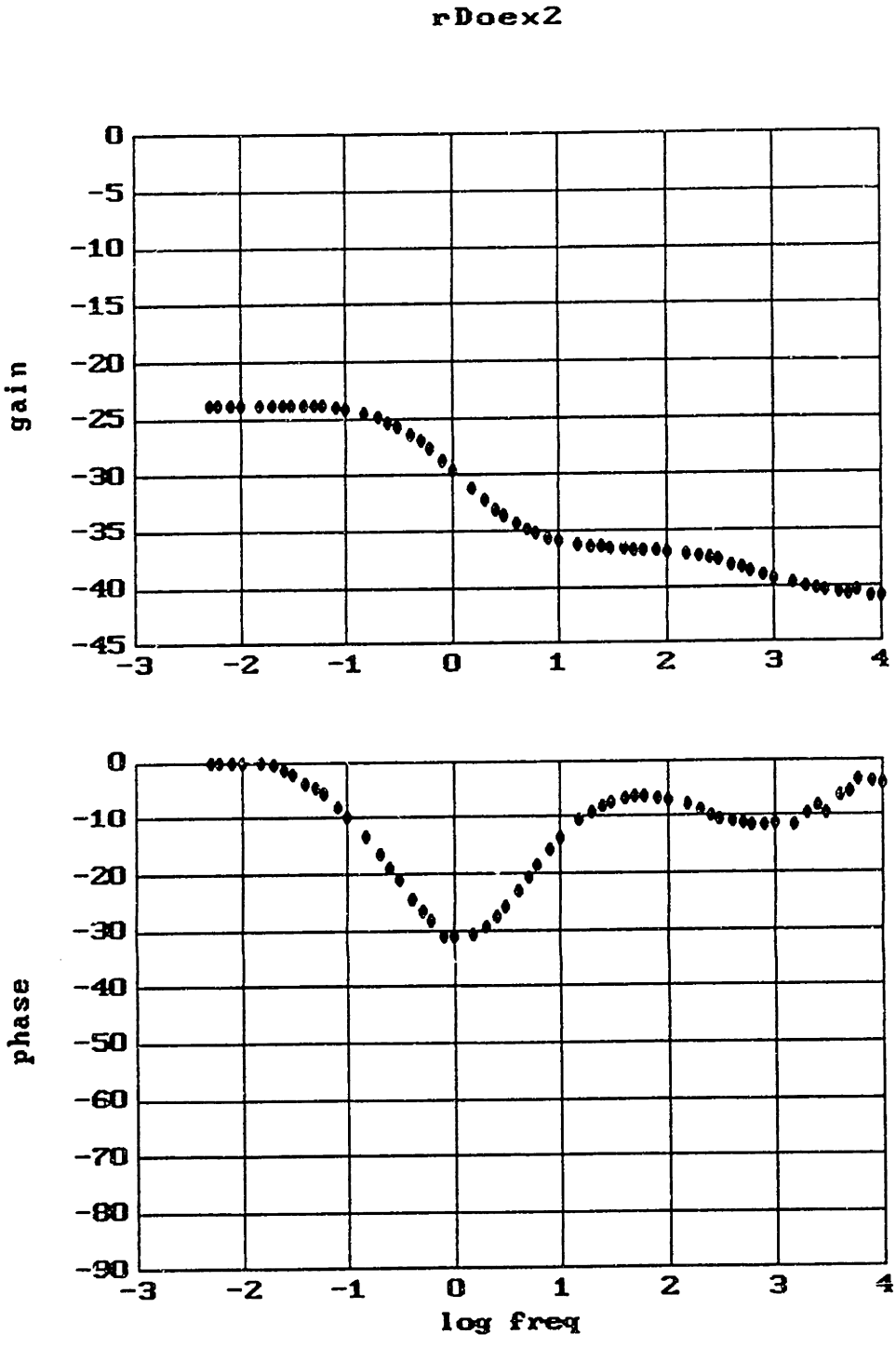

Figure 7.4: Response of Parylene Coated Macro Sensor to Silica Gel in Air

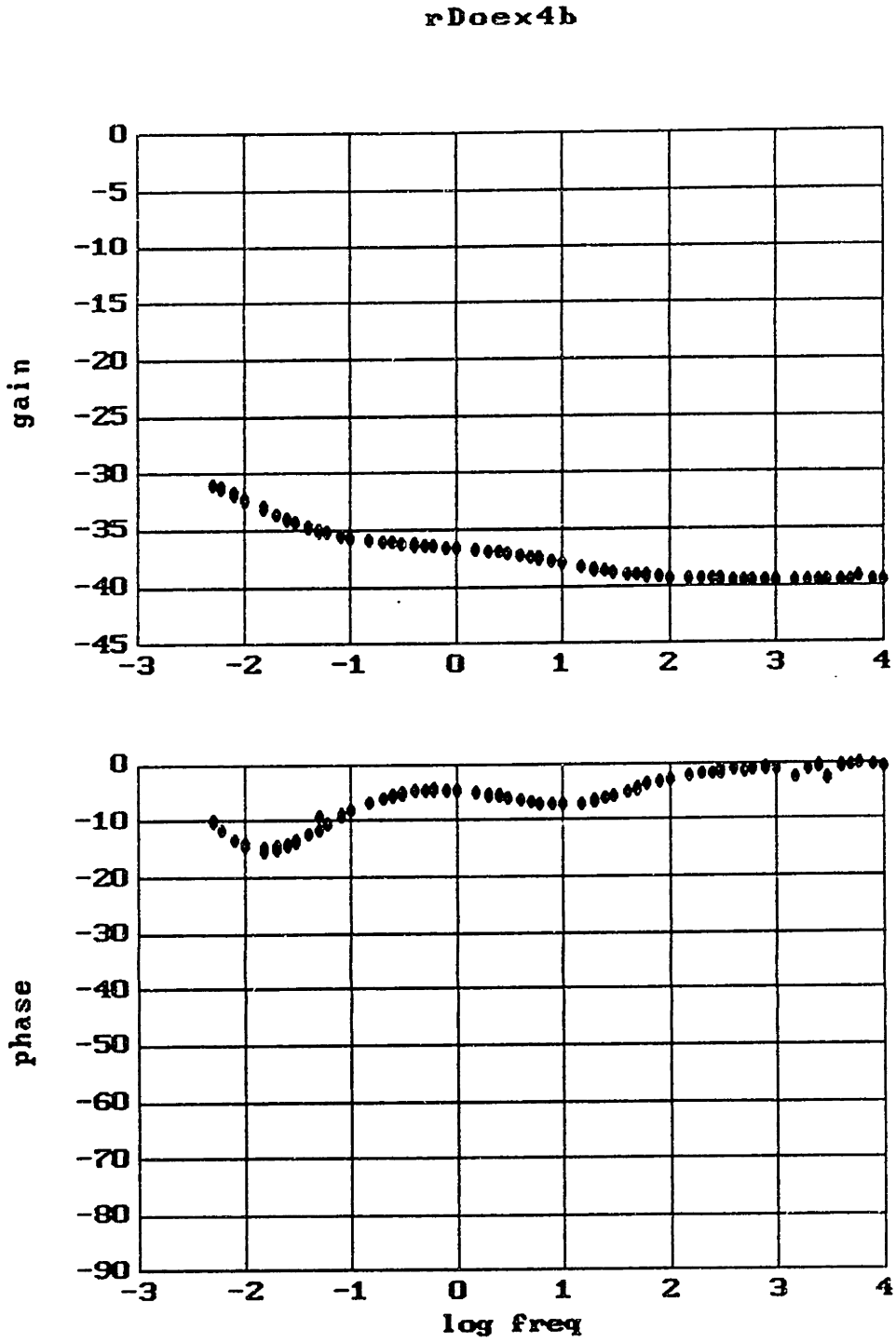

Figure 7.5: Parylene Coated Macro Sensor with Silica Gel in Oil w/ 25ppm Water

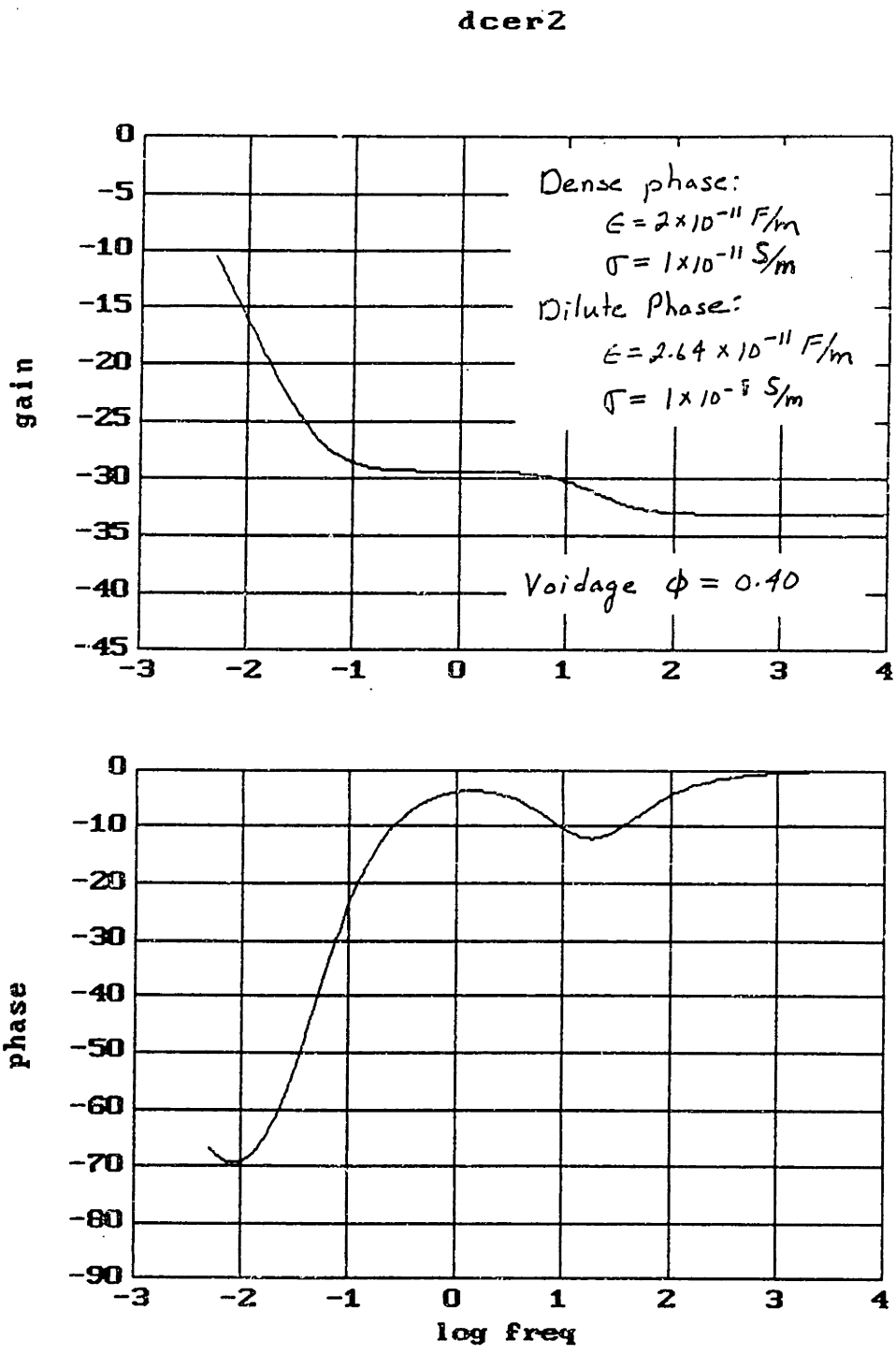

Figure 7.6: Predicted Response Using Lorentz Sphere Model with Complex ϵ

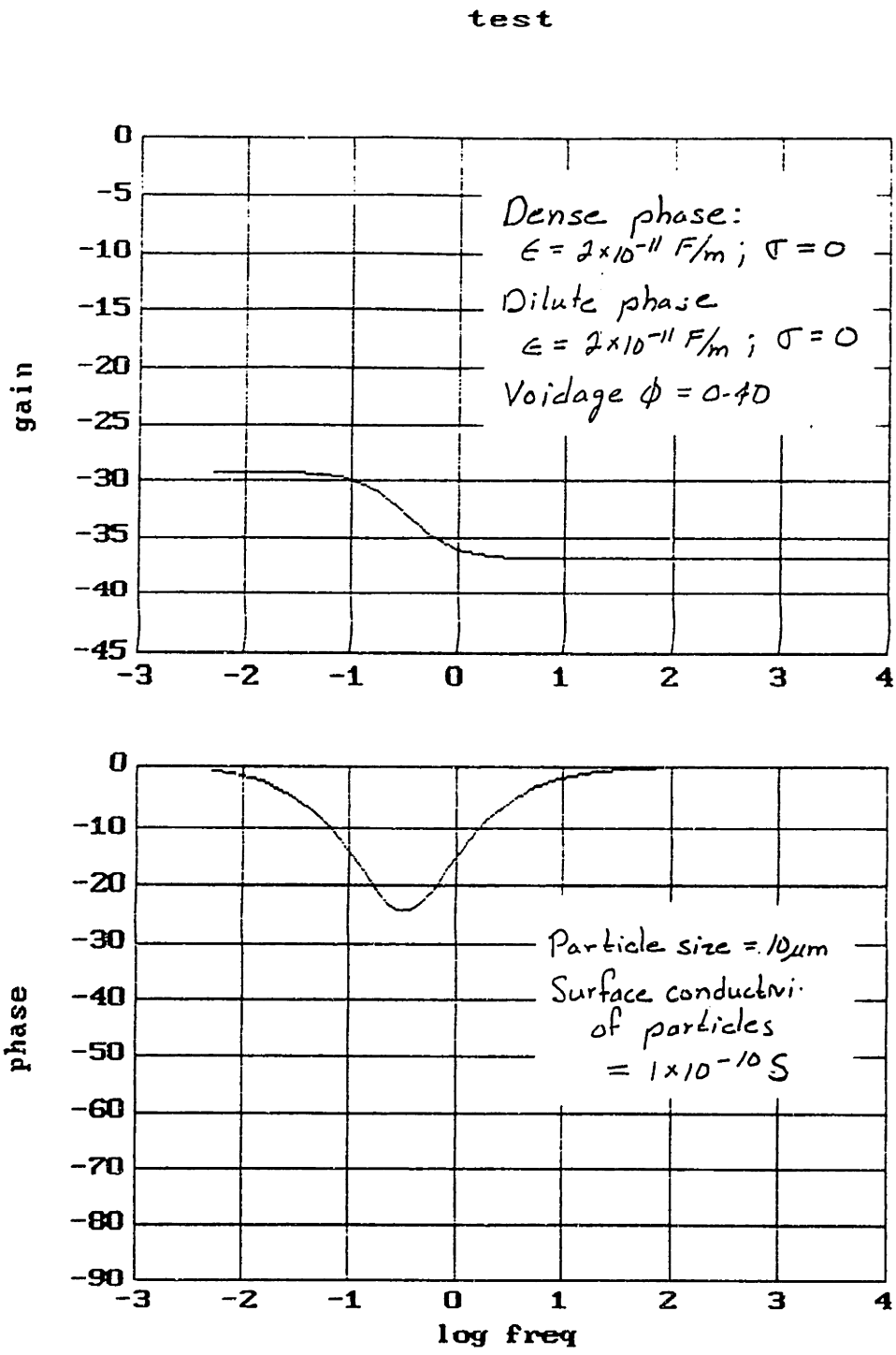

Figure 7.7: Insulating Particles in Insulating Medium with Surface Conduction on Surface of Particles

Another explanation for the two phase peaks observed in air might be that charge relaxes due to a conduction process on the particle surface as described before, and that the second phase peak is due to relaxation of charge between particles characterized by some contact resistance. This explanation seems more reasonable because the bulk of the silica gell should be very insulating. If that is the case, then the lorentz sphere model for particles in air would predict only one phase peak due to the relaxation of charge along the surfaces of the particles. In any case, more research is necessary before any conclusions can be drawn about the conduction mechanisms observed in this experiment.

7.3.2 Hydrophobic Silica Gell

In order to detect degradation substances in the oil other than water, a particle that is hydrophobic must be used. Cabosil N70-TS is a fumed silica (99.8% SiO_2) treated with an organosilicon compound to make it hydrophobic. These particles were not intended for use in a chromatographic capacity so that very little is specified about its absorption characteristics. Basically, the only motivation for trying these particles is their hydrophobic nature.

The second set of hydrophobic particles tested was the aforementioned porous, C_{18} coated, chromatographic grade silica. Basically, the C_{18} fills the cites on the particle which attract moisture. One consequence of this is that it will no longer absorb other polar molecules either.

Cabosil

The cabosil particles were placed in the filtration system and oxidized oil was passed through the bed of cabosil. Measurements of the conductivity before and after filtering showed very little change. However, the color of the oil after filtering was significantly lighter. Thus, the cabosil does seem to adsorb something from the oil, but not the constituents that determine its conductivity.

The response of a parylene coated macro sensor with cabosil in air was found to be flat at -42dB with no phase excursions. This is a strong indication that moisture is not a factor in the response of the system because the room air is close to 50% relative humidity. The response of the sensor with dried particles in dry oil (less than 7 ppm water) was found to have only a single peak as illustrated in Figure 7.8. Exposing the oil to moisture did not have an effect upon the response of the system. Moving the sensor from clean oil to oxidized oil had a small effect upon the position of the phase peak, but no more so than the change in bulk conductivity observed with a parylene coated sensor. The microdielectric measurements of the particles used in the oil filtration experiment look essentially like these other measurements. However, it would be reasonable to assume that the particles used for filtering the oil have adsorbed a much greater quantity of the degradation products in the oil than the particles exposed to oil by diffusion through a teflon membrane. However, this does not seem to be reflected in the dielectric measurments of these particles. Thus, it is possible that the substance affecting the color of the oil, which was filtered out by these particles, have no effect upon the dielectric properties of the oil particle

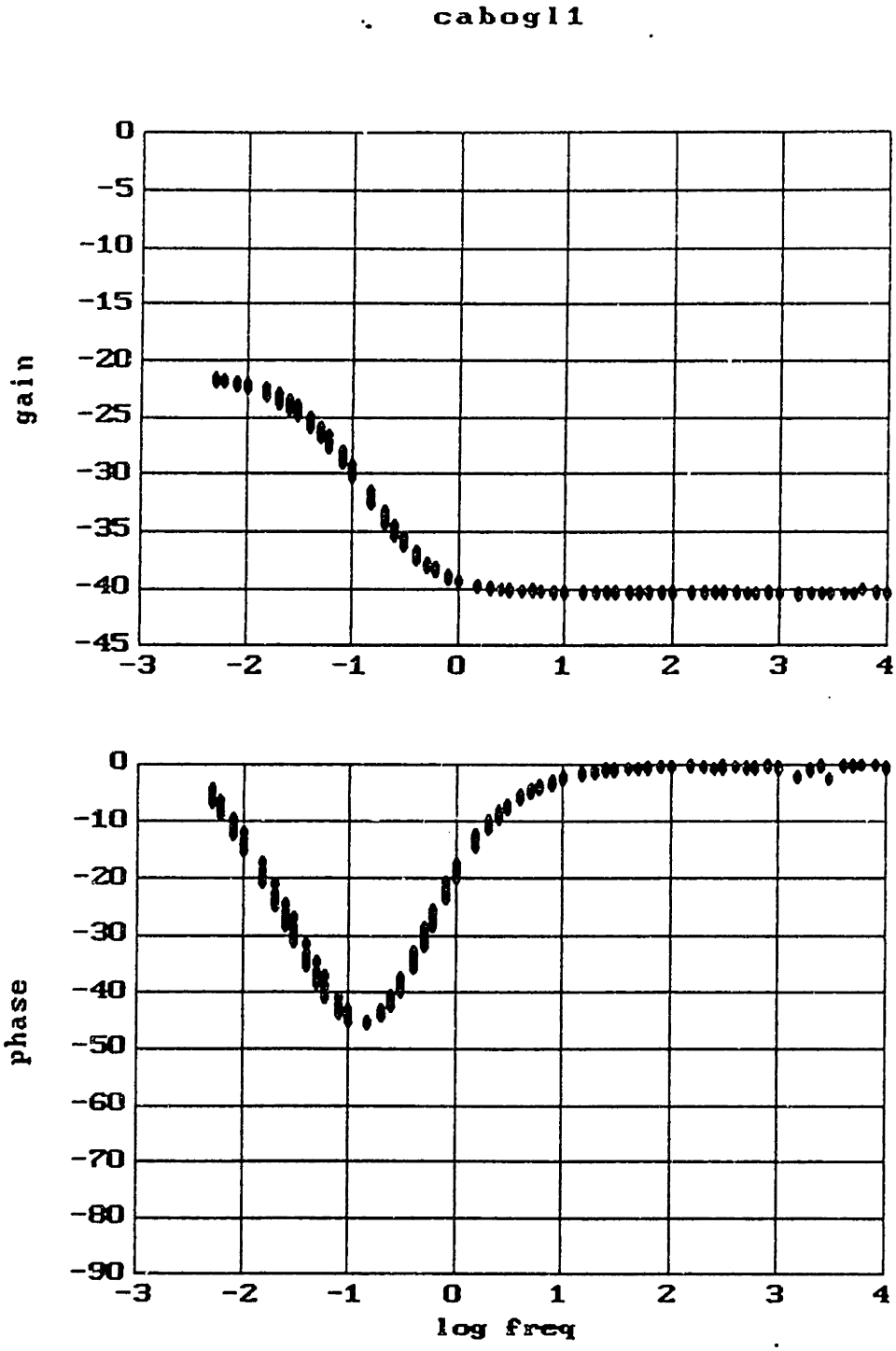

Figure 7.8: Parylene Coated Macro Sensor with Cabosil in Dry Oil

mixture. Thus, the value of using cabosil particles to detect degradation products in the oil is unclear. If the oil particle mixture truly becomes more conducting in going from clean to oxidized oil, and if it is a reversible process, then it may be useful because it allows detection of oxidation products at much higher frequencies than is possible from dielectric measurements of pure transformer oil. The tradeoff is that there is very little understanding of the conduction mechanisms in such a system. Before discussing possible conduction mechanisms in an oil/cabosil mixture, the experiments with the C_{18} coated chromatograpic grade silica gel are presented.

Carbon Treated Silica Gell

The porous silica particles used in this set of tests was treated by reacting them with a monofunctional silane carrying an 18 carbon alkyl chain to prevent adsorption of moisture. These particles were also tested to determine if they adsorbed any constituents from the oil associated with the oxidation of oil. Like the cabosil, it was found that the conductivity of the oxidized oil, before and after filtering, remained essentially the same. The color of the filtered oil, again, was significantly lighter. Thus, the particles have adsorbed components of the oil which affect its color and are associated with oxidation.

The response of a parylene coated macro sensor with C_{18} coated particles in air was found to be flat at -42.7 dB with no phase. Thus, the moisture present in the 50% relative humidity air does not seem to be contributing to any relaxation phenomena. The sensor, with dried particles, was then placed into new, dry oil (less than 7 ppm water). A single phase peak was observed (see Figure 7.9). The response is very similar to that observed for the cabosil particles. The response upon moving the sensor into oxidized oil, however, essentially did not affect the gain and phase response of the system. Measurements of the particles used in the filtration experiment was found to have the same gain and phase responses. Thus, these particles do not seem to be dielectrically sensitive to oxidation products in the oil.

Qualitative Discussion

The frequency of the phase peak for a parylene coated macro sensor's response to cabosil particles and C_{18} coated porous silica gell in oil was two orders of magnitude greater than the frequency of the phase peak that was found for the response of a parylene coated sensor to the same oil. This is an indication that the conductivity of the oil/particle mixture is much greater than the conductivity of the oil by itself. An attempt was made to match this data using the Lorentz sphere model without success. To predict a phase peak at the desired frequency, either the conductivity of the oil, the conductivity of the particle, or the surface conduction mechanism at the interface between the two, must increase drastically. It is unreasonable to assume that the conductivity of the oil has changed. It is possible that the conductivity of the particle has changed, but improbable. It is most likely that the surface conductivity of the particles has increased tremendously in the presence of oil, which might, for example, be due to the formation of double layers [43]. However, in any case, the oil will contribute a phase peak at the lower frequencies

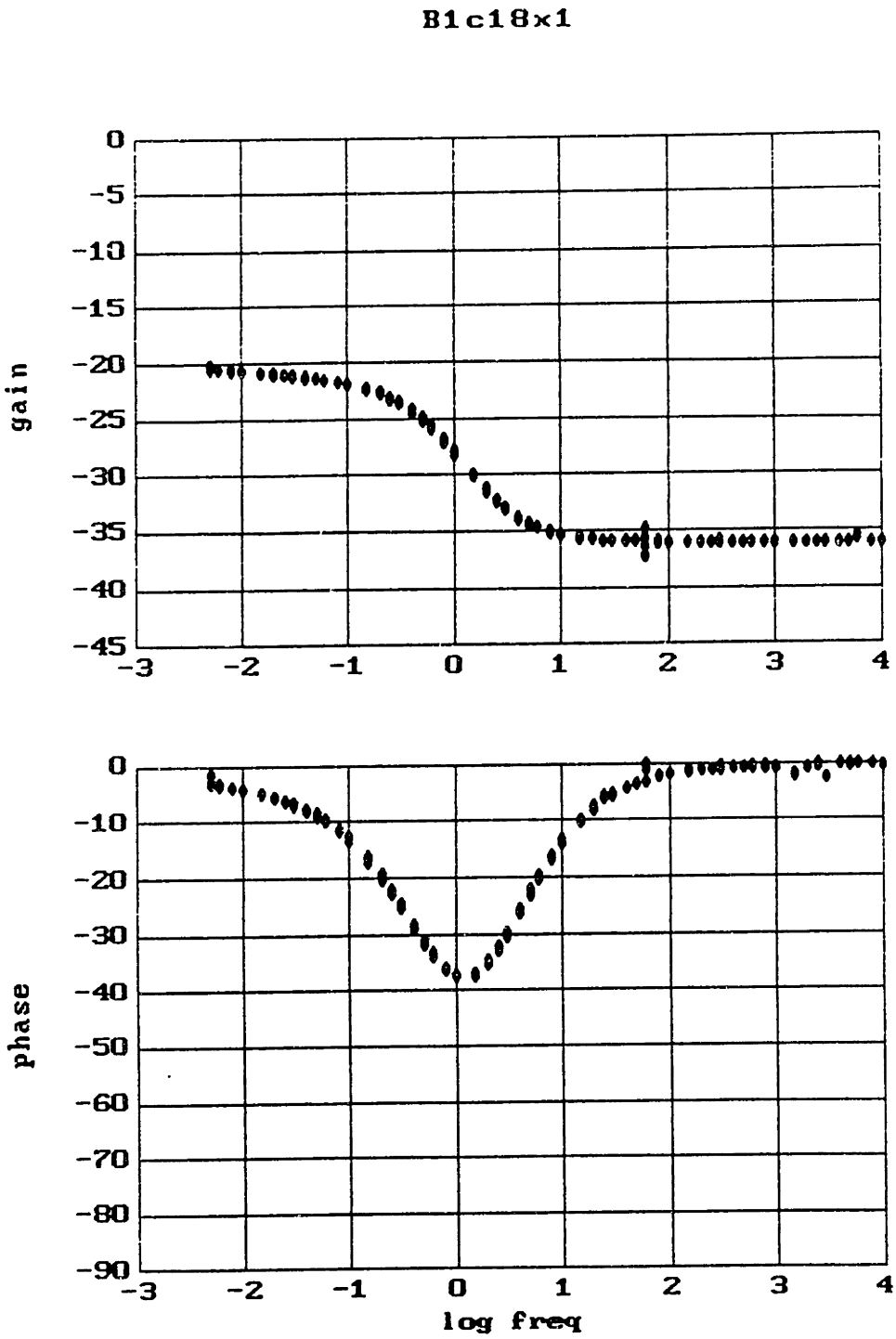

Figure 7.9: Parylene Coated Macro Sensor with C_{18} treated Silica in Oil

regardless of the other conductivity values. Thus, if the Lorentz sphere model is to be used, the lack of this phase information in the data must be explained. What other models to try becomes unclear at this point. However, the estimated dispersion of the cabosil particles is shown in Figure 7.10 with the log of the bulk permittivities and conductivities (estimated from the gain and phase) plotted vs. the log of the frequency. The data is also presented in Figure 7.11 as log ϵ' and log ϵ'' vs. log frequency (ω) where ϵ_∞ has been subtracted out. This is the same procedure used in analzying the dispersion observed for the paper insulation. Unfortunately, there is not enough information in Figure 7.11 to determine if it has the power law dependence described by Jonscher. Subtraction of ϵ_∞ from the dispersion curve has removed a significant portion of the ϵ' curve. Thus, the analysis of the dispersion in complex permittivity of the cabosil particles does not allow any conclusions to be drawn at this time.

The conclusion that can be drawn from these experiments is that the types of particles tested aren't very useful for enhancing the detection of degradation products due to oxidation. Other degradation procedures could also be tested, but at this point, some indication as to what to try based upon further physical insights about the system are needed. Thus, the results of using particles with the macro sensor weren't very useful in terms of developing a sensor for monitoring transformers, but the approach does have enough potential to perhaps justify further work. The second problem with the use of particles lies in the need for an appropriate model to help understand the physics of the conduction process, and to predict the responses for the system. Estimating the dispersion was the first step in trying to find an appropriate model. No conclusions, however, could be drawn from the dispersion relation.

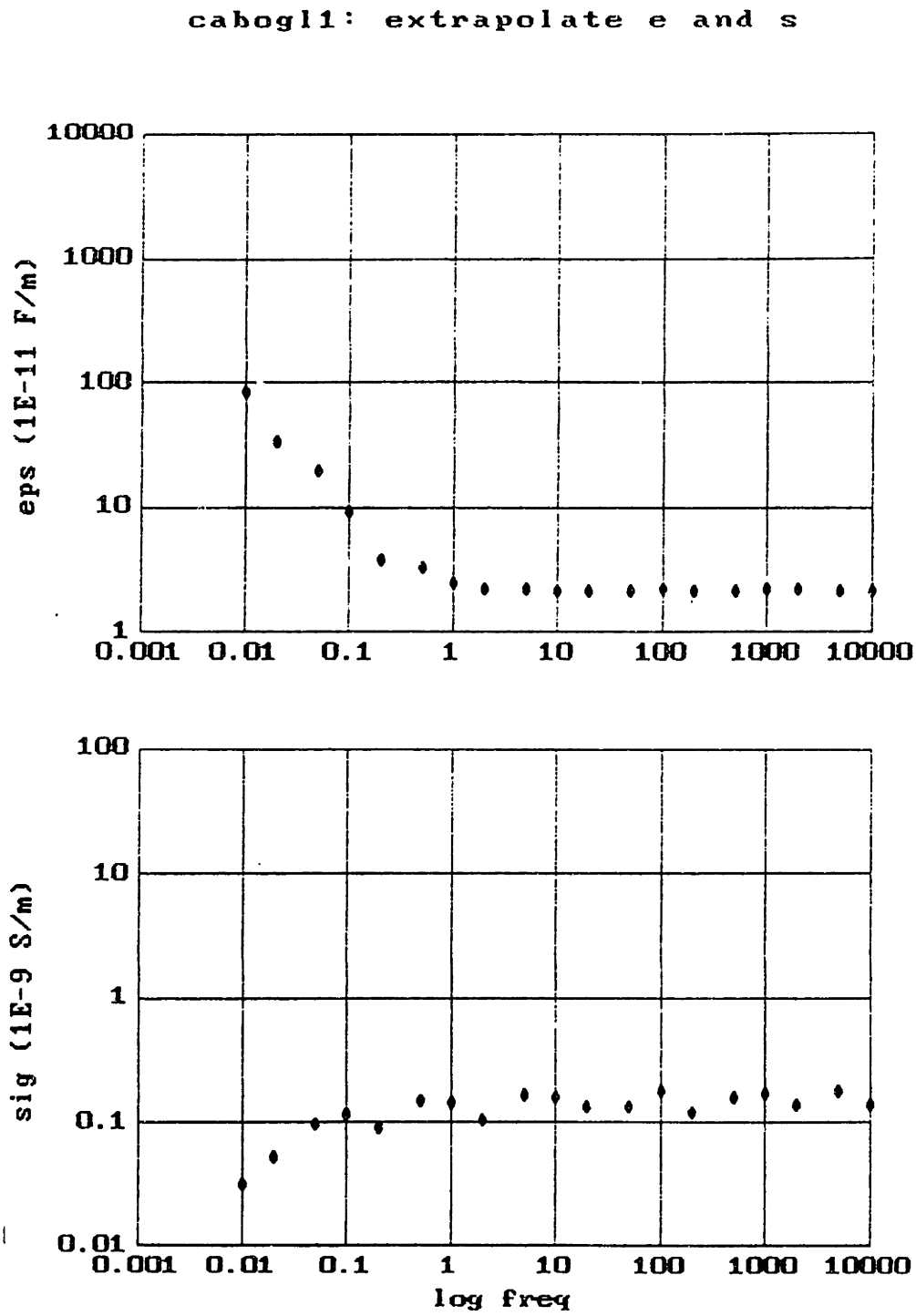

Figure 7.10: Dispersion of Epsilon and Sigma for Cabosil Particles

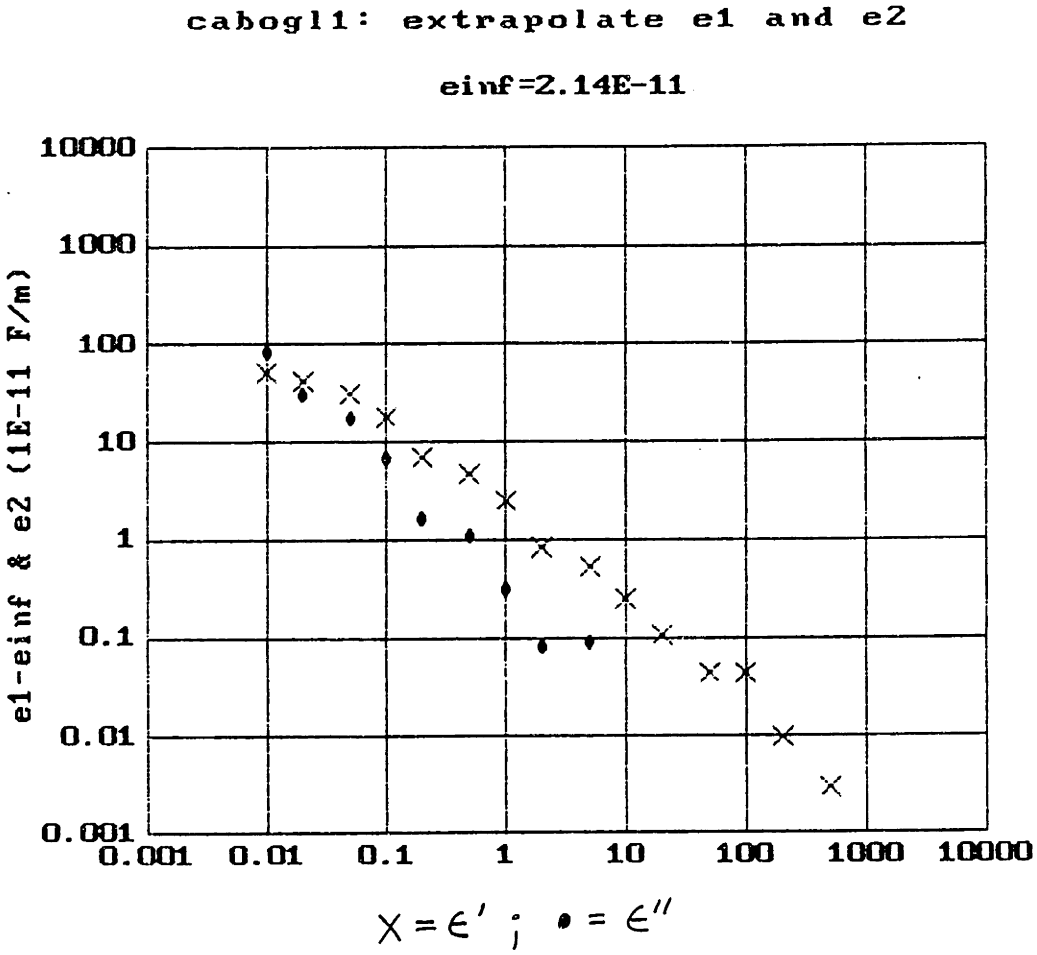

Figure 7.11: log ϵ' and log ϵ'' vs. log ω for Cabosil Particles

Chapter 8

Conclusion

8.1 Summary of Results

A millimeter wavelength "macro" sensor was developed to measure the bulk dielectric properties of insulating media in the transformer. This work included the design and testing of interface circuitry capable of making accurate measurements down to 0.005 Hz. Modifications of the continuum model for the interdigitated electrode structure were made to allow for accurate predictions of the parylene coated sensor's response to the bulk permittivity and conductivity of various materials. It was also discovered at this point that the macro sensor was relatively insensitive, compared to the micro sensor, to changes in permittivity. The reasons for this insensitivity were discussed, and a thinner oxide layer was suggested for better sensor performance. A thinner oxide layer also allows for discrimination between surface and bulk conduction phenomena. It was discovered upon testing the sensor in oil that a 5 to 10 μm coating of parylene was needed to passify the sensor to the effects of moisture.

Then, the permittivity and conductivity of various oils, estimated from macro sensor measurements (gain and phase frequency reponse), were compared with measurements of the same oils using conventional bridge techniques. Good agreement was found between the two sets of measurements. It was also found that oxidation of the oil increases its conductivity. To get maximum sensitivity to permittivity, and to also have temperature measurements available, it was suggested that a micro sensor be used in conjunction with a macro sensor for bulk dielectric measurements.

The ability to detect changes in the moisture content of paper insulation as reflected in frequency shifts of a phase peak was demonstrated. Attempts were made to understand the conduction process in the paper. Estimates were made of the conductivity, for various moisture levels in the paper, based upon an ohmic conduction model. The predicted response of the ohmic model, however, was unable to match the shape of the phase data associated with charge relaxation in the paper. Thus, it was concluded that dispersion of the the complex permittivity was responsible for the observed response. The dispersion in the complex permittivity of the paper at each frequency was estimated. It appeared to come very close to a power law dispersion relation.

The possibility of using a macro sensor to detect particulate contamination in the oil was also explored. It was found that under very special conditions, that the thickness of a sedimenting layer could be estimated. However, in a transformer, where these conditions don't exist, it becomes basically impossible to accurately measure the particulate contamination in the oil.

Microdielectric measurements were also made of Particle coatings as degradation products were adsorbed from the transformer oil. Fuller's earth was effective in adsorbing degradation products from the oil, but showed no change in its dielectric response. Plain, liquid chromatographic grade silica gel was tried, and moisture was found to dominate its response. Consequently, these two set of particles are not useful for monitoring degradation products in transformer oil. Hydrophobic chromatographic grade silica gel was then tried, along with hydrophobic cabosil particles. The responses of these two sets of particles were very similar. Both appeared to be insensitive to moisture, but showed very little change in response when measuring clean and oxidized oil. Again, these particles do not appear to be especially useful in the context of monitoring transformer oil. An attempt was made to explain the conduction mechanism, but no conlusions were drawn. The dispersion in the complex permittivity of the cabosil in oil was estimated for future reference.

8.2 Future Work

The sensitivity of the current macro sensor to changes in permittivity has been somewhat disappointing. A new macro sensor should be designed to optimize its performance and a sensor constructed and tested.

The strategy of placing "coatings" onto the macro sensor that are dielectrically sensitive to targeted degradation products is a valid approach. Other materials should be explored for sensitivity to degradation products.

Also, the dispersions that were observed in the paper and particles warrant further research. Physical insights into the problem would be of great value in trying to find an appropriate model. The power law dispersion relation should be explored in greater depth. Microdielectric measurements are, in general, sensitive to complex permittivity dispersions because of the 0.005 Hz to 10 kHz frequency range. Thus, it can be a very useful device for studying low frequency dispersions in other materials.

Appendix A

Modeling Layers with Spatially Varying Dielectric Properties

The objective is to enhance understanding of microdielectrometry by expanding the capabilities of the model for the interdigitated electrode structure. The model described in LEES report TR86-019 assumes that the material probed by the sensor be unifrom in the transverse direction and have at least step wise continuous properties in the normal direction. This restriction has made it difficult, in certain circumstances, to interpret data. Specifically, the model becomes very cumbersome when simulating layers with smoothly varying properties in the normal direction (variations in the transverse direction are not considered). Although the current sensor allows only for temporal frequency response, the sensor is still sensitive to property gradients. Consequently, the ability to model such phenomena would potentially allow for parameter estimation techniques to be used for the determination of these complex permittivity profiles.

The best the current model can do is to discretize such a layer into many smaller layers each with uniform properties. A more flexible approach is desired such that the inhomogeneity is input as a function instead of discrete points. This becomes important if parameter estimation routines are to be implemented. It is much simpler to estimate three or four coefficents of a distribution function than it is to estimate the values for each layer of the discretization which amounts to a great many more parameters. Before proceeding further, some knowledge of the details for the continuum approach used to model the interdigitated electrode structure is necessary.

A.1 Surface Capacitance Densities

There are two sets of inputs to the model. The first specifies the electrode array structure which include parameters such as the spatial wavelength, oxide layer thickness and permittivity, and relative electrode dimensions. The second describes the media above the electrodes in terms of a complex surface capacitance density C_n representing the response of the media to one fourier component of a potential

applied at the electrode surface (these fourier components are found by solving the "mixed boundary value problem" for the potential along the electrode surface [25].)

The surface capacitance density looking in from the j'th interface is defined in terms of the quantities evaluated just above that interface.

$$\hat{C}_n^{(j)} = \frac{\hat{D}_n^{(j)}}{\hat{\Phi}_n^{(j)}} \tag{A.1}$$

Calculation of the surface capacitance is centered around the assumption that the media have uniform properties in the tangential direction. Given this geometry, it becomes convenient to represent the field solutions using "transfer relations". These are simply a convenient representation of the field solutions within a layer when the potentials at the boundaries are known. [40]. The transfer relations are also valid when a fourier representation is used. Thus, given the fourier modes for the potential at the upper and lower boundaries, the fourier modes of the electric field can be determined (see Figure A.1).

$$\begin{bmatrix} \hat{D}_n^{(j)'} \\ \hat{D}_n^{(j+1)} \end{bmatrix} = \begin{bmatrix} \hat{A}_{11}^{(j)} & \hat{A}_{12}^{(j)} \\ \hat{A}_{21}^{(j)} & \hat{A}_{22}^{(j)} \end{bmatrix} \begin{bmatrix} \hat{\Phi}_n^{(j)} \\ \hat{\Phi}_n^{(j+1)} \end{bmatrix} \tag{A.2}$$

In the case where a layer has uniform complex permittivity, the transfer relation can be solved for analytically [40]:

$$\begin{aligned} \hat{A}_{22}^{(j)} &= -\hat{A}_{11}^{(j)} = \epsilon_j^* k_n \coth(k_n d_j) \\ \hat{A}_{12}^{(j)} &= -\hat{A}_{21}^{(j)} = \frac{\epsilon_j^* k_n}{\sinh(k_n d_j)} \end{aligned} \tag{A.3}$$

Then, to relate one layer to the next, there are two boundary conditions to be satisfied at each interface. At the j'th interface, the potential is continuous, but there is a complex surface permittivity ϵ_{sj}^* and hence a discontinuity in the dielectric flux.

$$\hat{\Phi}^{(j)} = \hat{\Phi}^{(j)'} \tag{A.4}$$

$$\hat{D}_n^{(j)} - \hat{D}_n^{(j)'} + k_n^2 \epsilon_{sj}^* \hat{\Phi}_n^{(j)} = 0 \tag{A.5}$$

where $\hat{D}_n^{(j)}$ is a complex quantity. From these equations, it follows that

$$\hat{C}_n^{(j+1)} = \hat{A}_{22}^{(j)} + \frac{\hat{A}_{21}^{(j)} \hat{A}_{12}^{(j)}}{\hat{C}_n^{(j)} - \hat{A}_{11}^{(j)} + k_n^2 \epsilon_{sj}^*} \tag{A.6}$$

This expression can be used repeatedly, starting from the top layer (j=1) and working down to the P'th layer. By definition, the surface capacitance density desired for evaluating the complex gain is

$$\hat{C}_n \equiv \hat{C}_n^{(P+1)} \tag{A.7}$$

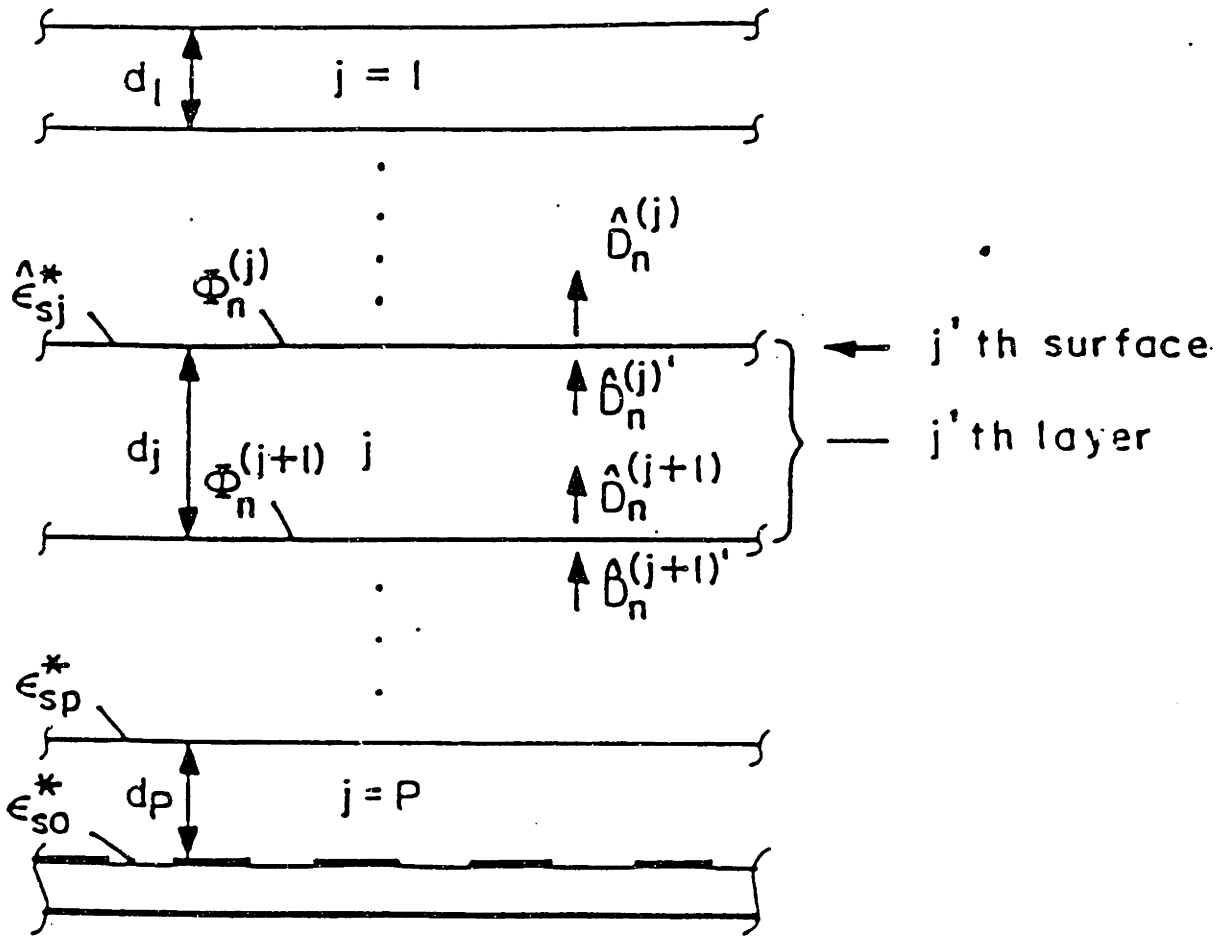

Figure A.1: Nomenclature for Layer Quantities

In addition, the first surface must be at infinity - the upper boundary of an infinite half space. In this case, the mutual terms in Equation A.6 are zero so that $\hat{C}_n^{(2)}$ can be evaluated without $\hat{C}_n^{(1)}$. Knowing this surface capacitance, all the other ones can be determined by back substituting.

To represent a layer with a complex permittivity profile in the context of surface capacitances, the transfer relation for that layer must be determined. Once the transfer relation is found, the layer can be incorporated into the model as described previously. Thus, a relation like Equation A.2 for a layer with complex permittivity gradient is desired.

The analytical result derived for the transfer relations of a uniform layer were found by writing Gauss' law in terms of the potential (irrotational electric field) with no free charge to get Laplace's equation,

$$\nabla^2 \Phi = 0 \tag{A.8}$$

and the assumption that the surface potential distributions take the form

$$\Phi = Re\tilde{\Phi}(x,t)e^{-j(k_y y + k_z z)} \tag{A.9}$$

If $\sigma = \sigma(x)$ and $\epsilon = \epsilon(x)$, then Gauss's law is no longer adequate and the governing equation becomes conservation of charge:

$$\frac{\partial \rho}{\partial t} + \nabla \cdot \vec{J} = 0 \tag{A.10}$$

Assuming a sinusoidal ($j\omega$) time dependence and substituting for ρ and $\vec{J}$ in Equation A.10 using Gauss' and Ohm's law gives an equation in the potential:

$$\epsilon^* \nabla^2 \Phi + \nabla \Phi \cdot \nabla \epsilon^* = 0 \tag{A.11}$$

where the complex permittivity is defined as

$$\epsilon^*(x) = \epsilon(x) - \frac{j\sigma(x)}{\omega} \tag{A.12}$$

Substituting Equation A.9 into Equation A.11 gives the partial differential equation describing the potential distribution in the layer.

$$\frac{\partial^2 \Phi}{\partial x^2} + \frac{1}{\epsilon^*} \frac{\partial \epsilon^*}{\partial x} \frac{\partial \Phi}{\partial x} - k^2 \Phi = 0 \tag{A.13}$$

where $k^2 = k_y y + k_z z$. This is a linear non-constant coefficient partial differential equation. The solution to this differential equation cannot, in general, be found analytically. Thus, a numerical method must be utilized. One way to integrate Equation A.13 is to first write it as two coupled first order equations

$$\frac{\partial \Phi}{\partial x} = -E \tag{A.14}$$

$$\frac{\partial E}{\partial x} = -\frac{1}{\epsilon^*} \frac{\partial \epsilon^*}{\partial x} E - k^2 \Phi \tag{A.15}$$

and then use a Runge-Kutta integration routine to numerically determine the solution (See appendix with program listings). The Runge-Kutta routine begins with the values of Φ and E at one boundary and "marches" accross the layer in small spatial increments calculating Φ and E at each position until the far boundary is reached. A strategy is now required for using this integration routine to extract the entries of the transfer relation matrix for this inhomogeneous layer.

There are at least two methods for extracting the entries to the transfer relation matrix. The strategies are similar in that both take advantage of setting one of the variables at a boundary to zero and the other to one. The first method is easily arrived at by looking again at the form of the transfer relation Equation A.2. If $\hat{\Phi}_n^{j+1}$ is chosen to be one and the electric field $\hat{E}_n^{j+}$ chosen such that the potential at the other boundary $\hat{\Phi}_n^{(j)}$ is zero, then the entries in the transfer relation are $\hat{A}_{22}^{(j)} = \hat{E}_n^{(j+1)}$ and $\hat{A}_{12}^{(j)} = \hat{E}_n^{(j)'}$. This method is not particularly efficient because the electric field must be found using a search routine. Thus, at least two integrations across the layer must be performed: an initial guess of the electric field at one boundary giving the potential at the other; and a second point to determine a "slope" so that the electric field which gives a potential of zero at the opposing boundary can be determined. This works because the problem is linear in nature and once the "slope" is known, the desired electric field value can be found exactly. In practice, however, a third integration is desireable to insure that numerical errors that accumulate during integration aren't significant. Also, when the layer is too thick (greater than the spatial wavelength or when looking at a fourier mode that is high enough) the electric field and potential at one boundary no longer affect those at the other. Under these conditions, the numerical integration routine encounters difficulties which can be detected by a third integration. In any case, a minimum of four integrations across the layer are necessary to determine the transfer relation.

The other method, which was used in the final implementation of the subroutine to calculate $\hat{C}_n^{(j)}$, begins with the following relationship which is similar to a transfer relation matrix.

$$\begin{bmatrix} \hat{\Phi}_n^{(j)} \\ \hat{E}_n^{(j)'} \end{bmatrix} = \begin{bmatrix} \hat{N}_{11}^{(j)} & \hat{N}_{12}^{(j)} \\ \hat{N}_{21}^{(j)} & \hat{N}_{22}^{(j)} \end{bmatrix} \begin{bmatrix} \hat{\Phi}_n^{(j+1)} \\ \hat{E}_n^{(j+1)} \end{bmatrix} \tag{A.16}$$

The matrix entries can be found by setting $\hat{\Phi}_n^{(j+1)} = 1$ and $\hat{E}_n^{(j+1)} = 0$ and marching accross the layer with the integration routine to get $\hat{N}_{11}^{(j)} = \hat{\Phi}_n^{(j)}$ and $\hat{N}_{21}^{(j)} = \hat{E}_n^{(j)'}$.

Similarly, if $\hat{\Phi}_n^{(j+1)} = 0$ and $\hat{E}_n^{(j+1)} = 1$, then integration accross the layer gives $\hat{N}_{12}^{(j)} = \hat{\Phi}_n^{(j)}$ and $\hat{N}_{22}^{(j)} = \hat{E}_n^{(j)'}$. These equations can then be rewritten as a transfer relation giving the following result:

$$\begin{bmatrix} \hat{E}_n^{(j)'} \\ \hat{E}_n^{(j+1)} \end{bmatrix} = \begin{bmatrix} \frac{\hat{N}_{22}^{(j)}}{\hat{N}_{12}^{(j)}} & \hat{N}_{21}^{(j)} - \frac{\hat{N}_{22}^{(j)}\hat{N}_{11}^{(j)}}{\hat{N}_{12}^{(j)}} \\ \frac{1}{\hat{N}_{12}^{(j)}} & \frac{-\hat{N}_{11}^{(j)}}{\hat{N}_{12}^{(j)}} \end{bmatrix} \begin{bmatrix} \hat{\Phi}_n^{(j)} \\ \hat{\Phi}_n^{(j+1)} \end{bmatrix} \tag{A.17}$$

Hence, the transfer relation entries $\hat{A}^{(j)}$'s have been found numerically and can be used directly in the surface capacitance representation which characterizes the material above the electrode plane.

Figures A.2 and A.3 are the predicted responses to a layer adjacent to the elctrode plane with a conductivity gradient. One was generated using the subroutine just outlined, and the other was generated using 100 different layers representing the discretization of the conductivity profile in that layer. Both give almost identical responses which validates the integration technique used. Also, both routines require approximately the same amount of computer time. On an IBM PC-AT, it takes approximately three hours to generate 58 predicted gain and phase data points. Parameter estimation of the coefficients for a polynomial modeling the profile is beyond the scope of this thesis and is left as further work to be done.

A.2 Second Order Runge-Kutta

The second order Runge-Kutta, or simplified Runge-Kutta integration technique is described by the following set of equations:

$$\Phi_{n+1} = \Phi_n + \frac{\Delta x}{2}\{f(x_n, \Phi_n, E_n) + f(x_n + \Delta x, \Phi_n + \Delta x f(x_n, \Phi_n, E_n), E_n + \Delta x g(x_n, \Phi_n, E_n))\} \tag{A.18}$$

and

$$E_{n+1} = E_n + \frac{\Delta x}{2}\{g(x_n, \Phi_n, E_n) + g(x_n + \Delta x, \Phi_n + \Delta x f(y_n, \Phi_n, E_n), E_n + \Delta x g(y_n, \Phi_n, E_n))\} \tag{A.19}$$

where

$$f(x_n, \Phi_n, E_n) = -E_n \tag{A.20}$$

$$g(x_n, \Phi_n, E_n) = \frac{-1}{\epsilon^*}\frac{\partial \epsilon^*}{\partial x} E_n - k^2 \Phi_n \tag{A.21}$$

and

$$x_{n+1} = x_n + \Delta x \tag{A.22}$$

A detailed explanatin of how this formula was derived is presented by Henrici in **Essentials of Numerical Aalysis with Pocket Calculator Demonstrations** [45].

A.3 Program Listings

```
c imp.c  Set's up call to integration routine and calculates transfer
c        relation matrix elements
c

         subroutine spimp(n2,L,re,rse,t,N,h2,num,steps)
         complex  z,z1,za,L(0:499),za1,za2,y1
         complex  ya,M11,M12,M21,M22,P
         complex  N11,N12,N21,N22
         complex  re(0:9),rse(0:9),tmp,tmp3,zreg(1:2)
         integer  n2,steps,k,q,num,N
         real     t(0:9),k1,d,h,xs,dummy,h2
         external integr

         PI = 3.141592654

         tmpa=cmplx(10.0,0.0)
 20      if ((n2 .le. N) .and. (real(tmpa) .ge. (.002)) .and.
     x        (xs .ne. -1.0)) then
                  d=t(1)
                  h=d/steps
                  k1=2*PI*n2
                  xs=0
                  z=cmplx(0.0,0.0)
                  za=z
                  ya=cmplx(1.0,0.0)
                  call integr(xs,ya,y1,z,za,z1,h,d,k1,re,steps)
                  N11=y1
                  N21=z1
                  xs=0
                  z=cmplx(1.0,0.0)
                  za=z
                  ya=cmplx(0.0,0.0)
                  call integr(xs,ya,y1,z,za,z1,h,d,k1,re,steps)
                  N12=y1
                  N22=z1
c  Calculate transfer matrix entries
                  M11=-N22/N12
                  M12= -N21 + N22*N11/N12
                  M21= -1/N12
                  M22= N11/N12

         tmp3=cmplx(0.0,aimag(rse(0))*k1)
         P=(1/((1/re(1))*(re(0)+tmp3)*k1-M11))*M12

 30      tmp=M21*P+M22
         tmp=tmp/(2*n2*PI)
         L(n2-1)=(1/tanh(2*PI*n2*h2))+tmp*re(num-1)
         if (n2 .gt. 1) then
                  tmp=(L(n2-2)-L(n2-1))/L(n2-2)
                  tmpa=cmplx(cabs(tmp),0.0)
         endif
         n2=n2+1
         goto 20
         endif

         return
         end
```

```
c  Integration routine using 2nd order Runge-Kutta

      subroutine integr(xs,ya,yl,z,za,zl,h,d,k1,re,steps)
              complex ya,z,za,zl,y,re(0:9),rc4,gfunc
              complex rc1,rc2,rc3,zal,yb,yl
              real    x,xs,eta,k1,h,d
              integer i,j,steps

                  y=ya
                  eta=log(aimag(re(1))/aimag(re(2)))/d
                    i=0
                    y=ya
                    x=xs
300                 if (i .lt. steps) then
                      rc4=gfunc(x,y,z,eta,k1,re)
                      yl=y + (h/2)*(2*z + h*rc4)
                      rc1=h*z+y
                      rc2=h*rc4+z
                      rc3=gfunc((x+h),rc1,rc2,eta,k1,re)
                      zl=(h/2)*(rc3+rc4)+z
                      y=yl
                      z=zl
                      x = x + h
                      i=i+1
                  go to 300
                  endif

      return
      end

      complex function gfunc(x,y,z,eta,k1,re)
      real x,eta,k1
      complex y,z,re(0:9),rc7,rc8


        rc7=cmplx(0.0,aimag(re(2)))
        rc8=cmplx(real(re(2)),exp(eta*x)*aimag(re(2)))
        gfunc= k1*k1*y - (1/rc8)*(z*rc7*eta*exp(eta*x))
        return
      end
```

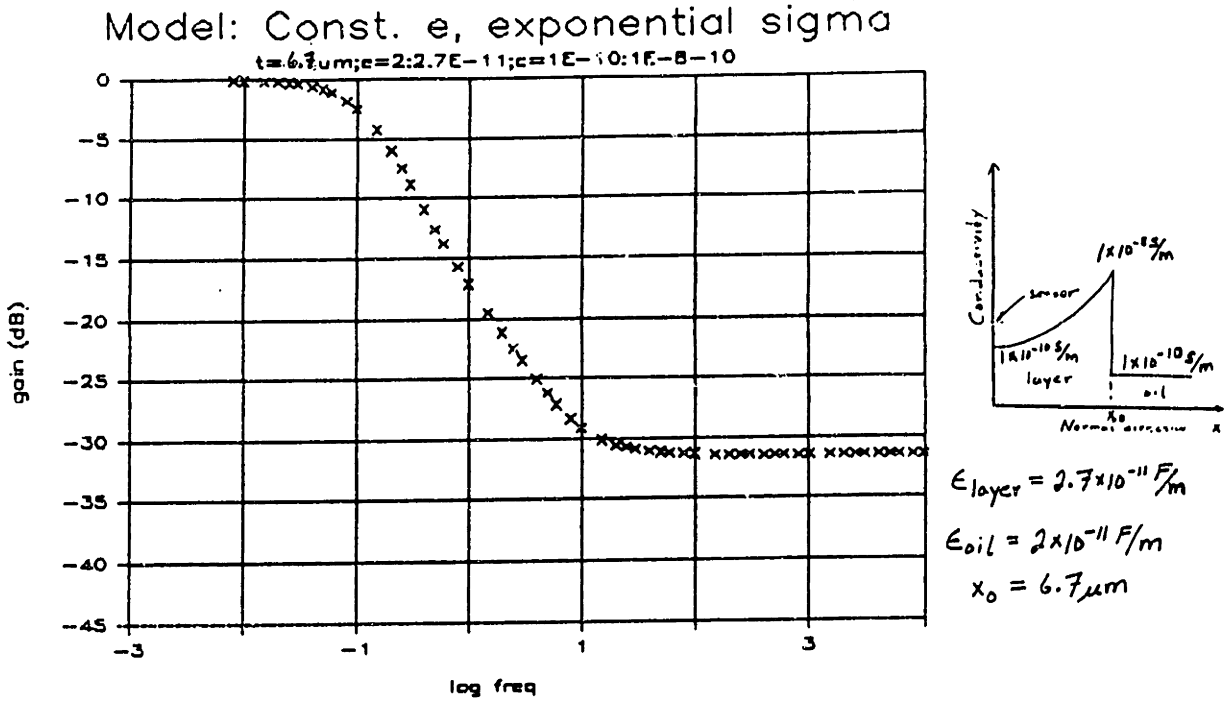

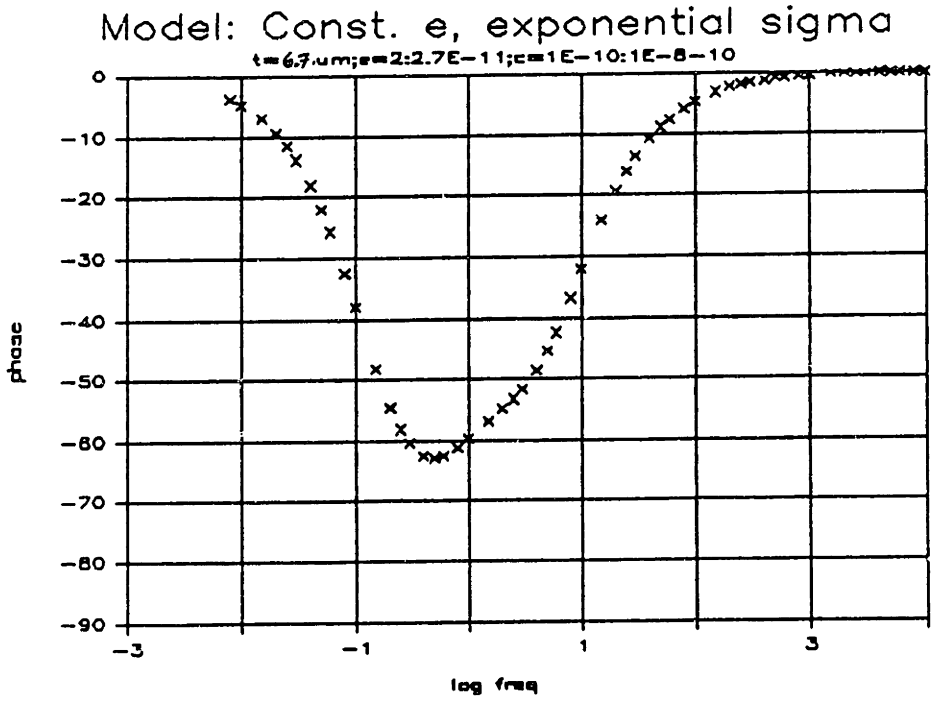

Figure A.2: Predicted Response to Layer with Conductivity Profile Using Integration

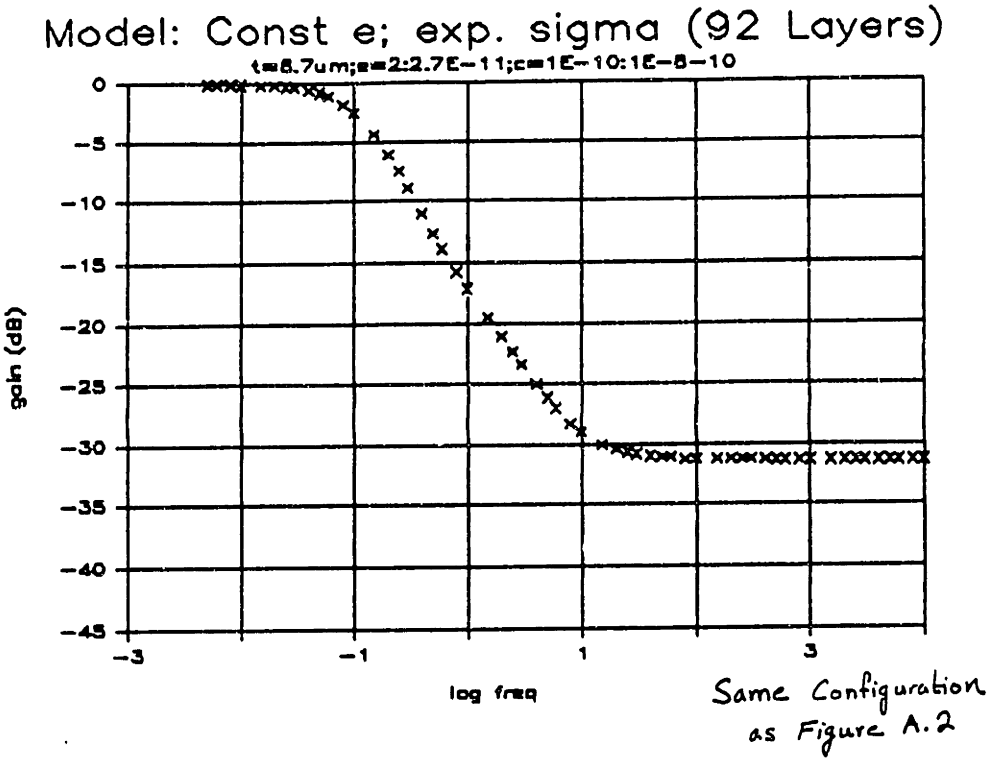

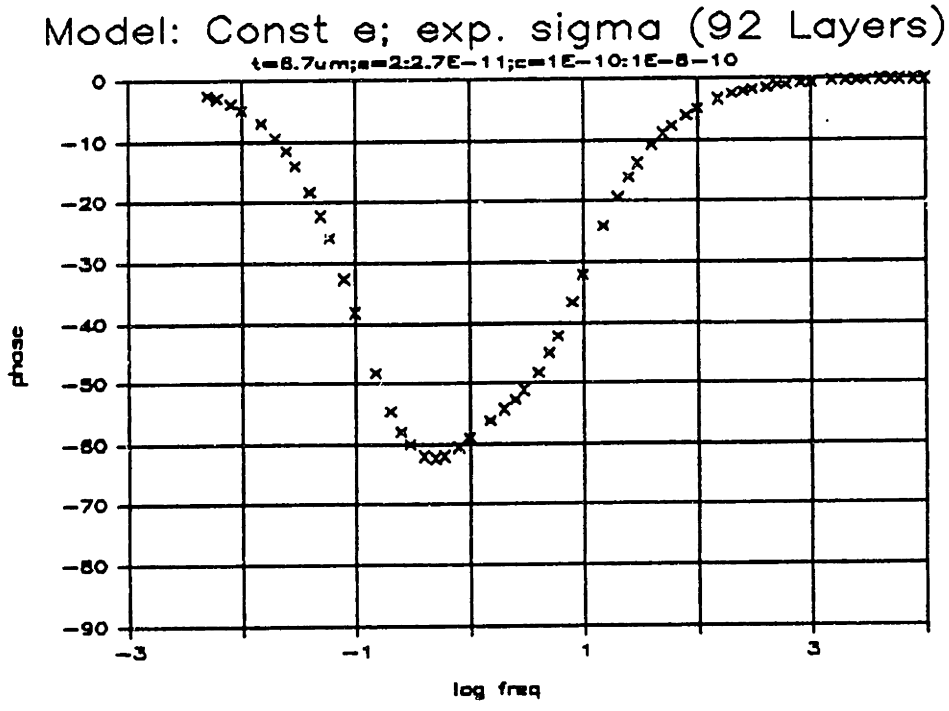

Figure A.3: Predicted Response to Layer with Conductivity Profile Using Discretization

Appendix B

Derivation of the Lorentz Sphere Model with Complex Surface Permittivity

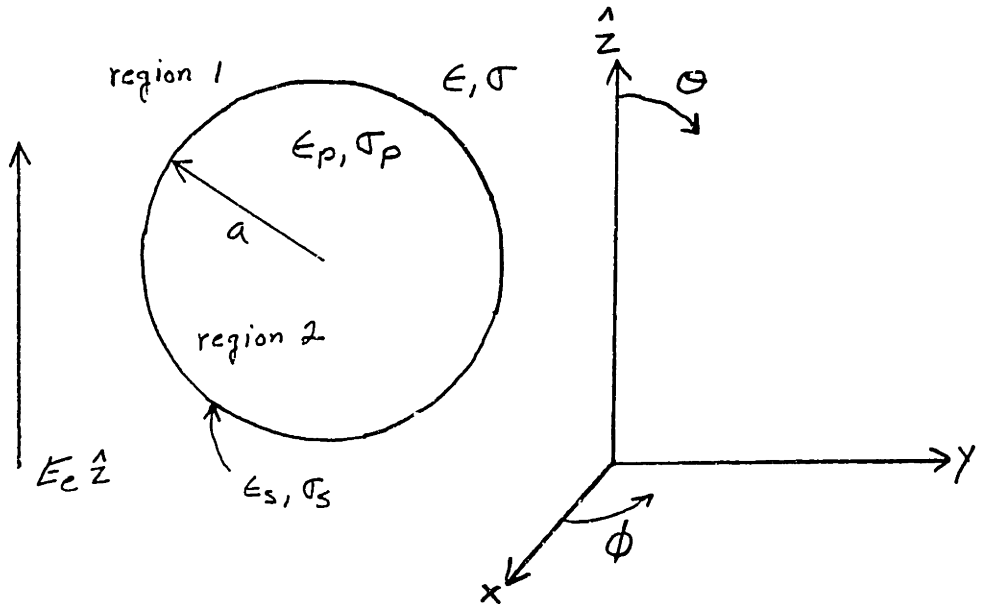

A sphere of radius a with permittivity ϵ_p and conductivity σ_p is embedded in a material with permittivity ϵ and conductivity σ. In addition, the sphere has a complex surface permittivity comprised of ϵ_s and σ_s. The sphere is stressed by an electric field which is uniform in the z direction at infinity ($E_e\hat{z}$). The potential in region (1) must satisfy Laplace's equation:

$$\Phi^{(1)} = -E_e r cos\theta + \frac{A cos\theta}{r^2} \tag{B.1}$$

where A is a constant to be determined. This is the superposition of a uniform field, and a dipole field which allows the boundary conditions at $r = a$ and $r = \infty$ to be matched. The potential in region (2) has only a uniform field contribution because the potential can't "blow up" at $r = 0$:

$$\Phi^{(2)} = B r cos\theta \tag{B.2}$$

where B is a constant to be determined. To find A and B, the boundary conditions at $r = a$ are used. The first boundary condition is continuity of the potential across the particle surface:

$$\Phi^{(1)}(r = a) = \Phi^{(2)}(r = a) \tag{B.3}$$

This gives one equation for A and B:

$$A = (B + E_e)a^3 \tag{B.4}$$

Conservation of charge specifies the other boundary condition:

$$\nabla \cdot \vec{J} + \frac{\partial \rho}{\partial t} + \nabla_\Sigma \cdot \vec{k} = 0 \tag{B.5}$$

where $\vec{J}$ is the bulk current density, and $\vec{k}$ is the surface current. Equation B.5 can be rewritten using the corresponding jump conditions assuming a sinusoidal time dependence:

$$\epsilon^* E_r^{(1)} - \epsilon_p^* E_r^{(2)} + \epsilon_s^* \nabla_\Sigma E_\theta = 0 \tag{B.6}$$

where the constitutive relations $J_r = \sigma E_r$ and $k = \sigma_s E_\theta$ have been used and $\epsilon^* = \epsilon - \frac{i\sigma}{\omega}$. Substituting for $E^{(1)}$, $E^{(2)}$, and E_θ using $\vec{E} = -\nabla\Phi$, gives the following relationship for A and B:

$$\epsilon^*(E_e + \frac{2A}{a^3}) + \epsilon_p^* B + \epsilon_s^* \frac{2B}{a} = 0 \tag{B.7}$$

Substituting for A using Equation B.4 and solving for B gives:

$$B = \frac{-3\epsilon^* E_e}{2\epsilon^* + \epsilon_p^* + \frac{2\epsilon_s^*}{a}} \tag{B.8}$$

Substituting for A and B into Equation B.1 gives:

$$\Phi^1 = -Er\cos\theta + a^3(E_e + B)\frac{\cos\theta}{r^3} \tag{B.9}$$

Comparing the second term in this equation with the solution for a dipole

$$\Phi_{dipole} = \frac{p}{4\pi\epsilon^*}\frac{\cos\theta}{r^2} \tag{B.10}$$

indicates that

$$p = 4\pi\epsilon^* a^3 E_e(1 + B) \tag{B.11}$$

The total polarization, P, is the polarization of one sphere times the density of spheres per unit volume, p_m, where p_m is given by:

$$p_m = \frac{1 - \phi}{4\pi a^3/3} \tag{B.12}$$

and ϕ is the "voidage", or space not occupied by the particles. Thus, the total polarization is given by:

$$P = 3(1 - \phi)\epsilon^*(1 + B)E_e \tag{B.13}$$

To calculate the effective permittivity, let's begin from the definition of the displacement vector D:

$$\vec{D} = \epsilon \vec{E_{avg}} + \vec{P} \tag{B.14}$$

where

$$\vec{E_{avg}} = \vec{E_e} - \frac{\vec{P}}{3} \tag{B.15}$$

and $\vec{P}/3$ is the depolarization field [41]. Substituting for $\vec{P}$ in Equation B.14 using Equation B.13, and substituting for E_e using Equation B.15 gives an equation in just E_{avg} from which the effective permittivity can be extracted:

$$\epsilon^*_{effective} = \left[\frac{3\epsilon_p^* + 6\epsilon_s^*/a + 2\phi(\epsilon^* - \epsilon_p^* - 2\epsilon_s^*/a)}{3\epsilon^* + \phi(\epsilon_p^* - \epsilon^* + 2\epsilon_s^*/a)}\right]\epsilon^* \tag{B.16}$$

Bibliography

[1] Rouse, T. O., *Evaluation of Alternative Insulating Oils for Use in Transformers and Other Electrical Apparatus*, EL-809-SY EPRI Research Project 562-1 (Prepared by General Electric: Project manager E. T. Norton)

[2] Wilson, A.C.M., *Insulating liquids: Their uses, Manufacture and Properties*, Peter Pereginus LTD., UK, 1980.

[3] Baehr, R., W. Breuer, F. Flottmeyer, J. Kotschnigg, R. Muller, and H. Nieschwietz, "Diagnostic Techniques and Preventive Maintenance Procedures for Large Transformers", CIGRE Conf., Sept., 1982, paper 12-13.

[4] Rogers, R.R., "IEEE and IEC Codes to Interpret Incipient Faults in Transformers, Using Gas in Oil Analysis", IEEE Trans. Electr. Insul., Vol EI-13, No. 5, Oct. 1978.

[5] Duval, M., C. Lamarre, "The Characterization of Electrical Insulating Oils by High-Performance Liquid Chromatography", IEEE Trans. Electr. Insul., Vol EI-12 No. 5, October 1977

[6] Duval, M., C. Lamarre, Y. Giguere, "Reversed-phase High Performance Liquid Chromatographic Analysis of Polar Oxidation Products in Transformer Oils", Jornal of Chromatography, 284 (1984) 273-280

[7] Burton, P.J., J. Graham, A.C. Hall, J.A. Laver, and A.J. Oliver, "Recent Developments by CEGB to Improve the Prediction and Monitoring of Transformer Performance", CIGRE Conf., Sept, 1984, paper 12-09

[8] ASTM Test D117-81

[9] Forster, E. O. "A Comparison of the AC and DC Conductivities of Liquid Hydrocarbons", 4th International Conf. on Conduction and Breakdown in Dielectric Liquids, Dublin, 1972.

[10] Bartnikas, R., "Dielectric Losses in Solid-Liquid Insulating Systems - Part I". IEEE Transactions on Electric Insulation, Vol. EI-5, No. 4, Dec. 1970

[11] Blythe, A. R.,*Electrical Properties of Polymers* Cambridge Solid State Science Series, Cambridge University Press NY, 1979

[12] Gartner, E. and Tobazeon, R.,"On the Behavior of Liquid/ Solid Insulations at Very Low Frequency". IEEE Transactions on Electrical Insulation, Vol. EI-12, No. 1, Feb. 1977.

[13] Hakim, R. M., "The Effect of Oxidation on the Dielectric Properties of an Insulating Oil", IEEE Transactions on Electrical Insulation, Vol. EI-7, no. 4, Dec. 1972

[14] Bartnikas, R., "Dilectric Loss in Insulating Liquids" IEEE Transactions on Electrical Insulation, Vol. EI-2, No. 1, April 1967.

[15] W. A. Fessler, F. S. Nichols, T. O. Rouse, "Tube Aging and Oxidation of Naphthenic and Paraffinic Transformer Oils" IEEE Internation Symposium on Electrical Insulation.

[16] I. Y. Megahed, A. A. Zaky, "Influence of Temperature and Pressure on Conduction Currents in Transformer Oil", IEEE Transactions on Electrical Insulation Vol. EI-4 no. 4 Dec. 1969

[17] C. Lamarre, J. P. Crine, M. Duval, "Influence of Oxidation on the Electrical Properties of Inhibited Naphthenic and Paraffinic Transformer Oils", IEEE Transactions on Electrical Insulation Vol. EI-22 No.1, Feb. 1987

[18] Bartnikas, R., "Electrical Conduction in Medium Viscosity Oil-Paper Films – Part II", IEEE Transactions on Electrical Insulation, Vol. EI-9, no. 3, Sept. 1974

[19] A. A. El-Sulaiman, A. S. Ahmed, M. I. Qureshi, "High Field DC Conduction Current and Spectroscopy of Aged Transformer Oil", IEEE Transactions on Power Apparatus and Systems, Vol. PAS-101, No. 11, Nov. 1982

[20] Stark, K. H., "Dielectric Loss of Insulating Oil", IEE Proceedings Pt IIA Vol. 100, 1953

[21] S. Yasufuku, T. Umemura, T. Tanii, "Electric Conduction Phenomena and Carrier Mobility Behavior in Dielectric Fluids", IEEE Transactions on Electrical Insulation, Vol EI-14 No. 1, Feb 1979

[22] S. D. Senturia, N. F. Sheppard, H. L. Lee, and D. R. Day, "In-Situ Measurement of the Properties of Curing Systems with Microdielectrometry", J. Adhesion, Vol. 15, 1982, pp. 69-90

[23] Lee, H.L., "Optimazation of a Resin Cure Sensor", SM Thesis, MIT, Aug., 1982

[24] Mouyad, L., "Monitoring of Transformer Oil Using Microdielectric Sensors", SM Thesis, MIT, Feb., 1985

[25] Zaretsky, M., L. Mouayad, J.R. Melcher, "Modal Approach to Obtaining Continuum Properties from Interdigital Electrode Dielectrometry", to be published in IEEE.

[26] Zaretsky, M., Ph. D. Thesis to be compeleted in summer of 1987 under supervision of Prof. J. R. Melcher.

[27] Micromet Instruments. Cambridge MA

[28] J. R. Melcher, H. A. Haus, *Electromagnetic Fields and Energy* Dept. of EE, MIT, 1983 (6.013 class notes–to be published)

[29] Paratronix Inc., Attleboro Mass.

[30] S. A. Stigant, A. C. Franklin *The J & P Transformer Book* John Wiley & Sons, New York 1973

[31] Stannett, A. W., "The Measurement of Water in Power Transformers". IEE Proceedings Pt. A, Supp. 3, Vol. 109, 1962

[32] Rushall, R. T., "Dielectric Properties of Oil-Soaked Pressboard as Affected by Water". IEE Proceedings Pt II A, Vol. 100, 1953

[33] Jonscher, A. K., *Dielectric Relaxation in Solids* Chelsea Dielectrics Press, London 1983

[34] O'Sullivan, J. B., "The Conduction of Electricity Through Cellulose - Part III. The Mobility of Hydrogen and Hydroxyl Ions in Cellulose Sheet". J. Textile Institute, 1947, vol. 38.

[35] O'Sullivan, J. B., "The Conduction of Electricity Through Cellulose - Part IV. The Mobility of Various Ions in Cellulose Sheet". J. Textile Institute, 1947, vol. 38.

[36] O'Sullivan, J. B., "The Conduction of Electricity Through Cellulose - Part V. The Effect of Temperature". J. Textile Institute, 1947, vol. 39.

[37] Hearle, J. W. S., "Electrical Resistance of Textile Materials: IV. Theory". J. Textile Institute, 1953, Vol. 44 No. 4

[38] Mark, Richard E.,*Handbook of Physical and Mechanical Testing of Paper and Paperboard, Vol. 2*, Chapter 21, "Electrical Properties: Theory", Gary A. Baum. Marcel Dekker, Inc., New York 1984.

[39] Potters Technical Quality Glass Beads. H series (High Density), Potters Industires Inc., P.O. Box 14, Carlstadt, N.J. 07072

[40] Melcher, J. R., *Continuum Electromechanics*, The MIT Press, Cambridge MA, 1981

[41] J. A. Kong, A. Sihvola, "Effective Permittivity of Dielectric Mixtures". Department of Electrical Engineering, MIT

[42] M. Zahn, S. Rhee, "Electric Field Effects on the Equilibrium and Small Signal Stabilization of Electrofluidized Beds", IEEE Transactions on Industry Applications, Vol. IA-20, No. 1, Jan. 1984

[43] Fuchs, M. ,"Dielectric Studies of Adsorption in Packed-Bed Systems". M. S. Thesis, Department of Electrical Engineering, MIT, Cambridge MA, 1986.

[44] *Chromatography: A Laboratory Handbook of Chromatographic and Electrophoretic Methods*, edited by Erich Heftmann, Van Nostrand Reinhold Company, New York 1975

[45] Henrici, P., *Essentials of Numerical Analysis with Pocket Calculator Demonstrationis.* John Wiley & Sons, New York, 1982